

https://dspace.org/

Ellagic acid-mediated inhibition of schistosoma japanicum glutathione transferase: enzyme kinetics and structural perspectives

Oyiogu, Blessing Oluebube

2018

https://hdl.handle.net/10539/27063

Oyiogu, Blessing Oluebube, (2018) Ellagic acid-mediated inhibition of Schistosoma japonicum glutathione transferase: enzyme kinetics and structural perspectives, University of the Witwatersrand, Johannesburg, https://hdl.handle.net/10539/27063.

Downloaded from a DSpace repository. https://dspace.org/

Ellagic acid-mediated inhibition of *Schistosoma japonicum* glutathione transferase: enzyme kinetics and structural perspectives

Blessing O. Oyiogu

A dissertation submitted to the Faculty of Science, University of the Witwatersrand, Johannesburg, in fulfilment of the requirement for the degree of Master of Science.

Johannesburg, September 2018.

Declaration

I declare that this dissertation is my own, unaided work. It is being submitted for the Degree of Master of Science at the University of the Witwatersrand, Johannesburg. It has not been submitted before for any degree or examination at any other University.



Blessing O. Oyiogu

28th day of September 2018.

Abstract

Schistosoma japonicum glutathione *S*-transferase (SjGST) is a homodimeric enzyme central to detoxification of electrophilic compounds in the parasite due to its lack of cytochrome P-450. Hence, SjGST is a potential therapeutic target for schistosomiasis. Akin to most cytosolic GSTs, SjGST is composed of two active sites per monomer, which are the glutathione binding site (G-site) and the hydrophobic binding site (H-site). Ellagic acid (EA), a polyphenolic compound ubiquitous in fruits and other plant-based products has been identified as a therapeutic agent against cancer, heart and liver diseases. The interaction between SjGST and EA was characterised in this study. Using 1-chloro-2,4 dinitrobenzene (CDNB) and glutathione (GSH) as SjGST substrates, EA was shown to inhibit SjGST activity, with an IC_{50} of 2.4 μM. The observed mode of inhibition with respect to the G-site and H-site was non-competitive and uncompetitive, respectively. The turnover rate of SjGST was reduced from 0.002 ± 0.0001 sec^{-1} to 0.0006 ± 0.00001 sec^{-1} in the presence of 9 μM EA, while the catalytic efficiency (k_{cat}/K_M) was reduced from 0.02 ± 0.0002 $M^{-1}s^{-1}$ to 0.009 ± 0.0001 $M^{-1}s^{-1}$. Using ANS as an extrinsic fluorescence probe, SjGST bound to ANS in a concentration-dependent manner in the absence (K_d = 40.6 ± 2.6 μM) or presence of EA (K_d = 30.3 ± 1.4 μM). This observation was further probed by the displacement of ANS by EA, which suggest that about 64.5% of ANS was displaced by EA. The ANS studies indicated that EA binds to the H-site of the enzyme. Secondary and quaternary structure analyses indicate that EA does not alter the secondary and tertiary structures of SjGST. Thermodynamic parameters obtained by isothermal titration calorimetry (ITC) indicate that the interaction between SjGST and EA is enthalpically-driven and compensated by a negative entropy change ($-T\Delta S$ = 20.40 ± 0.08 kJ/mol) because of enthalpy-entropy compensation. The free energy change (ΔG = -29.88 ± 0.07 kJ/mol) is also favoured by entropic contributions; therefore, indicating a strong hydrophobic interaction. A stoichiometry of 4 molecule of EA per mole of the dimeric enzyme was obtained. Molecular modelling studies suggests that EA binds more to the dimer interface compared with the H-site. Therefore, it is possible that EA may bind to two different sites in the enzyme, the H-site and the dimer interface.

Dedication

This work is dedicated to my lovely husband Uchechukwu, for your incredible love, support and motivation, my daughter Victoria Sochikayima, to my wonderful parents who thought me that “If you can think it, you can do it” and for their prayers.

Acknowledgements

My deepest gratitude goes to my supervisor and mentor **Dr Ikechukwu A. Achilonu** for his immense assistance and devoted supervision of my research work. I really appreciate your enormous contributions to this study.

The National Research Foundation and **Professor Heinrich W. Dirr** for financial support and opportunity to work in Protein-Structure Function Research Unit laboratory.

All my current and past colleagues of the Protein-Structure Function Research Unit, especially Babongiwe Hlabano, Tshireletso Mentor.

Table of contents

Declaration i

Abstract ii

Dedication iii

Acknowledgements iv

Table of contents v

List of Figures vii

List of Tables viii

Abbreviation ix

Chapter 1 Introduction 1

1.1 Problem statement 1

1.2 Rationale of the study 2

1.3 Definition of terms 2

1.4 Aims and objectives 3

1.5 Overview of the work 3

Chapter 2 Literature review 5

2.1 Overview of *Schistosoma* 5

2.2 The lifecycle of *Schistosoma* parasite 8

2.3 Current treatment of schistosomiasis 10

2.4 Overview of proteins as therapeutic agents 10

2.5 Glutathione transferase 12

2.6 *Schistosoma* glutathione transferase as a potential drug target 13

2.7 The structure of *Schistosoma japonicum* glutathione transferase 14

2.8 Ellagic Acid 17

2.9 Computational chemistry 18

Chapter 3 Materials, Methodology and Methods 21

3.1 Materials 21

3.2 Methodology and Methods 21

3.2.1 pGEX-4T-1 GST expression vector isolation and purification 21

3.2.2 Transformation of *E. coli* T7 Express with pGEX-4T-1 23
3.2.3 Overexpression of recombinant SjGST 24
3.2.4 Protein purification 24
3.2.5 Sodium dodecyl sulfate polyacrylamide gel electrophoresis 25
3.2.6 Quantification and qualitative analysis 26
3.2.7 Structural Characterisation 27
3.2.7.1 Secondary structure characterisation 28
3.2.7.2 Tertiary structure characterisation 29
3.2.7.3 Quaternary structure characterisation 31
3.2.8 Functional characterisation 32
3.2.8.1 GSH-CDNB conjugation assay 32
3.2.8.2 IC_{50} of Ellagic Acid 33
3.2.8.3 Kinetic analysis of SjGST 34
3.2.9 Isothermal titration calorimetry 36
3.2.10 Molecular modelling 37

Chapter 4 Results 38
4.1 Expression and purification of SjGST 38
4.2 Qualitative and quantitative analysis of recombinant SjGST 41
4.3 Structural Characterisation 43
4.3.1 Secondary structure 43
4.3.2 Tertiary structure 44
4.3.2.1 Intrinsic fluorescence 44
4.3.2.2 Extrinsic ANS fluorescence-binding studies 44
4.3.3 Quaternary structure 47
4.3 Functional characterisation 48
4.3.1 Kinetics analysis of SjGST 50
4.4 Thermodynamics of Ellagic acid-SjGST interaction 54
4.5 Molecular modelling studies 54

Chapter 5 Discussion 59
References 67
Appendix 79

List of Figures

Figure 2.1 Global distribution of schistosomiasis....8
Figure 2.2 Lifecycle of *Schistosoma* parasites....9
Figure 2.3 The structure of Praziquantel....10
Figure 2.4 Some inhibitors of *Schistosoma japonicum*....11
Figure 2.5 Schematic illustration of the active sites of typical dimeric GSTs....13
Figure 2.6 Cartoon Ribbon representation of SjGST....16
Figure 2.7 Structure of Ellagic acid....17
Figure 3.1 Map of pGEX-4T-1 vector....22
Figure 3.2 A ribbon representation of SjGST structure....29
Figure 3.3 GSH-CDNB conjugation reaction....34
Figure 4.1 SDS-PAGE analysis of over-expression of SjGST in *E. coli*....39
Figure 4.2 Purification profile of SjGST....40
Figure 4.3 Quantity and quality assessment of SjGST....42
Figure 4.4 Far-UV circular dichroism spectra of SjGST....43
Figure 4.5 Intrinsic fluorescence emission spectra of SjGST....45
Figure 4.6 ANS binding and displacement fluorescence analysis....46
Figure 4.7 SE-HPLC chromatogram of SjGST....47
Figure 4.8 Specific activity analysis using GSH-CDNB conjugation assay....48
Figure 4.9 IC_{50} of EA on its inhibitory effect on SjGST....49
Figure 4.10 Kinetic analysis of SjGST in the presence and absence of EA (GSH)....51
Figure 4.11 Kinetic analysis of SjGST in the presence and absence of EA (CDNB)....52
Figure 4.12 Inhibition kinetics of EA on SjGST....53
Figure 4.13 Calorimetric profile of the titration of SjGST....56
Figure 4.14 Molecular docking of SjGST bound EA....57
Figure 4.15 Molecular docking of EA bound to the H-site of SjGST....57
Figure 4.16 Molecular docking of EA bound to the H-site of GSTP1-1....58
Figure 4.17 Glide Emodel energy bar chart....58

List of Tables

Table 3.1 Non-standard materials and suppliers.....21

Table 4.1 Summary of the secondary structure content calculated.....44

Table 4.2 Kinetic parameters of SjGST.....54

Abbreviations

[Θ]	mean residue ellipticity
3D	three dimensions
Å	Ångström unit (1 Ångström unit = 0.1 nm)
A_{280}	absorbance at 280 nm
ANS	8-anilino-1-napthalene sulfonate
CD	circular dichroism
CDNB	1-chloro-2,4-dinitrochlorobenzene
C-terminal	carboxylic acid terminal
Da	dalton
ddH_2O	deionised-distilled water
DDT	dichloro-diphenyl-trichloroethane
dH_2O	distilled water
DNA	deoxyribonucleic acid
DTNB	5,5'-dithio-bis-(2-nitrobenzoic acid)
DTT	dithiothreitol
EDTA	ethylenediamine-tetra-acetic acid
GSH	glutathione (reduced form)
G-site	glutathione binding site
GST	glutathione *S*-transferase
H-site	hydrophobic electrophilic substrate binding site
IC_{50}	50% inhibitory concentration
IPTG	isopropyl β-D-1-thiogalactopyranoside
ITC	isothermal titration calorimetry
k_{cat}	turnover number
k_{cat}/K_M	catalytic efficiency
K_M	Michaelis-Menten constant
K_d	dissociation constant
kDa	kilodalton
kJ/mol	kilojoules per mole
LB	lysogeny broth
mdeg	millidegrees

Mr	relative molecular mass
Mw	molecular weight
nm	nanometer
nM	nanomolar
N-terminal	amino terminal
OD	optical density
PDB	protein data bank
rpm	revolution per minute
SDS-PAGE	sodium dodecyl sulfate polyacrylamide gel electrophoresis
SE-HPLC	size exclusion-high performance liquid chromatography
TEMED	N,N,N′,N′-tetramethylethylenediamine
Tris-HCL	tris(hydroxymethyl)aminomethane-Hydrochloric acid
UV	ultra violet
v/v	volume per volume
w/v	weight per volume
ΔG	Gibbs free energy
ΔH	enthalpy change
ΔS	entropy change
ε	molar absorption coefficient
μL	microlitre
μm	micrometre
μM	micromolar

Chapter 1

Introduction

1.1 Problem statement

Schistosomiasis is a chronic devastating parasitic disease caused by flat worms of the class trematoda (*Schistosoma* spp). The disease is mostly prevalent in Africa and endemic in about 42 African countries (Steinmann *et al.*, 2006). It has been estimated that ∼258 million people are infected, and ∼200 000 deaths recorded annually (King and Dangerfield-Cha, 2008). Schistosomes infections lead to many chronic disabilities such as anaemia, stunted growth and other morbidities, which are not fully reported. In addition, Schistosome infections enhance susceptibility to some other disease infections such as malaria (Utzinger *et al.*, 2001) and HIV (Secor and Sundstrom, 2007). Among the species that affect humans, *S. Japonicum* is the most severe and widespread. The World Health Organisation (WHO) has explored several means to contain the transmission of the disease. WHO tried reducing the densities of the intermediate host (snail) through the use of molluscicides, but abandoned the process due to the high cost and linked environmental hazards (Utzinger *et al.*, 2009). The use of chemotherapy and several drugs have also been tried, but the affected population can hardly afford the cost of chemotherapy and the drugs were not effective except as supplementary drugs (Caffrey, 2007; Doenhoff *et al.*, 2008).

Currently praziquantel is the only major drug for the treatment of schistosomiasis. It is effective against the adult worms, but its action against schistosomulae (immature worm) is limited (Colley *et al.*, 2014). Ross *et al*. (2002) reported that praziquantel is not a good option for chemoprophylaxis because it has a short half-life of about 1-2 h. There are claims of Schistosome resistance to praziquantel and tolerance in some endemic countries, also laboratory analysis reported Praziquantel resistant parasites (Doenhoff *et al.*, 2008). This clearly indicates the need to identify new drug therapies to treat schistosomiasis.

1.2 Definition of terms

Enzymes catalyse the rate of numerous bio-chemical reactions by converting substrates into products in a system within an optimum pH. The enzyme activity measures the quantity of active enzyme molecules available to catalyse a reaction. The activity of enzymes can be inhibited by some substrates or molecules, which disrupts their catalytic efficiency. Although I cannot dispute the possible existence of other biological activities of SjGST, in this study SjGST activity refers to GSH-CDNB conjugation reaction catalysed by SjGST. This reaction mimics the classical detoxification reaction carried out by cytosolic GSTs.

1.3 Rationale of the study

It is essential and urgent to develop new therapeutics for the treatment of Schistosomiasis, in case if the resistance to Praziquantel spreads extensively, or as a supplementary drug that can be administered in combination with Praziquantel to prevent the evolution of Praziquantel resistant strain of *Schistosoma*. Glutathione *S*-transferases (GSTs) is an essential detoxification enzyme in parasitic helminths. It has been identified as a major attractive therapeutic target against schistosomiasis and other parasitic diseases (Ramsay and Dilda, 2014). GSTs exhibits high capacity to bind various non-substrate ligands with varying affinity (Listowsky, 1993). Hence, they participate in the uptake and transportation of non-substrate hydrophobic compounds. The ligandin functions of GSTs has been associated with the regulation of GST activities because ligand-binding has the capacity to inhibit the catalytic properties of these enzymes (Yassin *et al.*, 2004). It has been reported that Praziquantel binds to *Schistosoma japonicum* GST (SjGST), but *in vitro* studies revealed that it does not inhibit the activity of the enzyme (Milhon *et al.*, 1997).

Humans have been using naturally occurring products such as fruits, vegetables and herbs since early days as medications and seasonings. In recent times, there has been an upsurge in the use of these products as nutritional supplements and for herbal medications. Ellagic acid (EA) (2,3,7,8 tetrahydroxy[1]benzopyranol[5,4,3-cde][1]benzopyran-5, 10-dione) is a natural dietary polyphenolic compound found mostly in fruits and herbs (Whitley *et al.*, 2003). EA is also a chemotherapeutic agent and has been shown to inhibit human GSTs (Hayeshi *et al.*, 2007). EA being a naturally occurring compound is of great benefit to this study, because it is readily available in our daily diet and can be modified into other derivatives or analogues with stronger effects against SjGST. In addition, the SjGST H-site is structurally different from that

of mammals, and this indicates a structural backbone for rational drug design of substrate analogue inhibitors for SjGST (McTigue *et al.*, 1995). More so, there are no published experimental data describing the interaction between EA and SjGST. However, in view of the need for an alternative drug for schistosomiasis and the major role of GST in the thriving of *Schistosoma japonicum*, can EA inhibit the GSH-CDNB conjugation activity of SjGST?

1.3 Aims and objectives

The study was aimed at determining if EA is a potential inhibitor of the GSH-CDNB conjugation activity of SjGST. This aim will be achieved by accomplishing the following objectives:

1. To heterologously express recombinant SjGST using pGEX-4T-1 expression vector, and purification will be performed using glutathione agarose affinity chromatography.
2. To determine the specific activity of the recombinant SjGST using GSH and 1-chloro-2, 4-dinitrobenzene (CDNB) conjugation assay.
3. To carry out secondary, tertiary and quaternary structure characterisation of SjGST using far-UV circular dichroism, intrinsic tryptophan fluorescence, extrinsic 8-analino-1-naphthalene sulfonate (ANS) fluorescence spectroscopy and size exclusion high pressure liquid chromatography (SE-HPLC).
4. To determine the IC_{50} of EA on SjGST activity.
5. To obtain the kinetic parameters (K_M, k_{cat}, and k_{cat}/K_M) of SjGST in the presence and absence of EA.
6. To determine the energetics of binding by exploring some thermodynamic parameters (ΔH, ΔS, ΔG, K_d and K_a) using isothermal calorimetry (ITC).
7. Molecular modelling studies will be performed using Induced Fit™ ligand docking and Glide docking algorithms implemented in Schrödinger Suite 2017-3, to simulate the binding site of EA on SjGST.

1.4 Overview of the work

In chapter one, the problem statement, rationale of the study and the aims and objectives of the study was described. This is followed by a review of relevant literatures from previous research works, in chapter two. Chapter three describes the methodology and methods applied in the

research work, while the obtained results are presented in the fourth chapter. Finally, the results were discussed, and conclusion outlined in chapter five.

Chapter 2

Literature review

2.1 Overview of *Schistosoma*

The genus *Schistosoma,* also known as blood-flukes, is of the class trematoda. They are parasitic flat worms majorly found in fresh water bodies. The various species of *Schistosoma* includes *Schistosoma haematobium, S. mansoni, S. japonicum, S. intercalatum, S. mekongi, S. bovis,* and *S. matteei* (WHO, 2016). Among these species of Schistosomes, *S. haematobium, S. mansoni* and *S. japonicum* are the most ubiquitous and contagious in humans (Jiang *et al.*, 2008). Fresh water snails of distinct species are the intermediate host of Schistosomes, *Oncomelania* spp for *S. japonicum*, *Biomphalaria* spp for *S. mansoni*, *Tricular* (*Neotricular aperta*) spp for *S. mekongi* and *Bulinus* spp for *S. haematobium* and *S. intercalatum*. These species of snail do not exist in the same habitat and they thrive in distinct environmental states. The spread of the snail species majorly determines the prevalence of the different Schistosome species in a particular region (Joannes Clerinx and Soentjens., 2017). This parasitic worm (*Schistosoma*) causes an acute and chronic diseases in humans called schistosomiasis, a major devastating disease next to malaria in developing countries of the world (WHO, 2016).

Schistosomiasis, also known as bilharzias or snail fever, is one of the neglected tropical diseases discovered by Theodor Bilharz in 1851, while working in Cairo as a surgeon (Nour, 2010). Schistosomiasis infection in human starts when the skin comes in contact with the cercariae released by the snail hosts in fresh water bodies, the cercariae penetrates through the skin (Joannes Clerinx and Soentjens., 2017). The disease becomes symptomatic resulting in immunologic reactions to the *Schistosoma* eggs confined in tissues. The eggs release antigens which stimulates a granulomatous reaction that involves macrophages, T-cells, and oesinophils resulting to a clinical disease. Manifestation and symptoms of the disease is dependent on location and the number of eggs caught up or trapped in the tissues (Ahmed, 2016b). Some studies proposed that the morbidity which occurs because of the Schistosome infections, is induced by *Schistosoma* eggs not the adult worms. Most of the eggs are embedded permanently in the intestines or liver because numerous numbers of them are not excreted, as in the case of *S. japonicum, S. mekongi and S. mansoni.* The eggs can also be lodged in the bladder and urogenital system as in the case of *S. haematobium* (Colley *et al.*, 2014).

S. japonicum was discovered in 1904 by Katsurada in Japan (Nakashima *et al.*, 2003). It is the most virulent of the other species of tropical blood flukes affecting humans, because of the large quantity of eggs it produces. Also, the eggs are much smaller in size than that of other species (Jia *et al.*, 2007). *S. japonicum* is prevalent in China and the Philippines, most times infection by this species results in a blood serum disease known as 'Katayama' fever (Al-Waheeb *et al.*, 2009). About 60% of brain *Schistosoma* disease is caused by *S. japonicum* due to the size of the egg. Cerebral schistosomiasis is usually predominant amidst *S. japonicum* infections. This is because of ectopic accumulation of the eggs, which moves to the central nervous system. Encephalopathy is usually a sign or an indication of this ectopic egg settlement. Some of its clinical presentations are signs of meningoencephalitis, migraine, nausea and Jacksonian epilepsy. If the spinal cord is infected, it may lead to paralysis, sensory loss and loss of bladder control (urinary incontinence) (Ross *et al.*, 2012). *S. japonicum* has zoonotic capabilities; it can infect cattle, water buffaloes and humans, it increases the disease burden in humans which results in socio-economic challenges (Doerig and Grevelding, 2015).

Schistosoma causes a wide variety of debilitating systemic morbidities and complications, which includes gastrointestinal bleeding, malnutrition, infertility, severe anaemia, carcinoma of the liver and bladder, neuroschistosomiasis, renal failure, spontaneous abortion, pulmonary hypertension and pregnancy complications from vulvar of fallopian granuloma (Ahmed, 2016a; King and Dangerfield-Cha, 2008).

Acute schistosomiasis, also known as Katayama syndrome or fever, mostly occurs in locations that are heavily infected. The symptoms are usually short term and mild, which arises as a result of the reaction between the immune complex of the host and the parasite. Symptoms usually manifest within two to twelve weeks after infestation (Ross *et al.*, 2002). The usual symptoms are headache, fever, cough, fatigue, myalgia, eosinophilia, etc. If acute schistosomiasis is not identified early and treated accordingly, it may lead to serious morbidity (Ahmed, 2016a).

Chronic schistosomiasis often evolves after the primary infection, which may take several months or years to occur. It results in prolonged health issues and could harm vital organs (Utzinger *et al.*, 2009). The eggs confined in tissues in the course of perivesical movement or those that clump up in the liver, lungs, cerebrospinal system or spleen usually lead to chronic schistosomiasis. Granulomatous response occurs and gradually develops fibrotic deposits in host tissue prior to the destruction of the ova. This response is triggered by proteolytic enzymes

released by the eggs (Gryseels *et al.*, 2009). The site where there is a maximum build-up of the eggs usually determines where the granuloma develops. For instance, it develops in genitourinary tract (for *S. haematobium*), in the intestine and liver (for *S. japonicum* and *S. mansoni*). It has also been observed that other types of tissues found in the brain, lungs, skeletal muscle, skin, and adrenal gland develop granulomas (Ross *et al.*, 2002). Some of the clinical manifestation of chronic schistosomiasis include bloody diarrhoea, cramping, pain while urinating/blood in the urine (urinary schistosomiasis), chest pain, liver failure, cerebral disease, transverse myelitis, seizures etc (Kinsley *et al.*, 2008b; Nmorsi O., 2007).

Schistosomiasis is still a public health challenge in so many countries of the world especially in Africa where indigent and rural societies are majorly affected. About 92% of the population in need of prophylactic chemotherapy for the disease reside in the African continent (GHO, 2016). Presently according to WHO, 74 countries are endemic to this disease and 52 countries have inhabitants in need of prophylactic treatment. It has been estimated that about 258 million people are infected with schistosomiasis with about 200,000 deaths annually and 123 million of the infected population are children, because it is obvious that children have a higher risk of contracting the infection (WHO, 2016). Furthermore, it was estimated that schistosomiasis is responsible for about 70 million disability-adjusted life years (DALYs) lost yearly. Problems and challenges encountered globally as a result of schistosomiasis have been estimated to be more than that caused by malaria and tuberculosis and much the same as DALYs that cannot be regained due to HIV/AIDS (Hotez and Fenwick, 2009). Figure 2.1 shows the global distribution of schistosomiasis, endemic and non-endemic countries.

S. Japonicum is endemic in Southern China, Indonesia, Thailand and Philippines. *S. mansoni* is prevalent in about 52 countries which includes the Caribbean, Brazil, Venezuela, countries in the Eastern Mediterranean region (Egypt, Afghanistan, Iraq, Iran, Saudi Arabia, Yemen etc.), all rain forest sub-Saharan and Southern African countries (Adenowo *et al.*, 2015; John *et al.*, 2008). *S. haematobium* is endemic in about 54 countries in the Middle East and Africa, while *S. Mekongi* affects populations living around the Mekongi River in South-east Asia, countries like Thailand, Kampuchea and Laos. *S. intercalatum* affects about 10 Central African countries around the rain forest region (Adenowo *et al.*, 2015). However, rural - urban migration, increased eco-tourism and travels are spreading the disease to new regions (Bottieau *et al.*, 2006; Meltzer *et al.*, 2006).

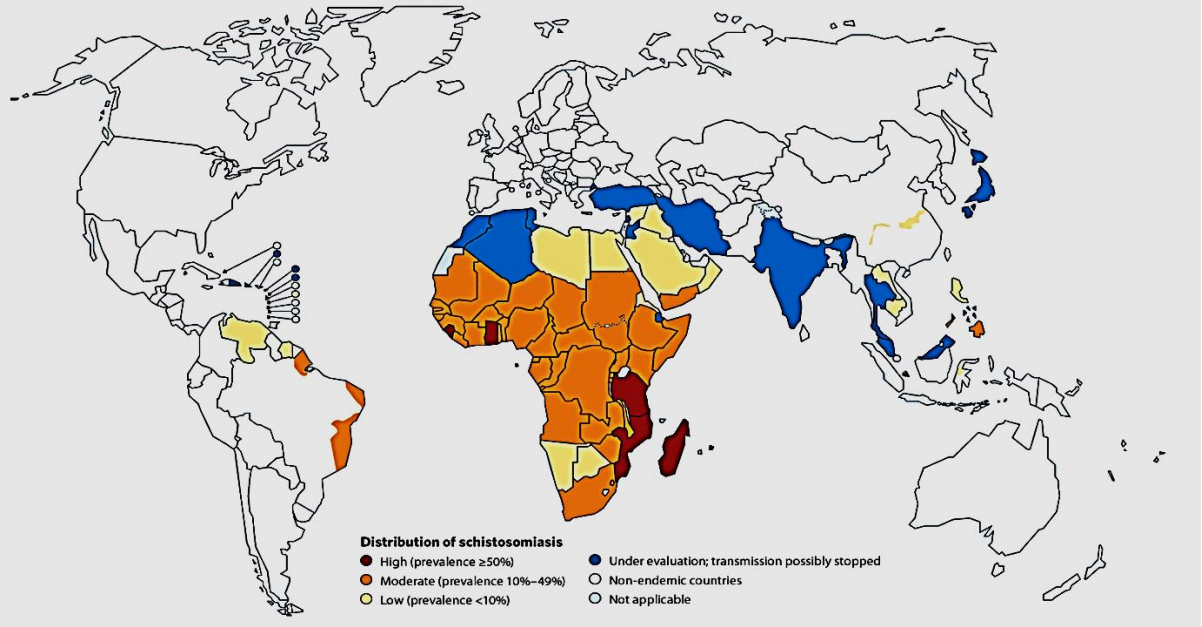


Figure 2.1 Global distribution of schistosomiasis. The distribution of schistosomiasis globally showing regions of high, moderate and low prevalence. It also indicates regions under evaluation in blue, non-endemic regions and regions unaffected by the disease. Source: WHO 2010.

2.2 The lifecycle of *Schistosoma* parasites

Schistosomes have a digenetic lifecycle; they reproduce sexually in their vertebrate host and asexually in snail host as shown in (Figure 2.2). Infected vertebrate host excretes eggs into the environment via urine or faeces, the eggs hatches in fresh water releasing a ciliated larva known as miracidia which infects an appropriate intermediate snail host. Asexual reproduction occurs in the snail in stages, the replication of multicellular sporocysts and the development of the cercariae, which is released within 4-6 weeks into water. The release of the cercariae happens mostly in the day time because it is triggered by light, and can be released in thousands daily by one snail for many months (Gryseels *et al.*, 2009). The virulent cercariae penetrates the human skin, sheds off its forked like tail permeating into the veins through the lungs where it develops into young worms (schistosomulae) then to the liver where it matures into adult worms or schistosomulae. The cercariae can only stay viable outside the human host for about 72 h. The schistosomulae moves via various tissues and phases into the portal veins, the female mates with the male by pairing; it enters gynecophoric canal of the male. They move in the opposite direction of blood flow to the veins in diverse tissues and organs with regards to their specific species (Ross *et al.*, 2007).

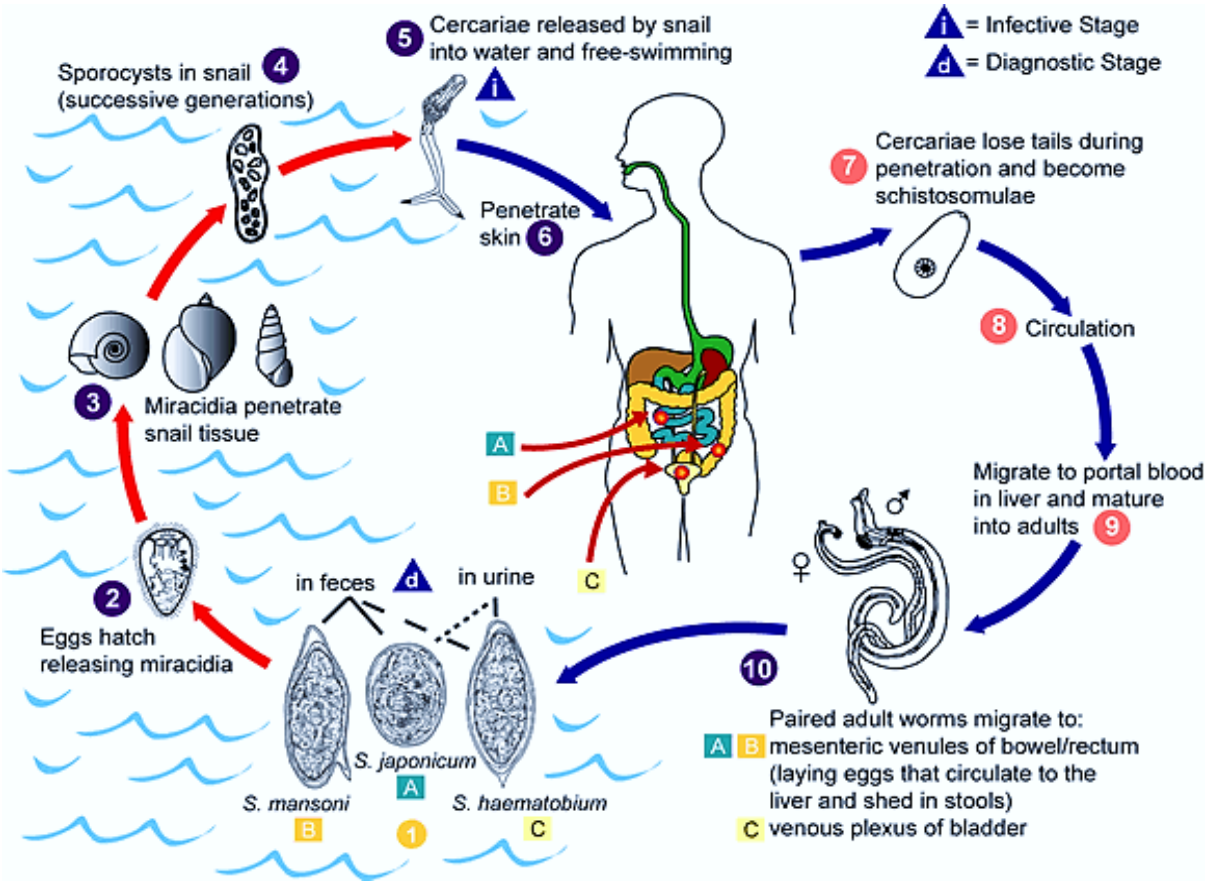


Figure 2.2 Lifecycle of *Schistosoma* parasites showing the two phases of the cycle in human and snails in fresh water.

S. japonicum is usually located in the mesenteric veins of the small intestine while *S. mansoni* is mainly seen in the large intestines. Nevertheless, the two species can be found in any of the intestines because they can migrate from one tissue location to another. *S. haematobium* is usually found in the vesicular veins and the rectal venules. The female worms produce eggs into the portal veins and perivesical system. The eggs proceed to the lumen of the bladder and ureter in the case of *S. haematobium*, to the intestinal lumen for *S. japonicum* and *S. mansoni* (WHO, 2017). Most of the eggs are excreted through faeces (*S. japonicum and S. haematobium*) and urine (*S. haematobium*), the remaining ones in the body re-enters the liver and causes inflammation (Yourgenome, 2016). The life span of the eggs from the moment it is laid by the adult female worm is within 1-2 weeks both for the excreted and retained. The excreted eggs hatch in water, release the miracidia, which infect their specific snail host; thus, completing the life cycle (Walker, 2011).

2.3 Current treatment of schistosomiasis

Currently praziquantel (acylated quinolone-pyrazine) is the primary drug used in the treatment of schistosomiasis. Its mode of action against the parasite is not yet well known or identified (Doenhoff *et al.*, 2008). Praziquantel (Figure 2.3) has no effect against the eggs or schistosomulae; hence, it requires a follow up treatment within 4-6 weeks after the initial treatment. A single dose of 40 mg/kg is usually effective for treatment, but *S. japonicum* requires more doses of 60 mg/kg (Renganathan, 1998). The average number of cure recorded using the normal dosage of praziquantel is about 60% within 1-2 months of treatment (Kramer CV *et al.*, 2014).

Artemether and artesunate derivatives of artemisinin are antimalarial drugs (Woodrow *et al.*, 2005), however they are also active against *Schistosoma* worms that are not fully developed to the adult stage (Utzinger *et al.*, 2000). In regions of high re-infection rate, artemisinin derivatives and praziquantel could be used together to enhance treatment. Oxamniquine has effect against *S. mansoni*; it is majorly used in Brazil (Fenwick *et al.*, 2003). It can cause remarkable side-effects like epileptic seizures, drowsiness etc.

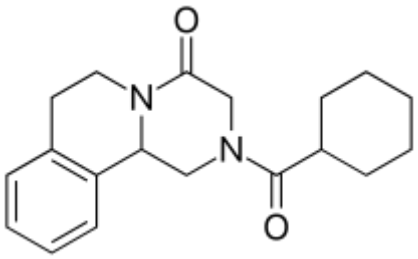


Figure 2.3 The structure of Praziquantel

2.4 Overview of proteins as therapeutic agents

Expansive research on the prospective molecular targets for schistosomiasis has gain much attention since the discovery of the genome (Caffrey *et al.*, 2009). Proteins such as proteases, kinases, G-protein-coupled receptors, ion channels, reductases and acetylases were discovered to be likely points of susceptibility, and are becoming evident and generally considered as new drug target to be explored (Babatunji *et al.*, 2014; Ferreira *et al.*, 2015). In addition, universal stress proteins (USP) have emerged as new potential drug targets against schistosomiasis, although their biochemical and molecular functions are yet to be well characterised (Masamba *et al.*, 2016).

Schistosome genes encoding histone acetyltransferases, deacetylases, methyltransferases and demethylases in *S. japonicum and S. mansoni* has been discovered, due to the identification of their genome sequences. The earliest research centred on the class I histone deacetylase (HDAC) 8 because comparison of catalytic site of the schistosome and human enzymes indicates key differences, suggesting the possibility of developing inhibitors specific for SmHDAC8 (Pierce *et al.*, 2012). The enzymes involved in lipid metabolism of schistosomes are regarded as interesting molecular targets for drug design because their sequence homology differs from the orthologs of mammals (Ferreira *et al.*, 2015). 3-oxoacyl-ACP reductases (OAR), has been speculated to be a metabolic bottleneck in schistosomes, belonging to the class reductases and a drug target for malaria and tuberculosis. Homology modelling and virtual screening were combined in discovering OAR inhibitors (Liu *et al.*, 2013). The research identified two inhibitors of OAR, which have antischistosomal action in cell assays and low cytotoxicity as well (Figure 2.4).

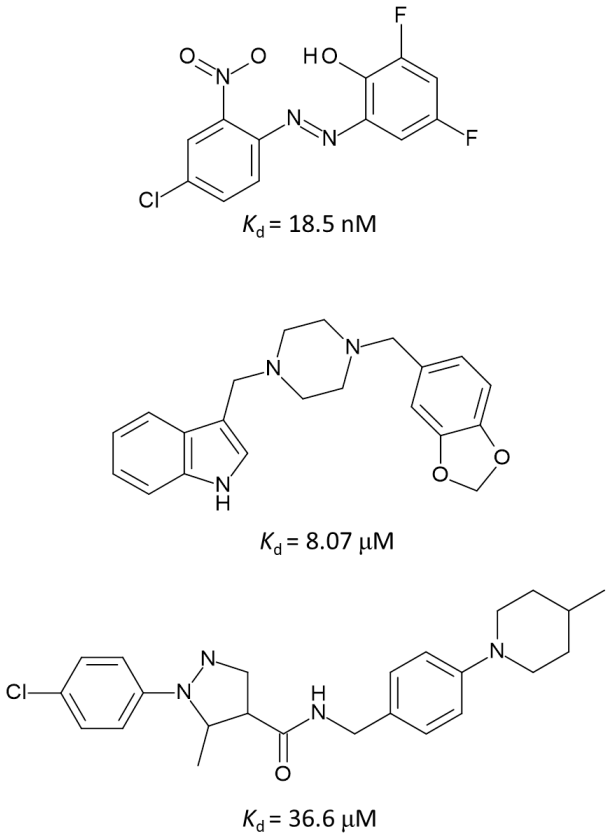


Figure 2.4 Some inhibitors of *Schistosoma japonicum* OAR identified through homology modelling and SBVS

The first step in the study involved molecular docking of molecule database selections, exhibiting drug-like properties which was carried out in comparison to *S. japonicum* OAR homology model. Thereafter, the identified virtual hits were assayed to check inhibitory activity on the recombinant enzyme (Ferreira *et al.*, 2015).

2.5 Glutathione transferase

Glutathione transferases (GST, EC 2.5.1.18) comprises a group of multi-gene isoenzymes, which detoxifies broad variety of exogenous and endogenous electrophilic compounds by glutathione (GSH) conjugation. They also carry out other activities such as transport of molecules, isomerisation, prostaglandin and leukotriene biosynthesis, catabolism of aromatic amino acids, modulation and/or development of ion channels and control in signal transcription processes (Torres-Rivera and Landa, 2008). They usually occur as dimeric enzymes, which can be in the form of a homo or heterodimers and their subunit molecular weight is approximately 26 kDa. Each dimer normally have 2 active sites (Figure 2.5) that perform independently (Alias, 2016). The active site comprises of the GSH-binding site (G-site) and a hydrophobic electrophile binding site (H-site). The H-site has low specificity; hence, its ability to bind an array of xenobiotics, including steroids, quinones, halogenonitrobenzenes, *αβ*-unsaturated carbonyl compounds, organophosphorus compounds, arylnitro compounds, aryl halides epoxides and isothiocyantates. GSTs take part in the phase II detoxification system and are of three major groups based on their localisation. They are the mitochondrial GSTs, microsomal GSTs or MAPEG (membrane proteins associated with ecosanoid and glutathione metabolism) and cytosolic or canonical GSTs (Torres-Rivera and Landa, 2008). The cytosolic GSTs (cGSTs) are many and are widely spread. They can be classified into organism-specific and the ubiquitous group. The organism specific class mostly exist in particular phyla, in plants as Tau (τ), Lambda (λ), Phi (Φ), and Beta (β) in prokaryotes, and in insect Epsilon (ε), Delta (δ). The Alpha (α), pi (π), Sigma (σ), mu (μ), Omega (ω, Ω) and Zeta (ζ, Z) classes are members of the ubiquitous cytosolic GSTs class found in mammals (Frova, 2006; Hayeshi *et al.*, 2007; Torres-Rivera and Landa, 2008). The Kappa (κ) is found in the mitochondrial GST group, it plays a major part in the *β*-oxidation of fatty acids and lipid peroxidation due to its localisation and high peroxidase activities. Four classes of the microsomal GSTs has been identified by some studies, although they are not well defined or characterised like the other GSTs (Frova, 2006). The classes include I, II, III and V (Jakobsson *et al.*, 1999).

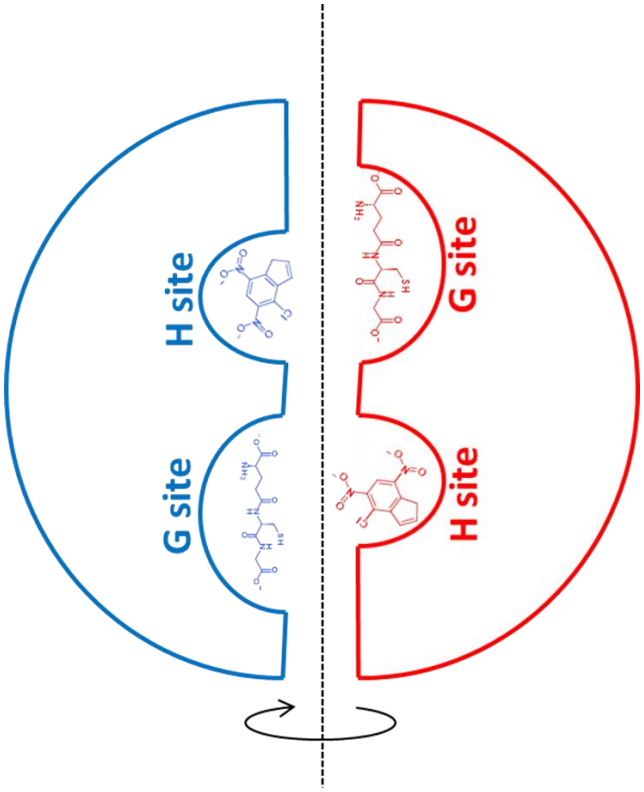


Figure 2.5 Schematic illustration of the active sites of typical dimeric GSTs. The active sites showing GSH bound to the G-site and CDNB bound to the H-site.

2.6 *Schistosoma* glutathione transferase as a potential drug target.

In most parasites, GSTs are notable for their role as the major detoxification process (phase I) because the activity of CYP450 (Cytochromes P450 cytochrome b5) is absent (McTigue *et al.*, 1995). Schistosomes are helminth organisms that are different because the enzyme activity levels of phase (I) one and other detoxification enzymes are usually not high, but low. However GSTs are normally expressed by schistosomes mostly in reaction to drug therapy (Sheehan *et al.*, 2001). Hence, GSTs are intriguing targets for developing vaccine and chemotherapeutic drugs. According to (Walker, 2011), it was observed that from classification viewpoint helminths have GSTs homologous to the Pi, Sigma and Mu classes of mammalian GSTs. The enzymes still exhibit adequate regions of structural disparity to the host enzymes which indicates potentials in the invention of drugs having parasitic specificity (Sheehan *et al.*, 2001)

GSTs metabolise xenobiotics and their actions can shield parasites from toxic impact of anthelmintic. They portray diverse actions and their substrates are specific, this enables diverse reactions between the GST and the anthelminthic compounds. The drug can inhibit or modulate

GST activity, which has been observed in schistosome GSTs (Nare *et al.*, 1992). Inhibition of schistosome GSTs could be favourable because the parasites will not have access to their main protection over oxidative stress, aversion of harmful xenobiotics and the production or movement of metabolites needed for the parasite to survive. The comparison of the parasite GST to its mammalian homologue shows that the G-site is conserved and it also emphasises the various structural dissimilarities of the H-binding site which presents chances of developing specific inhibitors (Baiocco *et al.*, 2006).

S. japonicum has two GSTs of 28 kDa and 26 kDa. They are isoforms and also similar to those of *S. mansoni* (Wright *et al.*, 1991). *S. mansoni* has five GST isoforms, GST1, 2, 3 with 28 kDa as the size of their subunits and two isoforms of 26 kDa. They are homologous to the mu class and similar to Pi and Alpha GSTs and for *S. haematobium* 28 kDa isoform has been discovered which is similar to 28 kDa of *S. bovi* (Trottein *et al.*, 1992). Each of these isoforms has their individual different function in the parasite because their kinetic properties differ. They also react differently to some inhibitors and substrates. The different locations of these isoforms in the parasite buttress their input in a specific metabolic pathway in schistosomes. The 28 kDa and 26 kDa are the main isoforms, they are located in tegument and in subtegumentary parenchymal cells. The 28 kDa GST isoform is found in undeveloped germinal cells of the male and female, then also in the ootype in the female genitals. The 26 kDa is found in the finger like part of the cytoplasm confined at the apical chamber outlined via the body of the flame cell. Hence, GST inhibition may probably interrupt metabolic processes in crucial regions (Huang *et al.*, 2012).

2.7 The structure of *Schistosoma japonicum* glutathione transferase

The 3-dimesional structure of the major GST (26 kDa) isoform of *S. japonicum* (Figure 2.6) has been solved using multiple isomorphous replacement (MIR), molecular replacement methods and set to *R*-factor of 19.7% at 2.4 Å resolution (McTigue *et al.*, 1995). Each subunit of SjGST contains 218 amino acid residues and it folds into N-terminal α/β domain made up of residues 1-76, containing 3 α helices and an antiparallel β-sheet made up of 4 strands. The C terminal α-helical domain is relatively larger in size and comprises of 5 α-helices with a long coil of residues 195-218 following the last helix (α8). The structure of the human GST does not have residues 211-218 (Gly-Gly-Gly-Asp-His-cisPro-Pro-Lys) being the final eight amino acids which create the open hairpin loop. The positioning of the 117 C^{α} locations from α helices

and β strands indicates that the complete fold of SjGST is similar to that of mammals. Residues 33-41 and 200-218 frames the segment of xenobiotic substrate binding site and also indicates the regions of highest difference between the structure of SjGST and human GSTs (McTigue *et al.*, 1995).

Each subunit has a binding site which becomes active when two subunits becomes a dimer of 57 Å × 47 Å × 44 Å dimensions, also between the folding axis of the two subunits is located a non-substrate binding site. This axis in-between the subunits is rotatable and is positioned at about 11° of the helical region of α4 which is symmetrical and crosses at angle of about 22°. The following residues are in proximity between the subunits- 50–53 (β-turn), 63-66 (β4), 67-76 (α3), 77-85 (loop), 88-109 (α4) and 129-136 (α5). At the point of association on the dimer Asp77-Arg89 and Glu51-Arg136 forms 2 salt bridges. Phe52 of one subunit penetrates and forms the main conspicuous hydrophobic contact found between 91-94 (α4) and 129-133 (α5) residues of the second subunit. Ser, Gln, Tyr, Asp, Leu100, Met69 and Arg polar side chains are the main amino acids that lines the long (40 Å) narrow cleft formed by the fitting together of the dimer (McTigue *et al.*, 1995)

Tyr103 of SjGST play an important role in the H-site for binding of xenobiotics and other endogenous substrates (Cardoso *et al.*, 2003). According to Rufer et al, the ligandin binding site (L-site) at the dimer interface, where Praziquantel binds, is partially occupied by Tyr103. They also observed that Arg107 and Tyr103, the vital and flexible residues of the L-site, in addition to the absence of a homologous tyrosine residue in mammalian GSTs could be of great importance to the design of specific drugs against Schistosoma GSTs (Rufer *et al.*, 2005).

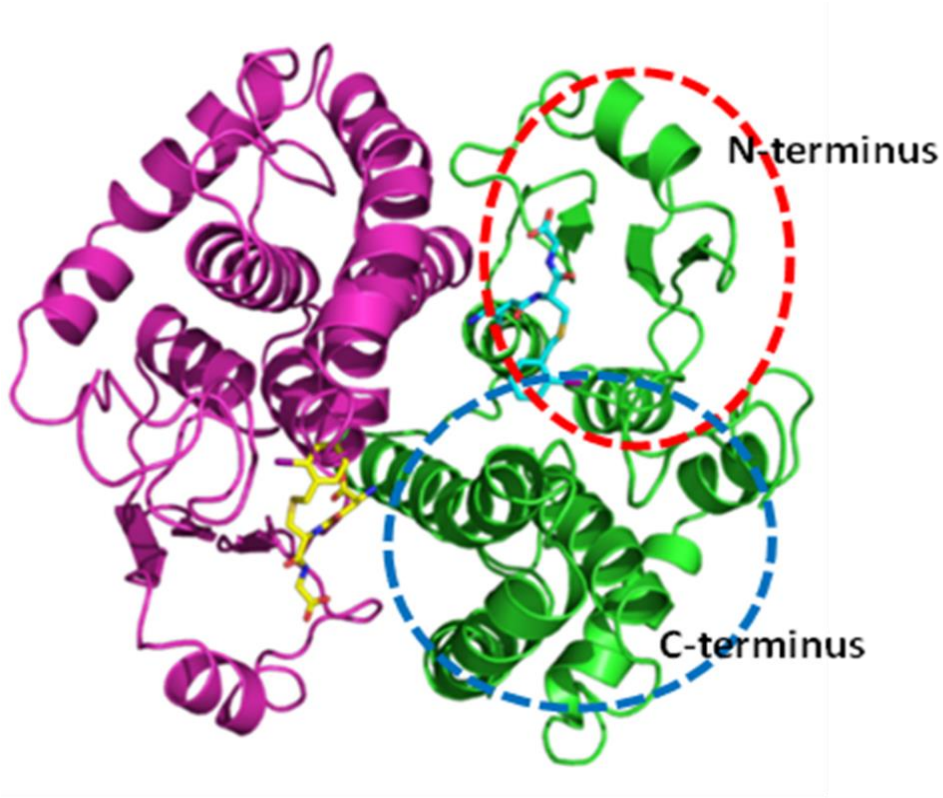


Figure 2.6 Cartoon Ribbon representation of SjGST. The quaternary structure of SjGST showing the active sites in yellow and cyan coloured rings on both units. The N and C terminus domains are indicated by red and blue circles respectively. Image is generated with PyMol PDB ID: 08515.

2.8 Ellagic Acid

Ellagic acid (EA) is an effective antioxidant found in organic sources with various nutritional advantages (Murugan *et al.*, 2009). EA is a bioactive polyphenolic substance ubiquitous in some nuts, fruits, and seeds like the pecans, pomegranates, cranberries, blackberries, raspberries, strawberries, almonds and walnuts (Landete, 2011). Phenolic compounds are modulators of numerous biological macromolecules and are classified into various groups based on their basic structure. The number of aromatic rings connected by structural moieties forms the bases that differentiates each group. Phenols have one or more aromatic rings with one hydroxyl group while polyphenols have more than one. EA is a planar molecule with four hydroxyl groups and two lactone groups (Figure 2.7).

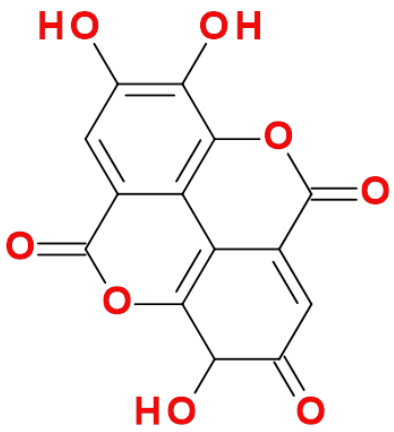


Figure 2.7 Structure of Ellagic acid

EA is a thermodynamically stable molecule and the four phenolic groups donates hydrogen bonds while lactone groups on EA (hydrophilic part) are the hydrogen bond acceptors (Bala *et al.*, 2006). Binding of EA to proteins seems to be irreversible, as no previous studies have made any contrary report (Walle *et al.*, 2003; Whitley *et al.*, 2003). The biological actions of polyphenols are highly dependent on their structure and concentration (Labieniec and Gabryelak, 2006). They have been shown to possess an extensive variety of biological actions and health functions, which include: anti-inflammatory properties, anticancer, antibiotic, antimalarial, anticancer, cardio-protective, analgesic, and antimicrobial proper. The antioxidant property of EA is induced by the aromatic conjugated –OH groups (Adedapo *et al.*,

2015; Barch *et al.*, 1996b; Galano *et al.*, 2014). Heur *et al* has been able to synthesise some analogues of EA (Flavellagic acid (3,4,5,3',4' -hydroxyl); 4,4'-hydroxl; 3,3'-hydroxyl and No-OH (benzopyrano[5,4,3-*c*,*d*,*e*][1]benzopyran-6,6'-dione)) (Heur *et al.*, 1992). EA is a tannin which results from the hydrolysis of ellagitannins using acids or bases, yielding hexahydroxydiphenic acid (HHDP). HHDP then undergoes a spontaneous reaction and lactonizes to EA (Landete, 2011).

According to a study carried out by (Hayeshi *et al.*, 2007), it was discovered that EA has the ability to inhibit the human GSTs (GST A1-1, A2-2, M1-1, M2-2, and GST P1-1) *in vitro*. Various studies proposed that EA counters the adverse effect of ROS produced during cellular metabolism in response to chemical and oxidative stress. Similarly, EA assists in antioxidant regeneration (GSH), inhibits carcinogen activation facilitated by phase-I enzymes, and stimulates apoptotic pathways causing the decrease of cancer and other chronic diseases (Khanduja *et al.*, 1999; Loarca-Piña *et al.*, 1998). EA also obstructs the tautomerase activity of human macrophage migration inhibitory factor (MIF) and proinflammatory reactions in peripheral blood mononuclear cells mediated by MIF (Sarkar *et al.*, 2015). Majid et al. also showed that there was an increased level of GSH and glutathione reductase in the liver of mice when fed with EA (Sabhiya Majid *et al.*, 1991). Additionally, EA in complex with tetracycline has been deduced to inhibit the formation of biofilm by reducing the production of extracellular polymeric substances with its associated virulence (Sivasankar *et al.*, 2016).

2.9 Computational chemistry

The calculation of molecular and atomic chemical properties obtained after the simulation of chemical events can be performed using computerised Newtonian law algorithms (Palermo and Vivo, 2015). Currently, molecular modelling and simulations are used for the effective study and dissection of complex events implicated in regulating proteins of pharmaceutical importance, such as metalloenzymes and membrane proteins (Martín-Santamaría, 2017). Molecular docking and virtual screening are regularly used *in silico* for drug discovery. They are computational strategies which considers structural flexibility and produces useful information to assist in the design of potent inhibitors (Martín-Santamaría, 2017). This aspect of chemistry facilitates rapid and cost effective possibilities for the design and discovery of new drug candidates, consequently optimising the whole drug design procedures within a short timeline (Jorgensen, 2004).

Docking protocols utilise the search strategy and scoring function. The search algorithm reveals the binding modes between the ligand and the protein by exploring the degrees of rotational and translational freedom together with the internal conformational degrees of freedom of the ligand and protein (Taylor *et al.*, 2002). The scoring function grades each conformation according to their efficiency and accuracy. It also distinguishes the experimental binding modes from other modes investigated by the search algorithm (Taylor *et al.*, 2002). Scoring methods involves molecular mechanics force field such as AMBER, OPLS or CHARM, and also empirical free energy scoring functions (Cornell *et al.*, 1995).

Crystal structure of protein-ligand complex make available data on the positions, interactions and possible interactions between the ligand and protein (Whittle and Blundell, 1994). Comparing the ligand binding mode predicted by docking with the crystal structure validates the accuracy of the docking. A threshold of 1.0 - 3.0 Å Root Mean Square Deviation (RMSD) between the x-ray pose and docked pose is mostly accepted as a successfully docked structure (Halperin *et al.*, 2002).

In addition, the essentials of molecular mechanics (MM) formed the basis of computational chemistry. Larger molecules are not always effectively estimated by semi-empirical treatments, hence, the inefficiency in acquiring some parameters from empirical data (Young, 2001). The molecules can be modelled using MM without using quantum mechanics (QM). Harmonic oscillator equation obtained using MM determines the total energy of a molecule, excluding the total electron density. The algebraic equation below (eqn.2.1) defines the energy associated with intermolecular forces (Van der Waals and hydrogen bonding), bond rotation, bending and stretching. One of the benefits of MM is modelling of large molecules such as proteins and DNA, which forms the foundation of computational biochemistry (Young, 2001).

$$\cup = \sum bonds\ E_{bend} + \sum angles\ E_{strech} + \sum dihedral\ E_{torion} + \sum pairs\ E_{non-bonded}$$

$Eqn.\ 2.1$

Force fields are used to predict energy associated with atoms coordinates in a system. Examples of force fields are GROMOS™, CHARMm (Chemistry at Harvard Macromolecular Mechanics), AMBER (Assisted Model Building with Energy Refinement), and OPLS (Optimised Potentials for Liquid Simulations) (Hu *et al.*, 2003). Force field parameters which

include: X-ray diffraction, NMR and neutron spectroscopy are obtained from experimental data (Eqn.2.2). For the purpose of this study, CHARMm and OPLS 2005 force fields was used.

$$E_{total} = \sum_{bonds}\left(r - r_{eq}\right)^2 + \sum_{angles} K\theta\left(\theta - \theta_{eq}\right)^2 + \sum_{adihedrals} \frac{V_n}{2}\left[1 + \cos n\emptyset - \gamma\right] + \sum^{LJ} i \sum i < j 4\varepsilon ij\left[\left(\frac{\sigma_{ij}}{r_{ij}}\right)^{12} - \left(\frac{\sigma_{ij}}{r_{ij}}\right)^{6}\right] + \sum_{i}^{Elec} \sum_{i<j} \frac{qiqj}{4\pi\varepsilon r_{ij}}$$

Eqn.2.2

Chapter 3

Materials, Methodology and Methods

3.1 Materials

Table 3.1 below shows the non-standard chemicals used in this study. All the other reagents used were of analytical grade.

Table 3.1: Non-standard materials and suppliers

Materials	Source	Location
PGEX-4T-1 expression vector	GE Healthcare®	Buckinghamshire, UK
GeneJET™ Plasmid miniprep kit	Fermentas®	Ontario, Canada
SDS-PAGE molecular weight markers	Fermentas®	Ontario, Canada
Isopropyl β-D-1-thiogalactopyranoside	Sigma-Aldrich®	St. Louis, MO, USA
Ellagic acid	Sigma-Aldrich®	St. Louis, MO, USA
Coomassie Brilliant Blue G250	Sigma-Aldrich®	St. Louis, MO, USA
Dithiothreitol (DTT)	Melford Laboratories Ltd.	Suffolk, UK
T7 Express Competent Cells	New England Biolabs	Ipswich, MA, USA
8 Anilino-1-naphthalenesulfonic acid (ANS)	Sigma-Aldrich®	St. Louise, MO, USA
Reduced L-glutathione (GSH)	Sigma-Aldrich®	St. Louis, MO, USA
1-Chloro-2,4-dinitrobenzene (CDNB)	Sigma-Aldrich ®	St. Louis, MO, USA
Yarra™ 3u SEC-2000, LC Column	Phenomenex	Torrance, CA, USA
Gel filtration standards	Bio-Rad®	California USA
Ampicillin and Chloramphenicol)	Roche Diagnostics	Manheim Germany

3.2 Methodology and Methods

3.2.1 pGEX-4T-1 GST expression vector isolation and purification

The GST Gene Fusion System is a multipurpose system for the expression, purification, and detection of GST-tagged proteins produced in *Escherichia coli (E. coli)*. The system is made up of three vital parts, which are, pGEX vectors, products for GST purification, and GST detection products. The pGEX vectors have been developed for inducible, optimal intracellular expression of genes as fusions with *Schistosoma japonicum* GST. Protein of interest is generated at the carboxyl terminus, and the GST moiety at the amino terminus when expressed in *E. coli*. The pGEX-4T-1 (Figure 3.1) is a bacteria expression vector with a T7 tac promoter

is derived from pGEX-2T, and it encodes for ampicillin resistance. Other features of pGEX-4T-1 include internal *laclq* gene, PreScission™ Protease, thrombin sites and mild elution conditions of the fusion proteins to reduce impact on their functional activity (Yourgenome, 2016).

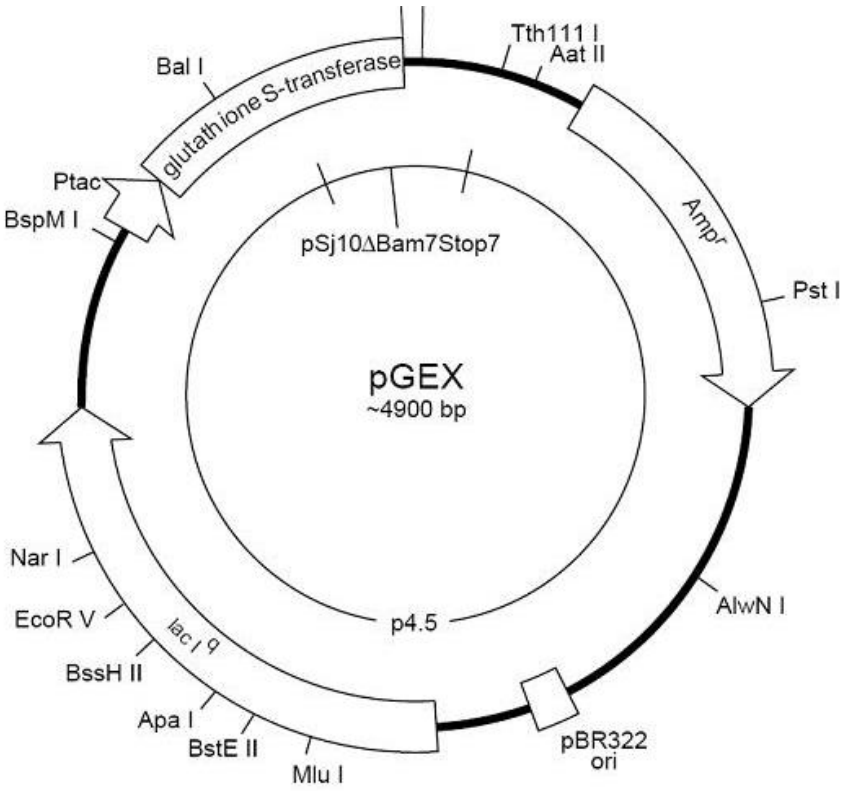


Figure 3.1 Map of pGEX-4T-1 vector. The map indicates restriction sites, the GST fusion gene (Bal l) and important sites of the vector including origin of replication (ori), multiple cloning sites and the ampicillin resistance gene.

The plasmid was extracted using the GeneJet™ Plasmid miniprep kit, which uses a unique silica-based membrane technology of a suitable spin column to prepare a premium plasmid DNA from recombinant *E. coli* cultures. The pGEX-4T-1 JM109 *E. coli* cell glycerol stock was generously provided by Dr Ikechukwu Achilonu. Lysogeny broth (LB) medium (10 mL) supplemented with 100 µg.mL^{-1} of ampicillin was inoculated with 5 µL of pGEX-4T-1 JM109 *E. coli* cell stock, and was incubated overnight (15 h) at 37℃ while shaking at 250 rpm. The bacteria culture was harvested by centrifugation at 6800×*g* using a microcentrifuge for 2 min at room temperature. The supernatant was decanted and the cells resuspended completely with 250 µL of the resuspension solution using a pipette. The resuspended cells were exposed to SDS alkaline lysis to liberate the plasmid DNA by adding 250 µL of the lysis solution containing SDS and NaOH, it was mixed thoroughly by gently inverting the tube to avoid

shearing of the genomic DNA. Neutralising solution (350 µL) containing sodium acetate, was added and thoroughly mixed by inverting the tube 4-6 times to precipitate larger genomic DNA and proteins. The observed turbid appearance indicates that the lysate has been neutralised, it was then centrifuged for 5 min at 6800×*g* to pellet the chromosomal DNA and bacteria cell debris. The supernatant was transferred carefully to a GeneJET™ spin column containing a silica-based membrane, without disturbing the white pellet (g DNA) and was centrifuged for 1 min at 6800×*g*. The flow-through was discarded and the adsorbed plasmid DNA was washed twice with 500 µL of the wash solution to remove contaminants by centrifuging for 1 min at 6800×*g*. The flow-through was discarded and centrifugation was repeated for 1 min to ensure that all the wash solution and ethanol were removed. The GeneJET™ spin column was placed into an Eppendorf tube, then 50 µL of the elution buffer (10 mM Tris-HCl, pH 8.5) was added to the centre of the column membrane and the vector was eluted. The eluted vector was incubated at room temperature and centrifuged for 2 min, the column was discarded, and the purified plasmid DNA was quantified using NanoDrop™ spectrophotometer and was stored at -20℃.

3.2.2 Transformation of *E. coli* T7 Express with pGEX-4T-1

Escherichia coli (E. coli) are obligate Gram-negative bacteria which have been the most popular means of recombinant protein production for decades. It proffers easy genetic manipulations, grows rapidly in a short time and low-cost media. A one-step heat shock method (Chung *et al.*, 1989), which makes *E. coli* cell membranes more permeable to external DNA was used to transform T7 Express Competent *E. coli* cells. The vector (2 µL) was incubated in 100 µL of T7 Express Competent *E. coli* cells for 30 minutes on ice, followed by a heat shock on a heating block at 42℃ for 50 seconds, and was placed back on ice for 10 min. Thereafter, 900 µL of SOC media (Super Optimal broth with Catabolite repression, made up of 2% (w/v) tryptone, 0.5% (w/v) yeast, 10 mM NaCl, 2.5 mM KCl, 10 mM $MgCl_2$, and 20 mM glucose) was added to the cells, and incubated at 37℃ for 1 h placed on a shaker (250 rpm). The cells were centrifuged at 6800×*g* for 1 min, 900 µL was decanted and the remaining was resuspended. The transformed bacteria cells (5 µL) were plated on 10 mL of LB agar [1% tryptone. 0.5% yeast and 0.5% NaCl] supplemented with ampicillin (100 $\mu g.mL^{-1}$) and chloramphenicol (34 $\mu g.mL^{-1}$), then incubated overnight at 37℃.

A single colony was selected from the plate and 50 mL of 2×YT media [1.6% (w/v) tryptone, 1.0% (w/v) yeast extract, 0.5% (w/v) NaCl] supplemented with ampicillin and chloramphenicol

34 μg.mL^{-1} each was inoculated. The bacteria culture was incubated at 37℃ overnight (12-16 h), shaking at 250 rpm.

3.2.3 Overexpression of recombinant SjGST

All subsequent inoculations and growths were performed in the presence of 100 μg.mL^{-1} ampicillin and 80 μg.mL^{-1} chloramphenicol, to create an environment that was favourable to only the cells of interest. Erlenmeyer flasks five times greater in volume of the culture was used to guarantee sufficient aeration during growth. Induction studies was performed to optimise IPTG concentration appropriate for over-expression. Cells from the overnight culture (2 mL) were incubated in 100 mL each of 2×YT media at 37℃, 200 rpm. Different IPTG concentrations of 0.25, 0.50, 1.00 mM each, was added to the cultures towards the beginning of their late-log phase (OD_{600} ~ 0.6) to induce optimal expression of SjGST plasmid. One of the cultures was left uninduced as the control sample. Cold induction was performed by chilling the cell cultures on ice for about 10 min before IPTG induction. The cells were further incubated at 30℃ for 6 h, while shaking at 200 rpm. Cells were harvested by centrifugation (5000×*g*, 5℃, 20 min). The supernatant was discarded, and the cell pellets resuspended with equilibration buffer [50 mM Tris-HCl, 150 mM NaCl, 10% (v/v) glycerol, 0.02% (w/v) NaN_3, pH 7.4] and stored at -20℃. The cells were subsequently thawed at 4℃, sonicated and then centrifuged at 23000×*g* 4℃ for 30 min. Samples of the pellets and supernatant were analysed with SDS-PAGE as described in section 3.2.5 to assess the optimal IPTG concentration required for SjGST over-expression. Subsequent SjGST over-expression, were performed using the procedure described above with 0.50 Mm final concentration of IPTG.

3.2.4 Protein purification

GSH-Agarose affinity chromatography was used to purify SjGST. This method enables for fast, mild, non-denaturing and highly selective purification of proteins containing glutathione binding sites. Glutathione-Agarose resin is made up of cross-linked agarose beads with glutathione covalently-bound to the resin at the SH moiety. GSTs have high affinity to the linked glutathione in the column. This resin performs efficiently with both small and large proteins tagged with GST in batch or column purifications. It also allows one step purification of proteins in their native conditions.

The GSH-Agarose column (20 mL) attached to Äkta FPLC (fast protein liquid chromatography) purification system was cleansed with five column volumes of 0.1 M borate buffer pH 8.5, and rinsed with equal volume of deionised water (ddH_2O). It was washed a second time with 0.1 M acetate buffer (pH 4.5) and rinsed with ddH_2O (five column volumes each), these washing steps assists to regenerate the column. The column was subsequently equilibrated using the equilibration buffer [50 mM Tris-HCl, 150 mM NaCl, 10% (v/v) glycerol, 0.02% (w/v) NaN_3, pH 7.4] (10 column volumes).

The frozen cells obtained after over-expression were thawed at 20℃ and 10 $\mu g.mL^{-1}$ of lysozyme was added and incubated at 20℃ for 30 min on a rotator. The cells were sonicated on ice using Sonicator Ultrasonic Processor (six cycles of 20 sec ON/OFF pulses, 15 amplitude) to enhance cell lysis. The debris was separated from the soluble cell fraction by centrifugation at 5000×*g*, 4℃for 20 minutes. The soluble cell fractions obtained was filter with 0.2 µm syringe filter to avoid clogging the column and was then loaded unto to the column. The column was washed with 10 column volume of equilibration buffer to wash off contaminants loosely bound to the resin. This was followed by a second wash with addition of 1% (v/v) Triton X-100 to the equilibration buffer (five column volumes), and then the resin was rinsed with 10 column volumes of the equilibration buffer. A one step elution was performed using the elution buffer [10 mM glycine, 0.02% (w/v) NaN_3 pH 10], the eluents were collected in fractions of 5 mL each using falcon tubes and the pH adjust to ~7.4 by adding 1 M Sodium phosphate pH 7.5 at 25% (v/v). The fractions were assessed for purity using discontinuous SDS-PAGE.

3.2.5 Sodium dodecyl sulfate polyacrylamide gel electrophoresis (SDS-PAGE)

Sodium dodecyl sulfate polyacrylamide gel electrophoresis (SDS-PAGE) is an analytical procedure that allows the separation of proteins or other molecules based on electrophoretic mobility. The migration of protein molecules depends on the size of the protein when exposed to an electric filed on polyacrylamide gel (Laemmli, 1970). SDS is an anionic detergent; it unfolds the protein and changes its native conformation by breaking the non-covalent bonds, hence the electrophoretic mobility of the protein molecules becomes a function of the size. The shorter polypeptide chains will migrate further through the gel than longer ones (Maurer, 1971). This technique was used to determine the homogeneity, identity and purity of the protein which is inferred by the appearance of a single band on the gel lane and the size calculated based on the distance migrated alongside a lane of protein standards of known size.

Reducing SDS-PAGE was performed as described by LaemmLi (1970) using PowerPac™ Basic Bio-Rad electrophoresis system and accessory unit. The unit is comprised of a gel-casting stand, casting gaskets, ten-well gel combs (1.5 mm thick), and 81.5 mm × 101.5 mm and 72.5 mm × 101.5 mm glass plates. The gel casting unit was assembled and running gel solution [12% (w/v) acrylamide, 1.35% (w/v) bisacrylamide, 1% (w/v) separating gel buffer [1.5 M Tris-HCl, pH 8.8] (3×), 0.3% (v/v) glycerol, 1.5% (w/v) ammonium persulfate, 0.005% (w/v) N,N,N´,N´-tetramethylenediamine (TEMED)] was applied in-between the glass plates and was overlaid with water to prevent inhibition of acrylamide polymerisation. When the mixture polymerised, the stacking gel solution [4% (w/v) acrylamide, 1.36% (w/v) bisacrylamide, 0.3% stacking gel buffer [500 mM Tris-HCl, pH6.8] (×3), 0.009% (w/v) ammonium persulfate, 0.005% (w/v) TEMED] was applied to the brim of the glass plates. The gel comb was inserted, and the mixture was allowed to polymerise. Protein samples (10 µL) were prepared in two-fold dilution by mixing with the reducing sample buffer [2% SDS (w/v), 5% β-mercaptoethanol (v/v), 20% glycerol (v/v), 0.05% (w/v) bromophenol blue and 125 mM Tris-HCl pH 6.8], and was warmed in hot water bath for 5 min to ensure that the protein is properly denatured. 10 µL of the samples were loaded on the gel wells, the first well was loaded with 10 µL of unstained Precision Plus Protein™ standards from Bio-Rad (California U.S.A). The unit was connected to the power pack and electrophoresis was performed at 120 volts till the gel front was about 0.5 cm to the bottom. The gel was stained with the staining solution [0.1 % (w/v) Coomassie Brilliant Blue R-250 dye in 1:5:4 (v/v/v) acetic acid-methanol-water solution] and was destained in [1: 5: 4 acetic acid: methanol: water] solution. The electrophoretogram was analysed with the Bio-Rad Gel Doc™ XR+ system and the molecular mass was obtained by plotting a graph of the log molecular weight of the standards against the distance migrated by the protein bands in the gel.

3.2.6 Quantification and qualitative analysis

This analytical procedure is based on the amount of light absorbed or transmitted when the light is passed through a sample. Ultraviolet (UV) and visible spectroscopy was used in determining the concentration of the protein sample, applying extinction coefficient method. Tryptophan and tyrosine exhibits more absorbance at 280 nm while phenylalanine contributes slightly. Absorbance increases as path length increases. Beer-Lambert law describes the relationship between absorbance and concentration and absorbance and path length

$$\boldsymbol{A} = \mathcal{E}\boldsymbol{\ell}\square \qquad (Eqn.\,3.1)$$

$$\boldsymbol{C} = \frac{\boldsymbol{A}}{\varepsilon \boldsymbol{\ell}} \qquad (Eqn.\ 3.2)$$

Where:

- $\boldsymbol{A}$ is Absorbance (a dimensionless number)
- $\boldsymbol{\mathcal{E}}$ is the proportionality constant called the molar extinction coefficient or molar absorptivity ($M^{-1}cm^{-1}$) at 280 nm measured in water. It is 42860 (per-monomer) and was determined using Expasy tool Protoparam algorithm (Gasteiger E. *et al.*, 2005)
- $\boldsymbol{\ell}$ is the path length (1 cm)
- C is concentration (M)

The quantification of the purified recombinant SjGST was performed by doubling dilution series and analysed using Jasco V-630 spectrophotometer (Jasco Inc., Tokyo Japan), monitoring absorbance at two different wavelengths ($A_{280\ nm}$ and $A_{340\ nm}$). A calibration plot of corrected absorbance versus dilution factor was used to obtain a gradient which was applied in the equation below (Eqn. 2.3) to calculate SjGST concentration.

$$conc\ mg/ml = \frac{slope \times Molecular\ mass}{\varepsilon \times path\ lenght\ (cm)} \qquad (Eqn.\ 3.3)$$

A ratio of absorbance at 280 nm to absorbance at 260 nm was established. The proportion of protein present relative to the amount of DNA was analysed by monitoring the absorbance ratio between 280 and 260 nm. Absorbance at 340 nm for each dilution was also monitored to check for protein aggregation.

3.2.7 Structural Characterisation

3.2.7.1 Secondary structure characterisation

Circular dichroism (CD) was used to analyse the secondary structure content of SjGST. The technique provides extensive study of large biological molecules. Chromophores in protein polypeptides are chiral in nature and hence absorb left and right circularly polarised light at different degrees and wavelengths (Greenfield, 2006). Information about secondary structural components of the protein namely the α-helices and β-sheets was deduced from the data obtained, and this is dependent on the characteristics of the protein under evaluation.

Circular dichroism could be carried out in the far-UV CD region or near-UV CD region; far-UV-CD analysis was used in this experiment. The region of far-UV CD is 180-240 nm wavelengths; this is the wavelength at which the secondary structure is analysed owing to the

fact that circularly polarised light is absorbed by the protein peptide backbones (tryptophan and tyrosine) at this region. Protein molecules which consists mainly of α-helices absorb right circular polarised light at 208 nm and 222 nm in a negative ellipticity and positive ellipticity at 190 nm, β-sheets conformation proteins absorb right polarised light at 218 nm in negative ellipticity and 195 nm positive ellipticity.

The far-UV CD spectra measurement of SjGST was obtained on Jasco J-810 spectropolarimeter with Spectra Manager software v1.5.00 (Jasco Inc., Tokyo, Japan) at 20℃, and wavelength range of 180-250 nm. The protein was dialysed in a GST storage buffer [5 mM sodium phosphate, 1 mM EDTA, 0.02% (w/v) NaN_3, pH 7.4] with a reduction in the concentration of sodium phosphate to reduce signal to noise ratio. 2 µL of SjGST samples were analysed in the absence and presence of EA [10 µM]. All spectra were recorded at scan speed of 200 $mm.min^{-1}$, data pitch of 0.2 nm, band width of 0.5 nm and 1 sec response time, using a 2 mm pathlength quartz cuvette. The spectra were obtained in average of 5 accumulations and were all buffer corrected. Mean residue ellipticity $[\Theta]$ ($deg.cm^2.dmol^{-1}$) calculation was applied to normalise the spectra using the formula below:

$$[\Theta] = \frac{100 \times \theta}{cnl} \qquad (Eqn. 3.4)$$

Where,

- Θ is the measured ellipticity signal in mdeg.
- c is protein concentration in mM.
- n is total number of residues in protein chain.
- l is the path length in cm.

The raw data obtained was submitted to Dichroweb algorithm server to analyse the percentage of the secondary structural components of SjGST (Whitmore and Wallace, 2008).

3.2.7.2 Tertiary structure characterisation

Intrinsic tryptophan fluorescence spectroscopy

Absorption of electromagnetic radiation transfers energy to molecules, which results in an excitation state (higher energy). A portion of the energy absorbed is re-emitted as light; the emitted light is usually of a longer wavelength (lower energy) than that of the excitation state. Fluorescence spectroscopy is a technique used in measuring the radiation energy emitted. The difference between excitation and emission is called the Stoke's shift and can be explained as the loss of energy due to vibrational relaxation (Head-Gordon and Head-Gordon, 1994). This technique is usually accurate at lower concentration of protein sample because fluorescence intensity increases as sample concentration increases. The excitation wavelength of tryptophan (Trp) indole group which is highly sensitive to polar environment is usually 295 nm and the emission is between 300 and 350 nm. In tryptophans, stoke shifts usually occurs, which implies that the emission wavelength is dependent on the tryptophan environment to a large extent; it can be affected by exposure to hydrophilic environment. When the tryptophans are buried (hydrophobic environment) they exhibit high quantum yield, hence high fluorescence intensity occurs. The three-dimensional structure of SjGST was characterised by this technique. The profile of the spectrum depends on the polarity of the tryptophans. SjGST contains four tryptophan residues on each subunit on the N-terminus domain as shown in (Figure 3.2).

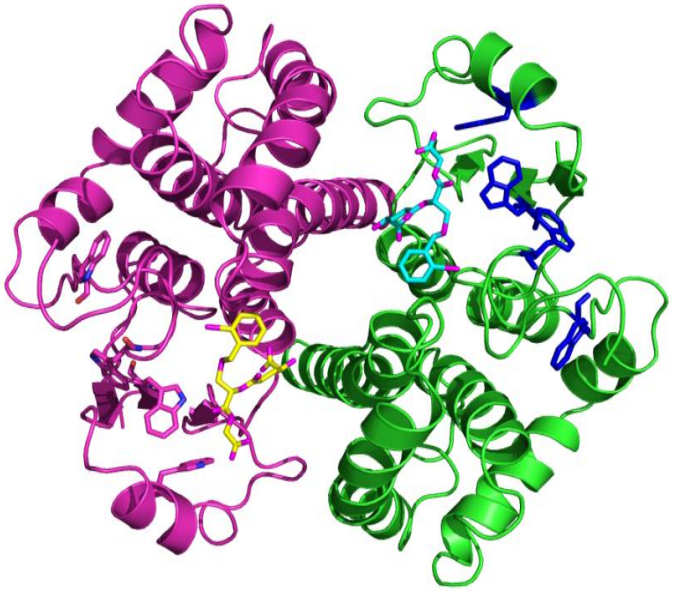


Figure 3.2 A ribbon representation of SjGST structure showing the positions of the tryptophans indicated in blue and magenta rings (PDB ID: 08515).

The fluorescence spectra of SjGST were obtained using Jasco FP-6300 with Spectra Manager software v1.5.00 (Jasco Inc., Tokyo, Japan) at 20℃, and 10 mm path length quartz cuvette. Fluorescence emission spectra of 2 µL SjGST in 20 mM sodium phosphate, 1 mM EDTA, 0.02% (w/v) NaN_3, pH 7.4, was recorded in triplicate and average of three accumulations. To probe the effect of EA on SjGST, 10 µM of EA was incubated with 2 µM SjGST for 30 min and the fluorescence emission spectra recorded afterwards. Emission spectra were obtained using excitation wavelength at 295 nm, 200 $nm.min^{-1}$ scan speeds, slit widths of 5 nm (excitation) and 2.5 nm (emission). Florescence emission was collected between 280 nm and 500 nm (to show Rayleigh scatter) and all spectra were also buffer corrected.

Extrinsic ANS-fluorescence spectroscopy and ANS binding studies

Extrinsic ANS-fluorescence spectroscopy was used to probe ANS-accessible hydrophobic binding cavities in SjGST. The fluorescence dye 8-anilino-1-naphthalene sulfonic acid (ANS) is an extrinsic fluorescent dye applied in various aspect of protein analysis, such as the characterisation of protein folding intermediates, measuring surface hydrophobicity and detecting aggregation or fibrillation (Hawe *et al.*, 2008). ANS has low fluorescence intensity in polar environment, but upon interacting with proteins the intensity is increased. Electrons of the dye molecules are excited by absorbing light and they move from the ground state to higher state (excited state). Processes such as vibrational relaxation and/or internal conversion, solvent relaxation, and twisted intra-molecular charge transfer usually compete with fluorescence; this may result to energy loss and thus a red shift of fluorescence emission due to absorption (Stokes shift). The change in polarity will increase the intensity and quantum yield ($\Delta\Phi$), resulting to a blue shift between 500 nm and 480 nm wavelengths.

ANS (10 mM) stock solutions were prepared using 20 mM sodium phosphate, 1 mM EDTA, 0.02% (w/v) NaN_3, pH 7.4, and the concentration was measured spectroscopically by monitoring its absorbance at 340 nm. An extinction coefficient (ε) of 5000 $M^{-1}cm^{-1}$ (Gregorio Weber and Young, 1964) at 350 nm, was used to calculate the concentration. The solution was wrapped in a foil paper to prevent photodecomposition, and it was stored at 4℃.

SjGST samples (2 µM) were incubated with freshly prepared 100 µM of ANS in 20 mM sodium phosphate, 1 mM EDTA, 0.02% (w/v) NaN_3, pH 7.4, for 1 h in the dark to enhance proper binding of ANS to SjGST. Blank samples containing only ANS were also prepared. All the

samples were analysed using Jasco FP-6300 fluorimeter with excitation at 390 nm, 20 ℃, with 5 nm slit widths, and emission was monitored between 400-600 nm wavelengths at a scan speed of 200 nm.min^{-1}. The spectra of free ANS was subtracted from ANS bound SjGST spectra in the presence and absence of EA.

Kinetic analysis of ANS binding were performed with increasing concentrations of ANS (0-100 μM) titrated against 2 μM of SjGST in the absence and presence of EA (100 μM) in 20 mM sodium phosphate, 1 mM EDTA, 0.02% (w/v) NaN_3, pH 7.4. The ANS was incubated for 1 h before adding EA, and the mixture was incubated for 30 min. Fluorescence emission was monitored at 492 nm upon excitation at 390 nm, also the fluorescence intensity at 492 nm for free ANS was subtracted from that of the corresponding intensity of ANS bound to SjGST. The data obtained was fitted using Sigma plot v 13.0. Single site ligand-binding equation shown below was applied.

$$F_{cor} = \frac{F_{max}\,[ANS]}{k_d\ + [ANS]} \qquad (Eqn\ 3.5)$$

Where F_{cor} is the corrected fluorescence, F_{max} is the maximum fluorescence and k_d is the dissociation constant.

For ANS displacement studies, 2 μM of SjGST was incubated with a freshly prepared ANS (100 μM) for 1 h at 20℃, this was followed by the titration of varying EA concentrations (0-100 μM). The fluorescence emission at 493 nm was collected and plotted against varying concentrations of EA. Spectra of ANS bound to SjGST in the presence of EA were corrected for background fluorescence by subtracting the corresponding ANS:EA spectra. All fluorescence emission spectra were collected in triplicate and three accumulations each.

3.2.7.3 Quaternary structure characterisation

Analytical size exclusion-high pressure liquid chromatography (SE-HPLC) is a technique which separates proteins based on hydrodynamic size, surface properties and diffusion coefficient. It is often preferred to size exclusion chromatography (SEC) due to its higher resolution and rapid molecule separation (Tayyab *et al.*, 1991). The diameter of the column (LC Phenomenex HPLC column) is 7.8 mm and a length of 300 mm filled with permeable silica beads arranged 3-dimensionally to retard the migration of the molecules through the

stationary phase of the column. Tiny sized protein molecules permeate through the pores in the beads and their movements becomes retarded, whereas the larger proteins migrate freely round the beads and elutes before the smaller molecules.

This technique was used to obtain the native size of SjGST at 20°C in 20 mM sodium phosphate, 500 mM NaCl, 2 mM DTT, 0.02% (w/v) NaN_3, pH 7.4, using Phenomenex Gel Filtration/Size Exclusion silica column, Yarra 3u SEC-2000 coupled to Phenomenex Security Guard ULTRA guard column. The column was connected to Shimadzu Prominence HPLC system (SPD20A), and was equilibrated using 20 mM Sodium phosphate, 500 mM NaCl, 2 mM DTT, 0.02% (w/v) NaN_3, pH 7.4 at 0.25 $mL.min^{-1}$ flow rate which was maintained for all sample analysis. Column calibration was performed using Bio-Rad Gel Filtration standards containing Bovine thyroglobulin (670 kDa), γ-globulin (154 kDa), Ovalbumin (44 kDa), Myoglobulin (17 kDa) and Vitamin B12 (1.35 kDa). 100 μM of SjGST was centrifuged and 20 μL was loaded on the column, then the protein was eluted using the column equilibration buffer. To ascertain the effect of EA on the native size of SjGST, 100 μM of SjGST was incubated with 10 μM of EA for 1 h, the mixture was loaded to the column which has been equilibrated with the equilibration buffer containing 10 μM EA. The SjGST bound EA was eluted with the same buffer.

The quaternary structure of SjGST both in the presence and absence of EA was determined using calibration curve of the gel filtration standards used to calibrate the column. All samples were analysed in triplicate.

3.2.8 Functional characterisation

3.2.8.1 GSH-CDNB conjugation assay

CDNB is a substrate with a wide range of ability to detect isozyme, it is also very easy to monitor the reaction progress (Habig *et al.*, 1974). CDNB conjugation with GSH proceeds through a nucleophile aromatic substitution of chlorine by the thiol group of GSH, producing a dinitrophenyl thioether and chloride ion (Figure 3.3). Formation of product (1- (*S*- glutathionyl)-2,4-dinitrobenzene) is followed by the appearance of an absorption band at 340 nm; this enables a spectrophotometric assay for GST activity. The presence of GST leads to a gradual increase of dinitrophenyl thioether chromophores. The reaction of CDNB and GSH is slow relative to the enzyme catalysed reaction. The activity of SjGST was assayed in the presence and absence of EA using GSH-CDNB conjugation assay.

The assayed samples were prepared by varying the concentration of SjGST in the absence and presence of 10 µM EA in 3 mL final volume containing 100 mM sodium phosphate, pH 6.5, 1 mM EDTA, 0.02% (w/v) NaN_3, 1 mM GSH and 1 mM CDNB. The rate of product formation was obtained by measuring change in absorbance using UV-visible light spectrophotometer (Jasco V-630, Jasco Inc., Tokyo Japan) and the progress of the reaction monitored at 20℃, 340 nm (ε = 9600 $M^{-1}.cm^{-1}$) for 60 s. All samples were analysed in triplicate and were also corrected for non-enzymatic reaction using the blank sample. The specific activity ($\mu mol.min^{-1}.mg^{-1}$) was obtained by plotting the slope of the initial velocity of complex formation against mass of SjGST (mg).

3.2.8.2 IC_{50} of Ellagic Acid

The half maximal inhibitory concentration (IC_{50}**)** evaluates or determines the potency of a substance in inhibiting a specific biochemical activity. It estimates the concentration of an inhibitor at which the response or its capacity to bind is reduced by 50% (Neubign, 2003). This quantitative technique stipulates the amount of a particular substance or inhibitor required to inhibit an enzyme activity by half.

The IC_{50} of Ellagic acid on SjGST was performed by monitoring the enzyme activity in the presence of varying concentrations of Ellagic acid using the GSH-CDNB conjugation assay as described in section 2.2.7.8. All samples were analysed in triplicate using 30 µM of SjGST incubated with varying concentrations of Ellagic acid for 1 h, and the progress curve monitored spectrophotometrically at 340 nm for 60 s. The progress curves were blank corrected and standard deviations were also calculated for each data point. The IC_{50} was obtained by plotting percentage activity values against the log inhibition concentration, and the data was fitted using the four-parameter logistic equation on Sigma plot v 13.0 shown below (Eqn. 2.6).

$$y = min + \frac{max - min}{1 + \left(\frac{x}{IC_{50}}\right)^{-Hillslope}} \qquad (Eqn.\ 2.6)$$

The four parameters include:

- Max – top of the curve
- Min – bottom of the curve
- X – IC_{50}
- Hillslope – Slope of the curve at its midpoint.

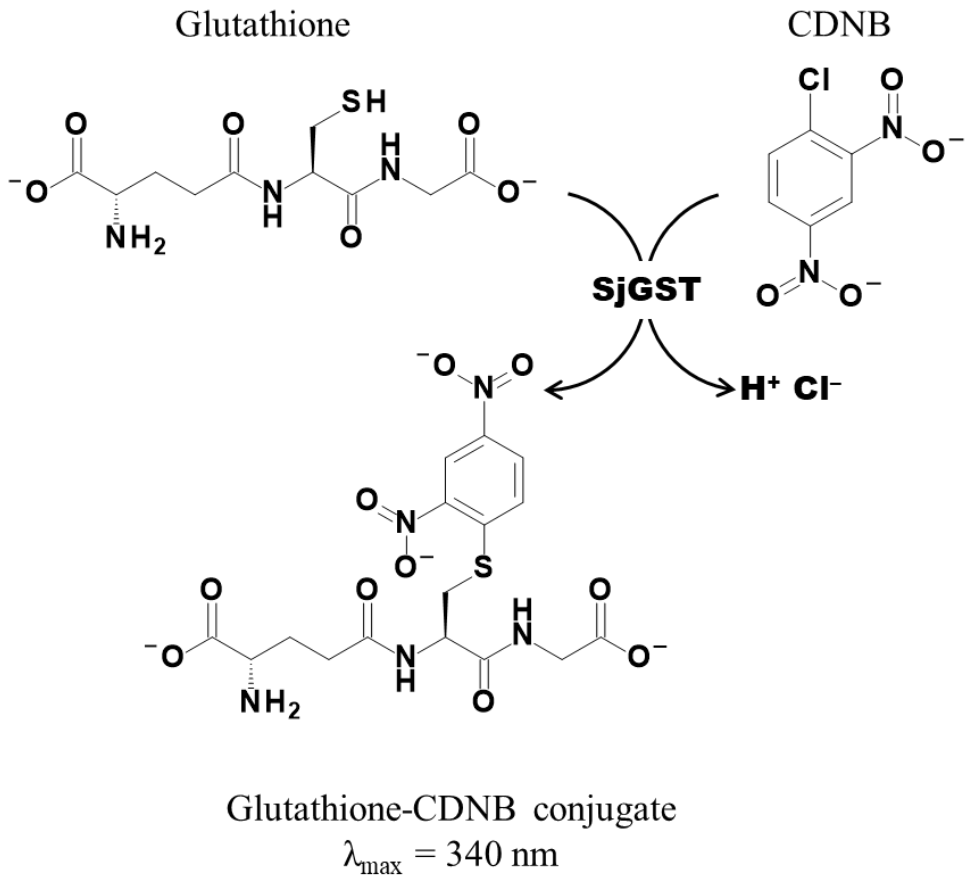


Figure 3.3 GSH-CDNB conjugation reaction. The reaction is catalysed by SjGST, Glutathione-CDNB conjugate and H^+ CL^- was released as products.

3.2.8.3 Kinetic analysis of SjGST

The mechanism of reactions catalysed by enzymes is usually calculated through kinetic measurements on enzyme substrate reaction systems; this includes evaluating rates of the enzyme catalysed reaction at different enzyme and substrate concentrations (Bowden, 1995). Enzymatic reactions are usually observed using spectrophotometer by monitoring the colour development over time, a spectroflourimeter could be used by applying a fluorescence probe.

The maximum velocity (V_{max}) is a kinetic parameter which indicates the maximum rate of reaction progress with an increasing concentration of a substrate using a constant concentration of enzyme. K_M is the concentration of substrate needed to produce a velocity that is one-half of V_{max}, when K_M value of an enzyme is small it means that the enzyme will achieve maximum catalytic efficiency at low substrate concentration. Therefore, the smaller the K_M value, the more efficient the enzyme.

The k_{cat} is the turnover number of the enzyme, which is the micromole of products made per minute per micromole of enzyme. The k_{cat} is the 1st order reaction rate constant for the conversion of the enzyme-substrate complex to product. The k_{cat}/K_M is the kinetic efficiency of the enzyme (specificity constant), it is the 2nd order rate constant for the reaction of an enzyme and a substrate to produce a product measured in $M^{-1}min^{-1}$. It enables the ranking of enzymes according to how efficient they are with different substrates.

Steady state kinetic measurements for SjGST were analysed using GSH-CDNB conjugation assay as described previously. The analysis was performed at 20℃ in 100 mM sodium phosphate pH 6.5, 1 mM EDTA, 0.02% (w/v) NaN_3, 1 mM GSH and 1 mM CDNB, using Jasco V-630 from Jasco Inc., Tokyo Japan. Total volume of each assay sample was 3 mL, all samples were analysed in triplicate and blank corrected. To obtain the apparent V_{max} and K_M, different concentrations of GSH (0-10 mM) and CDNB (0-1.50 mM) were used as the substrates. Samples were analysed both in the absence and presence of different concentrations of Ellagic acid [0.9, 2, 5 and 9 μM] in triplicate and the data points were fitted to Michaelis Menten single substrate model using Sigma plot v 13.0. The mode of inhibition was obtained using the Lineweaver-Burk plot. A double reciprocal plot of the inverse initial velocity as a function of inverse substrate concentration for both GSH and CDNB yielded a liner plot.

$$V = \frac{V_{max}[S]}{K_M + [S]} \qquad (Eqn.\ 3.7)$$

Taking the reciprocal of the Michaelis Menten equation above (Eqn. 2.7) gives equation 2.8

$$\frac{1}{V} = \frac{1}{V_{max}} + \frac{K_M}{V_{max}} \cdot \frac{1}{[S]} \qquad (Eqn.\ 3.8)$$

Where:

V = reaction velocity

K_M = Michaelis Menten constant

V_{max} = maximum velocity

$[S]$ = substrate concentration

The k_{cat} was obtained by varying the concentration of SjGST from 0-30 nM and keeping substrate (GSH) concentration constant at 1 M in the absence and presence of 10 μM of Ellagic

acid. The linear plot of velocity versus the enzyme concentration yielded the k_{cat} (sec^{-1}). The k_{cat}/K_M was obtained experimentally by varying the substrate (GSH) concentration, using concentrations far below the K_M value (0.00-0.04 mM) in the absence and presence of different Ellagic acid concentration (0.9, 2, 5 and 9 μM). A linear plot of the reaction velocity versus the substrate concentration was obtained. All data points are average of triplicate experiments and were blank corrected.

3.2.9 Isothermal titration calorimetry

The energetics of Ellagic acid binding to SjGST was measured by Isothermal titration calorimetry (ITC). This technique measures the binding affinity as well as the magnitude of the two parameters defining the binding affinity which is the enthalpy (ΔH) and entropy (ΔS) changes with high accuracy and precision. ITC mechanism involves measuring the binding interactions by detecting the absorbed or released heat during a binding reaction.

The binding interaction between SjGST and Ellagic acid was observed with the Nano ITC Standard Volume (TA Instruments, Delaware USA). Water-in-water titration was performed to equilibrate the machine. SjGST was thoroughly dialysed in 20 mM sodium phosphate, 2 mM TCEP-HCl, 1 mM EDTA, 0.02% (w/v) NaN_3, pH 7.4. The final dialysate was used to prepare 50 μM of SjGST and 2 mM Ellagic acid to ensure that both the ligand and protein has the same pH. The sample cell was loaded with 1000 μL of SjGST, the reference cell was filled with ddH_2O water, and 250 μL of the Ellagic acid (ligand) was loaded to the syringe. Ligand titration was performed automatically by the machine, injecting 5 μL of ligand every 300 seconds into the sample cell and the analysis was performed at 293.15 K. The amount of heat released by each injection decreases as the binding sites becomes saturated. A blank experiment was performed by titrating ligand (Ellagic acid) into buffer and the heat of dilution profile was subtracted from ligand into protein profile. The experiment was performed in triplicate. The thermodynamic parameters (ΔH, N, K_a) were obtained directly by integrating the area under each obtained peak with NanoAnalyze software, fitting the data with independent variable mode for non-linear least squares model for single site binding. ΔG and ΔS values were derived by applying the equation below (Eqn. 2.9).

$$\Delta G = \mathrm{RT}\ln\frac{1}{k_d} \qquad (Eqn.\,3.9)$$

$$\Delta G = \Delta H - \mathrm{T}\Delta S \qquad (Eqn.\,3.10)$$

Where R is the gas constant (8.3145 J/mol/K) and T is the absolute temperature in kelvin.

3.2.10 Molecular modelling

Molecular docking provides precise information about interactions between ligands (Ellagic acid) and the protein (SjGST) residues. The crystal structure of SjGST was obtained from the Protein Data Bank (PDB) with ID: 1DUG. Possible structural defects like missing loops and side chains were amended using the Protein Preparation Wizard (Madhavi Sastry *et al.*, 2013; Schrödinger, 2017b). The protein structure was also optimised (preparation and minimisation step) to reduce the energy level from that of a crystal structure to a level that can be observed in a solution. All water molecules with less three hydrogen bonds were removed. The ligand (Ellagic acid) was constructed using Maestro Elements 10.1 (Schrödinger, 2017a). Ligand preparation and energy minimization was also performed using a MacroModel algorithm (Schrödinger, 2017a) two minimization steps (500 cycles of steepest descend and 5000 cycles of conjugate gradient) were performed. The force fields were changed from OPLS-3 to OPLS-2005.

After preparation and minimization of both SjGST and Ellagic acid, molecular docking was performed using the Induce Fit™ docking algorithm (Farid *et al.*, 2006; Schrödinger, 2017a). This method uses OPLS 2005 force field and the protocol is initiated by docking ligands with Glide™ which produces multiple poses by using Van der Waals radii and an increased Coulomb-Van der Waals cut off. The docking of Ellagic acid to SjGST structure with minimal energy produces complexes ranked using the GlideScore™. Emodel energy (kcal/mol) enables the selection of best poses than GlideScore™ because it incorporates other force field components such as the electrostatic and Van der Waals energies (Shivakumar *et al.*, 2010). It also combines GlideScore™, ligand strain energy and ligand-receptor molecular mechanics interaction energy (Bottegoni *et al.*, 2008). Poses with higher binding affinity exhibits lower Emodel energy (kcal/mol).

Chapter 4

Results

4.1 Expression and purification of SjGST.

To express recombinant SjGST for this study, *E. coli* T7 Express® cells were transformed with pGEX-4T-1 vector containing a gene which encodes SjGST. Cells were induced to express for 6 h with varying concentrations of IPTG at 30℃ when the OD_{600} of the culture was 0.6. Figure 4.1 shows the electrophoretogram of the over-expression. The results show that 0.25 mM IPTG is required to over-express SjGST at 30℃. There is no observable difference in SjGST expression on the samples induced with IPTG as shown on lanes 2 - 4 (Figure 4.1). The percentage of SjGST relative to the protein fraction is 95%. There was no background expression in lane one which contains uninduced cell samples, this indicates that the promoter is tightly controlled. Lane 5 shows that SjGST was in the insoluble pellet, but at low amount (5%).

The soluble recombinant GST was purified using GSH-Agarose affinity chromatography, which allows for fast and non-denaturing purification of GST proteins. SjGST binds to the glutathione-agarose resins was eluted using 10 mM glycine. Non-specific proteins and DNA contaminants, which do not have affinity for GSH in the column as shown on peak 1 on the elution profile (Figure 4.2 A) increases the absorbance at 280 nm. Triton-X100 wash also triggered another increase in absorbance (peak 2) due to the presence of the phenyl group on Triton-X100 which absorbs strongly at 280 nm. A single step elution showing a symmetrical sharp peak (peak 3) was observed as recombinant SjGST eluted the column. Collected fractions were analysed for purity.

The purity and molecular mass of SjGST were analysed using 12% acrylamide SDS-PAGE. The obtained electrophoretogram indicates that the protein is pure, because the sample on lane 4 is a single band (Figure 4.2 B). Lane 1 represents the soluble cell fraction loaded into the GSH-Agarose column, while lane 2 is the flow-through, indicating that most of the soluble SjGST bound to the column. Lane 3 is sample from the Triton X-100 wash, no protein band is observed, indicating that no protein was lost during this wash step. The single band observed in lane 4 resolved at a relative molecular mass of approximately 25 kDa. This indicates that the

purified protein is SjGST, which is the protein of interest (SjGST). The distance migrated by the protein was compared to that of the known protein standards under similar conditions to calculate the protein's apparent monomeric mass as shown in Figure 4.2C. The calculated molecular mass is ~26 kDa, which corresponds to the expected theoretical size of 26 kDa (Figure 4.2C) (McTigue *et al.*, 1995).

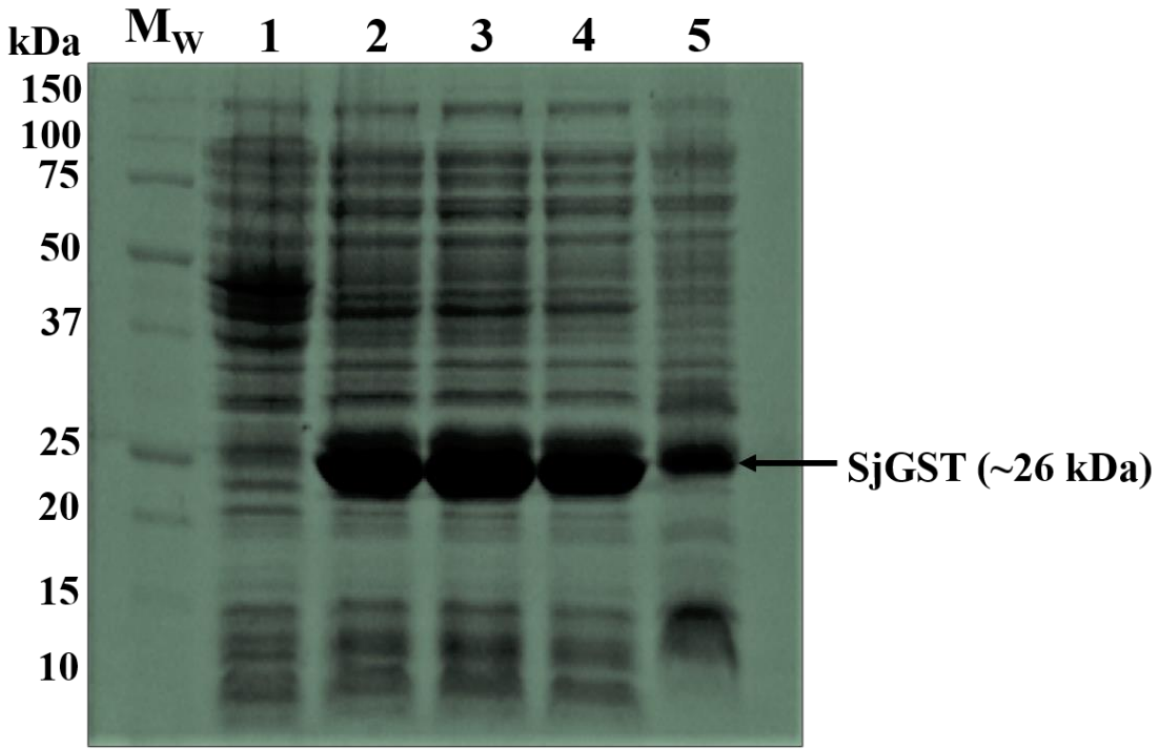


Figure 4.1 SDS-PAGE analysis of over-expression of SjGST in *E. coli*. T7 *E. coli* cells transformed with pGEX-4T-1 vector were induced (lanes 2 to 4), un-induced (lane 1) to express SjGST at 30℃ for 6 h. Cells were harvested and fractionated into soluble and insoluble cell fraction. Lane 1-4 contains soluble cell fractions of cells induced with 0 (un-induced), 0.25, 0.5 and 1 mM IPTG respectively. Lane 5 contains insoluble cell fraction from cells induced with 0.5 mM IPTG. All lanes contain approximately equal amount of cells. The over-expressed protein band resolved on the (12% acrylamide) gel at approximately 26 kDa

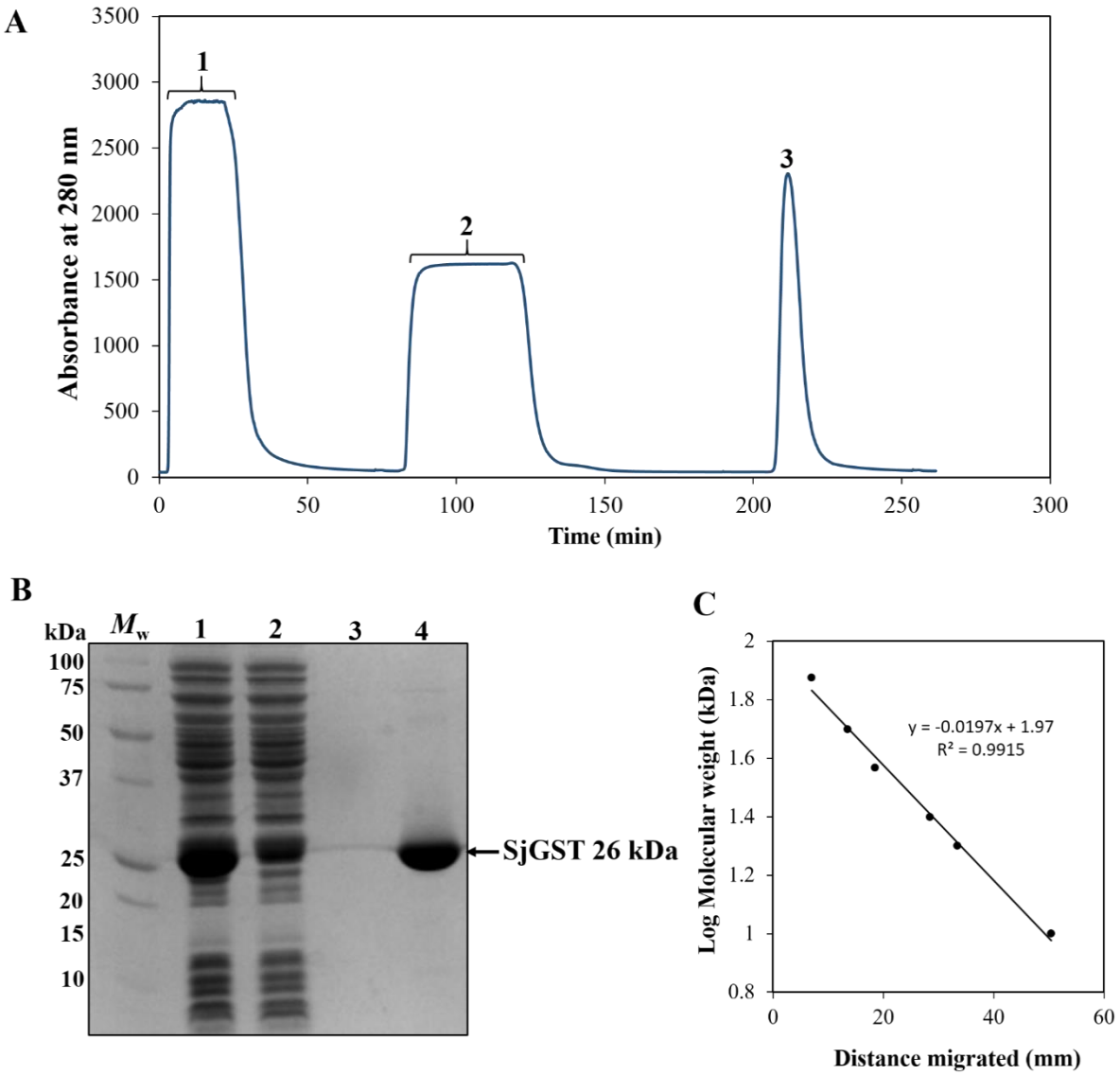


Figure 4.2 Purification profile of SjGST. (*A*) GSH-Agarose affinity chromatography purification profile for SjGST. The soluble cell Lysate was injected into the GSH-Agarose column as shown in Peak 1, which is the breakthrough (flow-through) peak representing unbound proteins. Wash buffer which is made up of the equilibration buffer (50 mM Tris-HCL) pH 7.4 and Triton X-100 was used to wash off unbound protein as depicted in peak 2. Peak 3 shows elution of the bound protein using 10 mM Glycine at pH 10. (*B*) Purity of the eluted protein sample was analysed using 12% SDS-PAGE. Lane 1 is the soluble cell fraction, the flow through was loaded in lane 2 (peak 1), lane 3 (peak 2) is a sample collected during the Triton X-100 wash, while lane 4 (peak 3) is the eluted pure protein sample indicated by one band of about 26 kDa. (*C*) Standard curve used to determine the mass of the protein. Log molecular weight of known protein standards was plotted against the distance migrated by each, linear regression analysis ($R^2 = 0.99$) was used to calculate the molecular weight of SjGST.

4.2 Qualitative and quantitative analysis of recombinant SjGST

The quality of the purified SjGST was analysed using ultraviolet (UV) spectroscopy. This technique enables the detection of nucleic acid contaminants and aggregations (Raleigh scatter) between 240 – 340 nm wavelengths. A single peak was observed at 280 nm wavelength and none at 260 and 340 nm wavelengths (Figure 4.3A). The A_{260}/A_{280} absorbance ratio is 0.53, indicating a pure non- nucleic acid contaminant sample. A serial dilution method was used to determine the protein concentration in the pooled fractions by monitoring absorbance at 280 nm and 340 nm, spectrophotometrically. Corrected absorbance was plotted against the dilution factor (Figure 4.3B). The equation derived from the linear plot is

$$y = 7.305x - 0.0129 \qquad (Eqn.\ 4.1)$$

The $R^2 = 0.9993$ and the derived slope was substituted in equation 3.2:

$$conc\ (mg/ml) = \frac{Slope \times Molecular\ mass}{Molar\ extinction\ coeficient} \qquad (Eqn.\ 4.2)$$

$$conc\ \ (mg/ml) = \frac{7.3053 \times 52\,000}{2 \times 42860} = 4.43\,mg/ml$$

$$conc\ mol/L = \frac{reacting\ mass}{molar\ mass} \qquad (Eqn.\ 4.3)$$

$$conc\ \ mol/L = \frac{4.43}{52000} = 0.0000852\,mol/L \sim 85\ \mu M$$

The calculated protein concentration is 85 µM.

The total protein obtained for the 20 mL purified sample is $4.43\,mg/mL \times 20\,mL = 88.6\,mg/20\,mL$

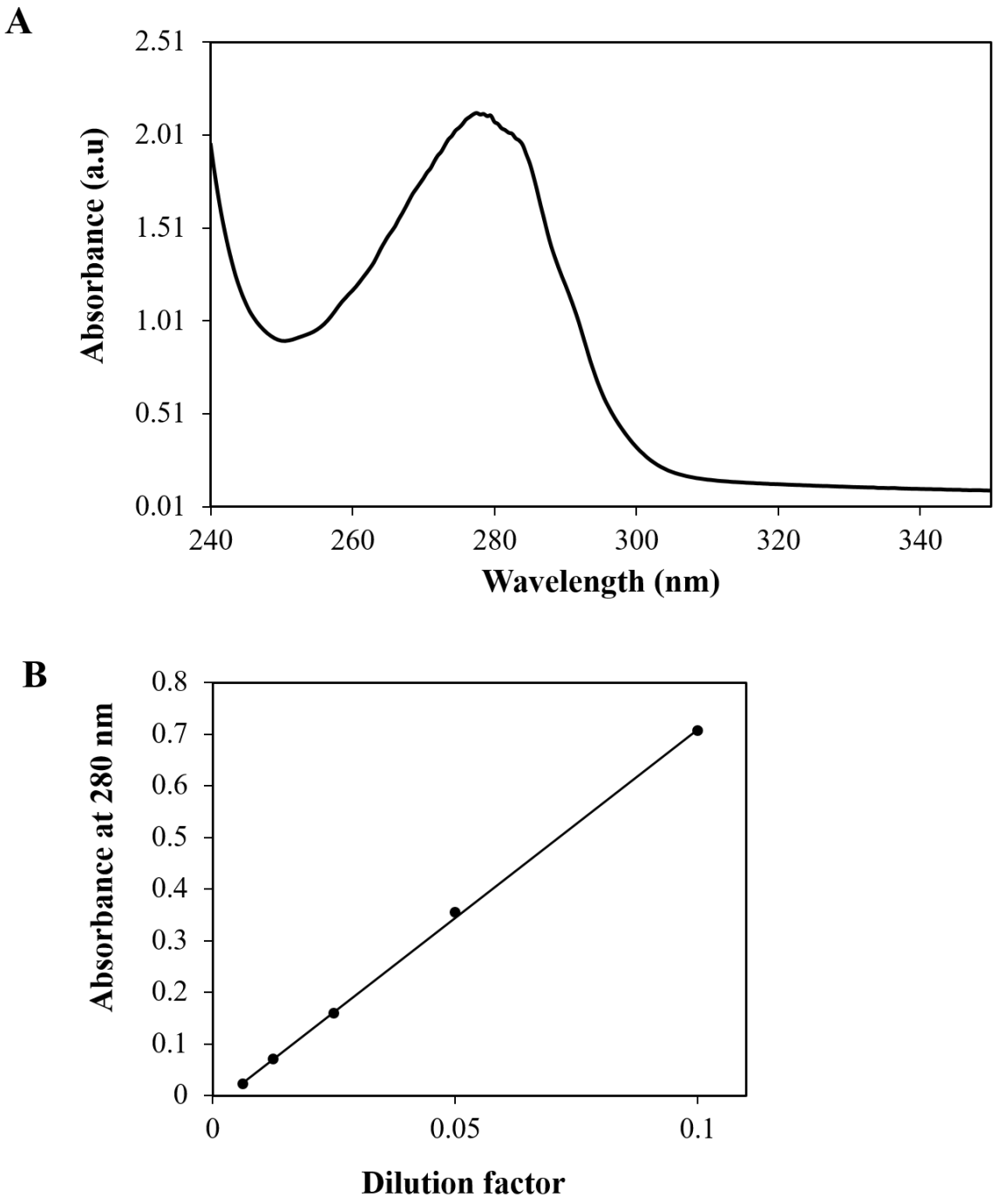


Figure 4.3 Quantity and quality assessment of SjGST. (*A*) UV absorption spectrum monitored between 240 nm and 350 nm wavelengths was used to analyse quality of the purified SjGST. The peak at 280 nm wavelength showing absorbance greater than 1.7 indicates a protein sample with an insignificant nucleic acid contamination. There are no peaks at 260 nm and 340 nm indicating the absence of DNA contamination and protein aggregation, respectively. (*B*) Dilution plot to determine the concentration of pure SjGST. Corrected absorbance ($A_{280\ nm} - A_{340\ nm}$) was plotted against the dilution factor, R^2 of 0.9996 was obtained. The resulting slope (7.3053) was used to calculate the protein concentration.

4.3 Structural Characterisation

4.3.1 Secondary structure

Far-UV circular dichroism (CD) spectroscopy was used to assay the secondary structure content of SjGST. The spectra (Figure 4.4), was collected between 190 nm and 250 nm wavelengths at 20°C, pH 7.4 and shows positive maxima at 191 ± 1 nm for (SjGST only), 192 ± 1 nm for (SjGST + EA), negative minima at 209 and 220 ± 1 nm, 206 and 222 ± 1 nm for SjGST and SjGST in the presence of EA respectively.

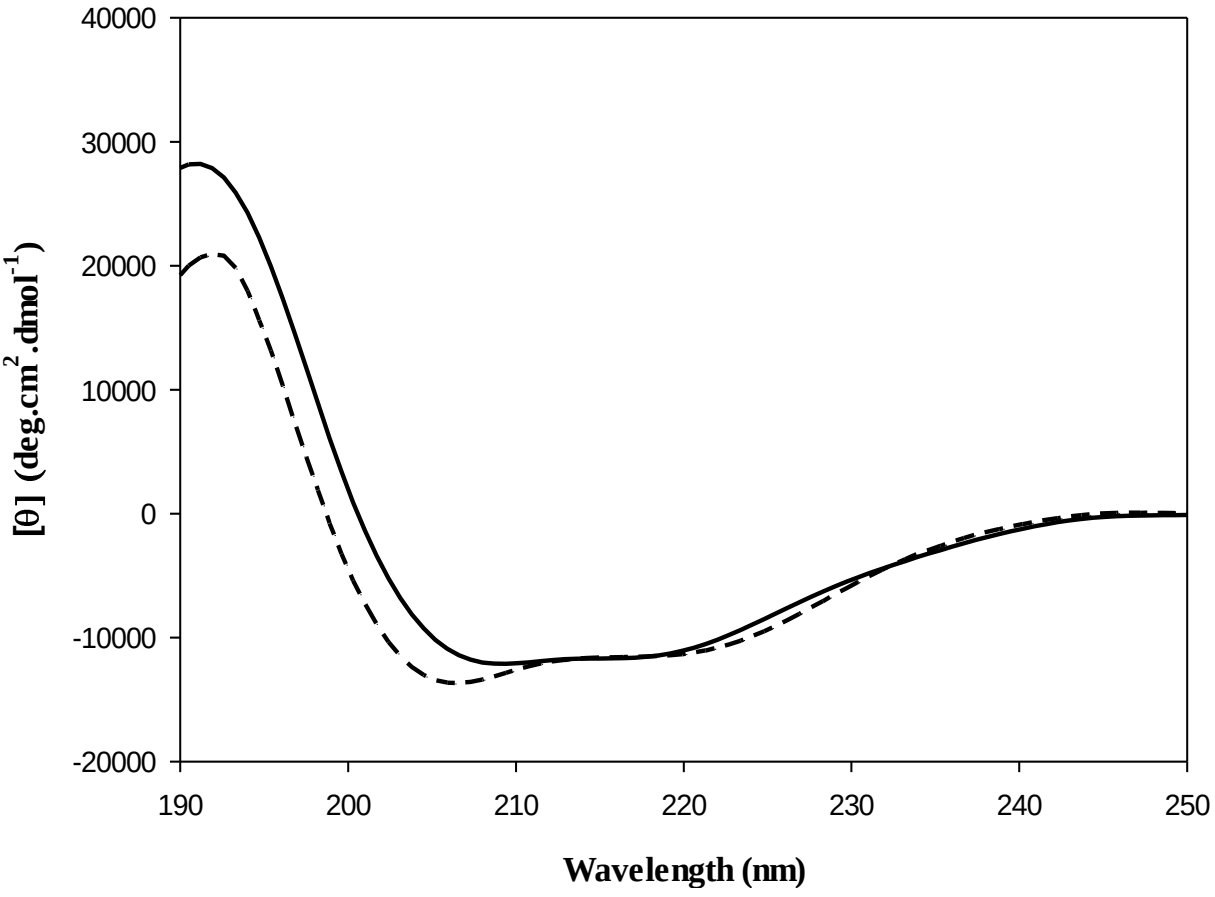


Figure 4.4 Far-UV circular dichroism spectra of SjGST. Far-UV CD spectra represents results obtained in the absence (bold line) and presence (dotted line) of 10 µM EA using 2 µM of SjGST in 5 mM sodium phosphate buffer of pH 7.4. Spectra from three scans were averaged and the blank (buffer alone) was subtracted. The experiment was performed at 20°C using JASCO J810.

Table 4.1
Summary of the secondary structure content calculated using CONTILL algorithm implemented in the Dichroweb server.

Protein	α Helix (%)	β Strand (%)	β Turn (%)	Unordered (%)	NRMSD
SjGST	98.9	1.1	0	0	0.084
SjGST + EA	99.1	0.9	0	0	0.078

Normalised root-mean-square deviation (NRMSD) indicates the goodness of fit of calculated data compared to obtained experimental data, with <0.1 acceptable as good fit (Sreerama and Woody, 2000).

4.3.2 Tertiary structure

4.3.2.1 Intrinsic fluorescence

Intrinsic fluorescence spectroscopy was used to analyse the tertiary structure of SjGST in the presence and absence of EA in relation to the local environment of tryptophan residues in the enzyme. SjGST has a total of eight tryptophan residues (four per monomer), located on the N-terminus thioredoxin-like domain, also Trp206 is in close proximity to the active site (McTigue *et al.*, 1995). The tryptophans were selectively excited at 295 nm and emission was monitored between 300 nm and 500 nm wavelength. The fluorescence spectra obtained (Figure 4.5) shows maximum emission wavelengths at 341 nm and 342 nm for SjGST and SjGST in presence of EA respectively. Fluorescence intensity of the protein sample containing EA decreased significantly by 60% as a result of changes in the microenvironment of the tryptophan

.

4.3.2.2 Extrinsic ANS fluorescence-binding studies.

ANS binding assay was used to probe the existence of hydrophobic patches on SjGST. The recombinant SjGST sample was analysed in the presence of 100 µM ANS, and also in the presence of EA. A significant increase in quantum yield and a concomitant blue shift in emission maxima was observed by monitoring a sample of SjGST in the presence of ANS, and also for SjGST-EA complex, following excitation at 390 nm. Free ANS emitted maximally at 519 nm, ANS bound to SjGST shows maximum emission at 492 nm, while 486 nm emission was observed for ANS bound to SjGST-EA complex (Figure 4.6A). The fluorescence spectra for ANS bound SjGST in the presence of EA also shows a decrease in quantum yield and a bluer shift.

In an effort to elucidate the observation above, ANS displacement studies were performed by varying the concentration of EA from 0 – 100 µM in the presence of 100 µM ANS bound to SjGST. The exponential decay profile obtained indicates that about 64.5% of ANS was successfully displaced as EA concentration was increased, which resulted in a decrease in fluorescence intensity as shown in (Figure 4.6B).

Further characterisation of the ANS binding environment on SjGST was performed to ascertain the affinity of ANS to the recombinant SjGST in the presence of EA. Saturation curve in the presence or absence of EA was obtained by measuring the quantum yield as a function of ANS concentration. The hyperbolic function of sigma plot was used to fit the data and obtain the K_d of ANS to SjGST in the absence of EA (40.6 µM ± 2.3) and in the presence of EA (30.3 µM ± 1.4) as shown in Figure 4.6C.

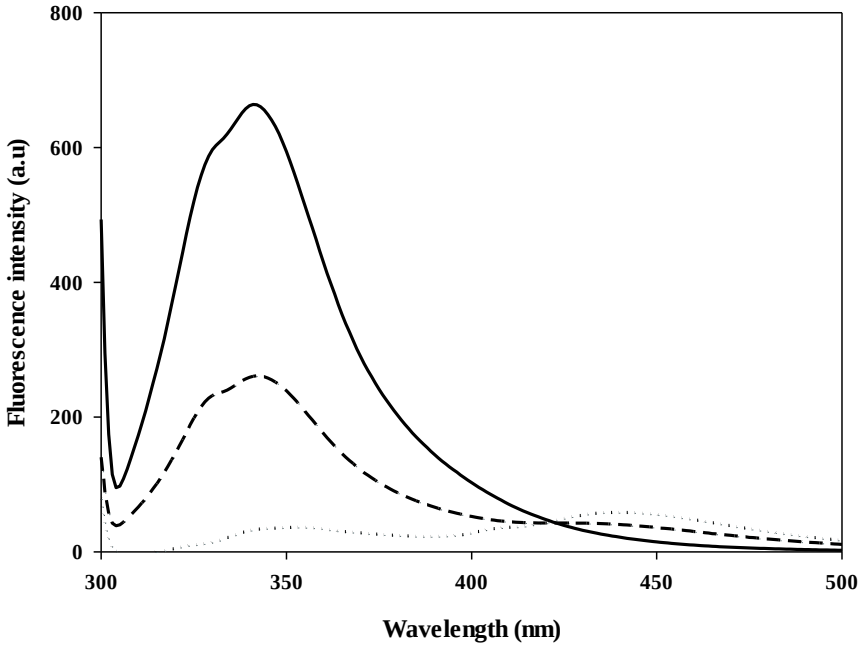


Figure 4.5 Intrinsic fluorescence emission spectra of SjGST. The bold line shows the emission spectrum of SjGST only, the dashed line is the spectrum of SjGST in the presence of EA, while the dotted line represents EA spectrum. The reaction was measured using 2 µM SjGST in 5 mM sodium phosphate buffer pH 7.4, at 295 nm excitation wavelength. Emission was collected from 300 nm to 500 nm wavelength at 20℃. Each spectrum is an average of three accumulations of three replicate experimental samples, with the subtraction of the control spectrum.

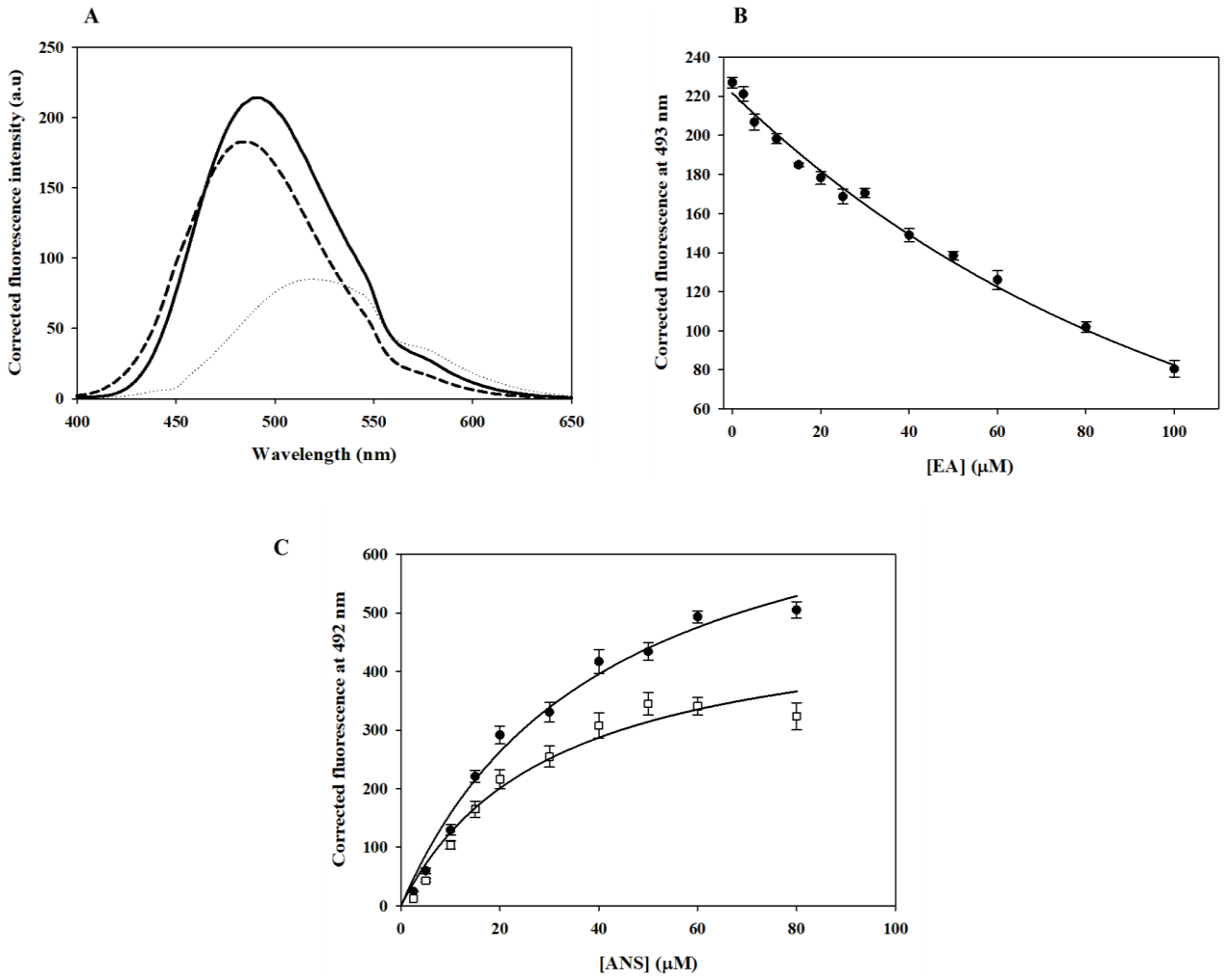


Figure 4.6 ANS binding and displacement fluorescence analysis. *(A)* Extrinsic ANS fluorescence spectra of unbound ANS (dotted line), ANS bound to SjGST (solid line), ANS bound to SjGST in the presence of EA (dashed line) and absence of EA (dotted line). Concentration of ANS was 100 µM and 2 µM SjGST. ANS was excited at 390 nm, and the spectrum emission was collected from 400 to 600 nm. *(B*) Spectrum of ANS displacement using EA. Varying concentrations (1-100 µM) of EA was used to displace 100 µM of ANS bound to 2 µM of SjGST. Emission at 493 nm was recorded and excitation was at 390 nm. *(C)* ANS concentration dependent fluorescence spectra of SjGST (●) and SjGST bound EA (□). 2 µM of SjGST only was titrated with increasing concentration of ANS as well as 2 µM of SjGST in the presence of 100 µM of EA. The experiments were performed in triplicate, the average obtained represents each data point. The error bars represent ± SD of each replicate experiment.

4.3.3 Quaternary structure

The quaternary structure of SjGST was characterised by SE-HPLC using 20 mM Na_2HPO_4, pH 7.4, 500 mM NaCl, 1 mM EDTA and 0.02% (w/v) NaN_3 buffer. Inset in Figure 4.7 shows a standard curve of the gel filtration standards used to calibrate the column and also to estimate the oligomeric size of SjGST. The protein eluted with a single peak (both in the absence and presence of EA) at approximately 54 kDa and 52 kDa respectively, corresponding to its native homodimeric quaternary structure (Figure 4.7).

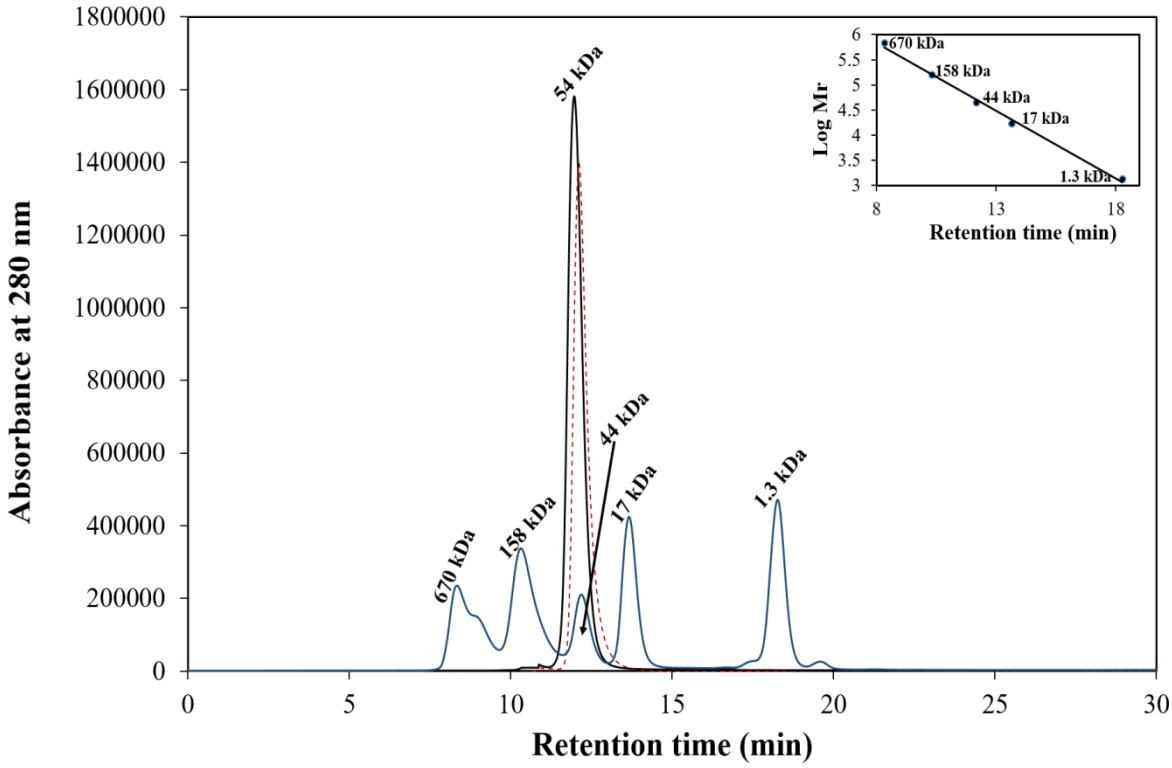


Figure 4.7 SE-HPLC chromatogram of SjGST. The elution profile was resolved by SE-HPLC using 20 mM sodium phosphate pH 7.4, 500 mM sodium chloride and 2 mM DTT. The black solid line is the profile for SjGST (100 µM), red dashed line represents the profile for SjGST (100 µM) in the presence of EA (10 µM), blue solid line is the chromatogram of the gel filtration standards. Inset is a standard curve of used to determine the molecular mass of the samples.

4.3 Functional characterisation

GSH-CDNB conjugation assay was used to determine the specific activity of SjGST both in the absence and presence of EA (10 µM), using 100 mM Na_2HPO_4, pH 6.5, 1 mM EDTA, 0.02% (w/v) NaN_3 buffer. The progress curve (Figure A1), for each triplicate data was monitored at A_{340} for 60 seconds, the slope for each reaction curve provides the initial velocity (υ_0), which was plotted against each enzyme concentration. Subsequently, the calculated activity for each enzyme concentration was plotted against each enzyme mass to obtain the specific activity (Figure 4.8). The specific activity of SjGST is 24 µmol min^{-1} mg^{-1} and 6.8 µmol min^{-1} mg^{-1} in the absence and presence of EA respectively. SjGST activity was reduced to approximately 28% by EA.

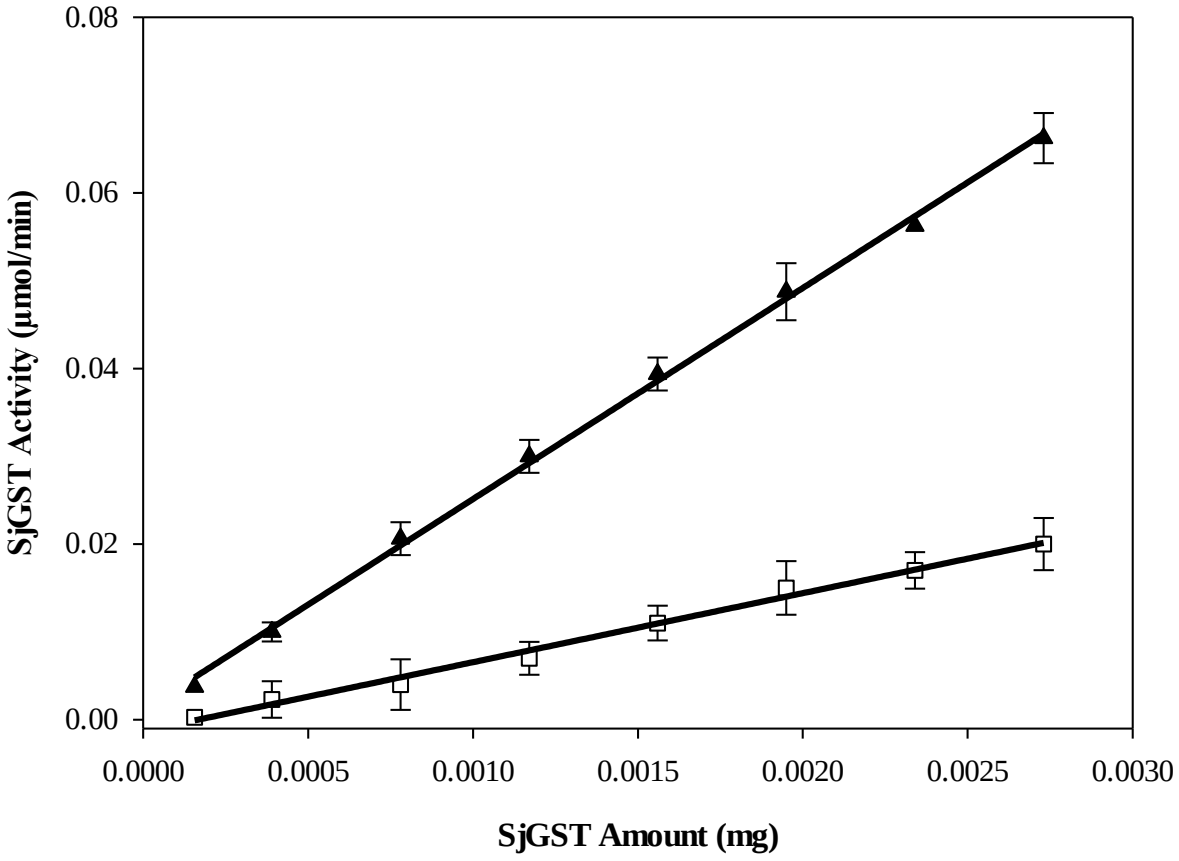


Figure 4.8 Specific activity analysis using GSH-CDNB conjugation assay. ***A plot of SjGST activity*** against the amount of enzyme in the absence (▲) and presence (□) of 10 µM Ellagic acid (EA) monitored by measuring change in A_{340} versus time (min) of the product (1-(S-glutathionyl)-2, 4 di-nitrobenzene). 1 mM sodium phosphate buffer, pH 6.5 was used to perform the reaction in triplicate with 1 mM GSH and 1 mM CDNB. The slopes (SjGST 24.05 (µmol/min/mg), R^2 = 0.9985 and SjGST + EA 6.8 (µmol/min/mg) R^2 = 0.9977) obtained is the specific activity of the enzyme. Average of the triplicate values were plotted with error bars indicating their standard deviations.

The half maximal inhibitory concentration (IC_{50}) of EA on SjGST was performed to gain more insight on the effect of EA on the activity of SjGST. GSH-CDNB conjugation assay was used to obtain the IC_{50} curve by plotting the activity calculated from the obtained progress curves against the log concentration of EA (Figure 4.9). The data was fitted with the four-parameter non-linear regression for sigmoidal curve, implemented in Sigma plot V13 and the IC_{50} was calculated to be approximately 2.4 µM EA.

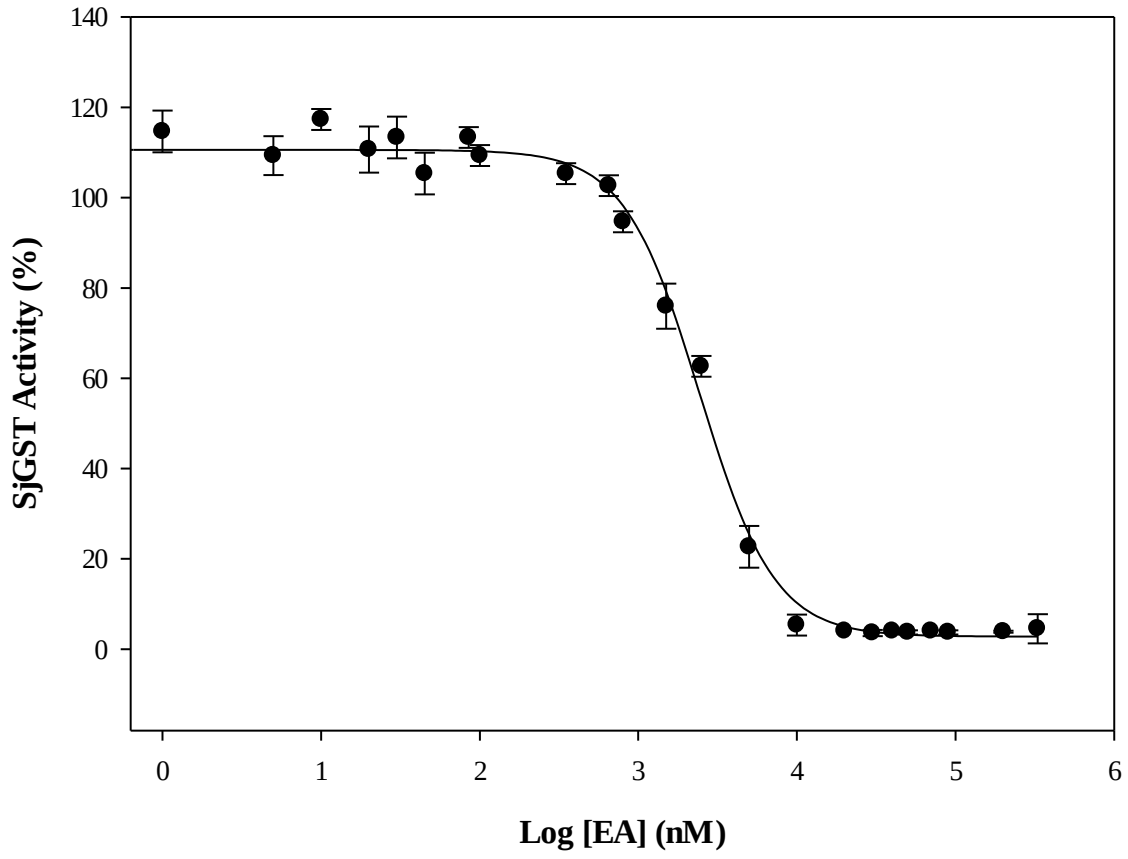


Figure 4.9 IC_{50} of EA on its inhibitory effect on SjGST. Varying concentrations of EA were incubated with SjGST (30 nM) in 100 mM sodium phosphate pH 6.5 for 30 min. The activity of the protein was monitored at 340 nm for 60 s. The percentage activity was plotted against the Log concentration of EA. Each data point is a representative of three separate experiment. The error bars represent ± SD of each replicate experiment.

4.3.1 Kinetics analysis of SjGST

The impact of EA on the mechanism of SjGST-catalysed reaction was further analysed using kinetic evaluation of the enzyme substrate reaction systems (using GSH-CDNB conjugation assay) in 100 mM Na_2HPO_4, pH 6.5, 1 mM EDTA, 0.02% (w/v) Na_3N buffer. The progress curves of the enzyme activity was monitored specrophotometrically at A_{340} for 60 s each. SjGST activity was measured using different substrate concentrations, in this case GSH or CDNB (Figure 4.10A and 4.11A), in the prescence of varying concentrations of EA. The reactions for GSH and CDNB followed the Michaelis Menten kinetics. A plot of the reaction velocity as a function of the substrate concentration (GSH and CDNB) was fitted using a hyperbolic function implimented in Sigma plot V13, and the calculated V_{max} and K_M obtained is shown in Table 4.2. The mode of inhibition of EA for both substrates was determined using the Lineweaver burk plots as shown in Figure 4.10B and 4.11B for GSH and CDNB, respectively. The SjGST-catalysed GSH-CDNB (varying GSH) conjugation reaction in the presence of EA show that EA does not compete with GSH (non-competitive). However, varying the concentration of CDNB as a substrate indicates an and un-competitive inhibition.

To probe further the impact of EA on SjGST catalytic efficiency and the rate of product formation, the k_{cat} and k_{cat}/K_M were determined. GSH-CDNB conjugation assay was also used to perform the reaction using GSH as the substrate in the presence and absence of EA. To determine the k_{cat}/K_M, a GSH concentration below the K_M was varied and the progress curve of the velocity was plotted against the various substrate concentration (Figure 4.12A). For k_{cat}, GSH concentration was kept constant while SjGST concentration was varied in the presence or absence of EA (Figure 4.12B). The obtained results (Table 4.2) indicates that the kinetic efficiency of SjGST was reduced.

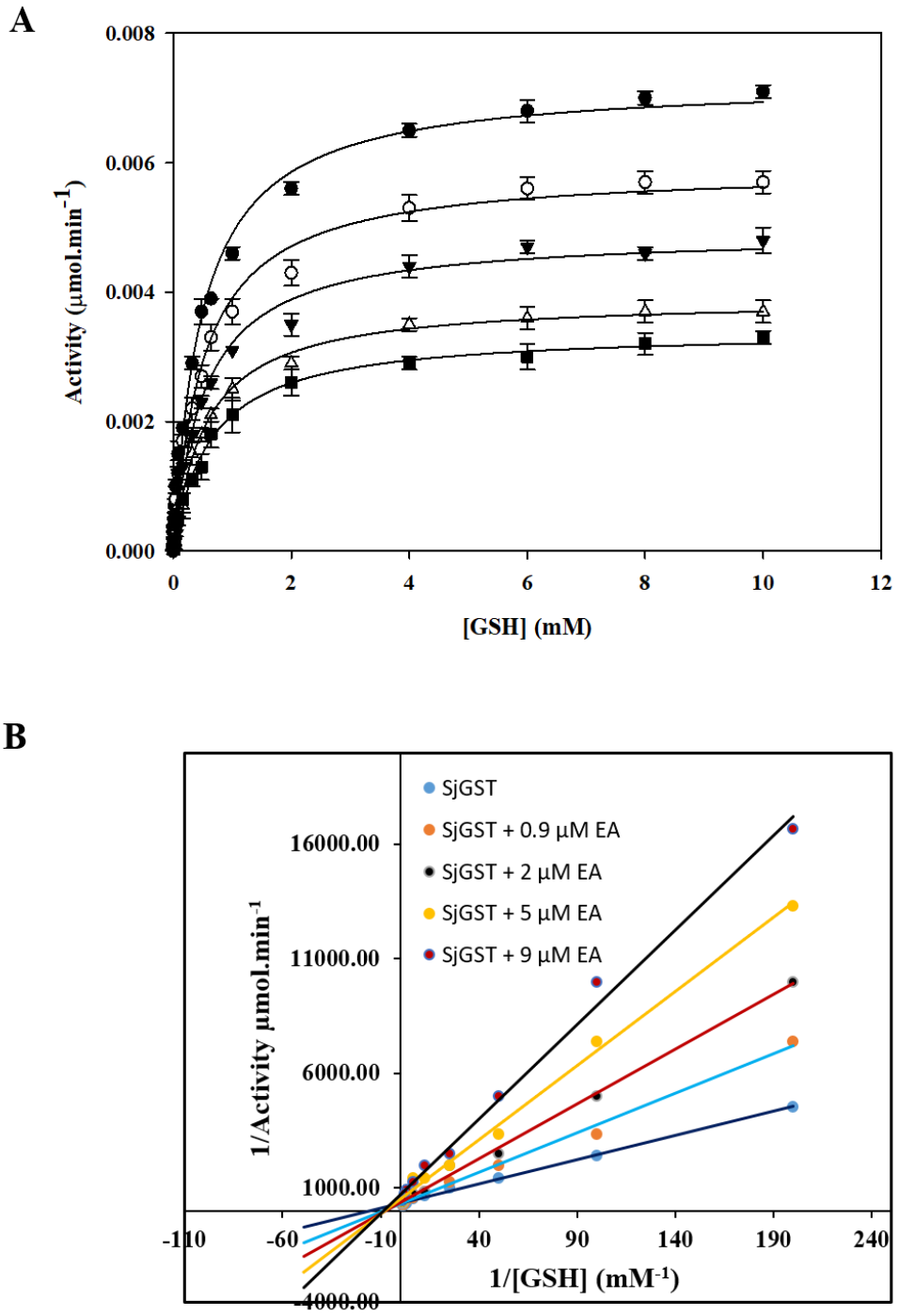


Figure 4.10 Kinetic analysis of SjGST in the presence and absence of EA. (*A*) Michaelis-Menten kinetics of SjGST–GSH conjugation in the presence of 1 mM CDNB monitored at 340 nm for 60 seconds. Hyperbolic curve (●) represents the reaction of SjGST in the absence of EA, (○) is the curve obtained when 0.9 µM of EA was added, (▼) shows the curve for 2 µM EA, (Δ) 5 µM EA and (□) 9 µM EA. The reaction velocity was plotted against a varied concentration of GSH. (*B*) Lineweaver burke double reciprocal plot of the rate of inactivation of SjGST activity as a function of the concentration of EA. The reaction was monitored for 60 seconds. The error bars represent ± SD of each replicate experiment.

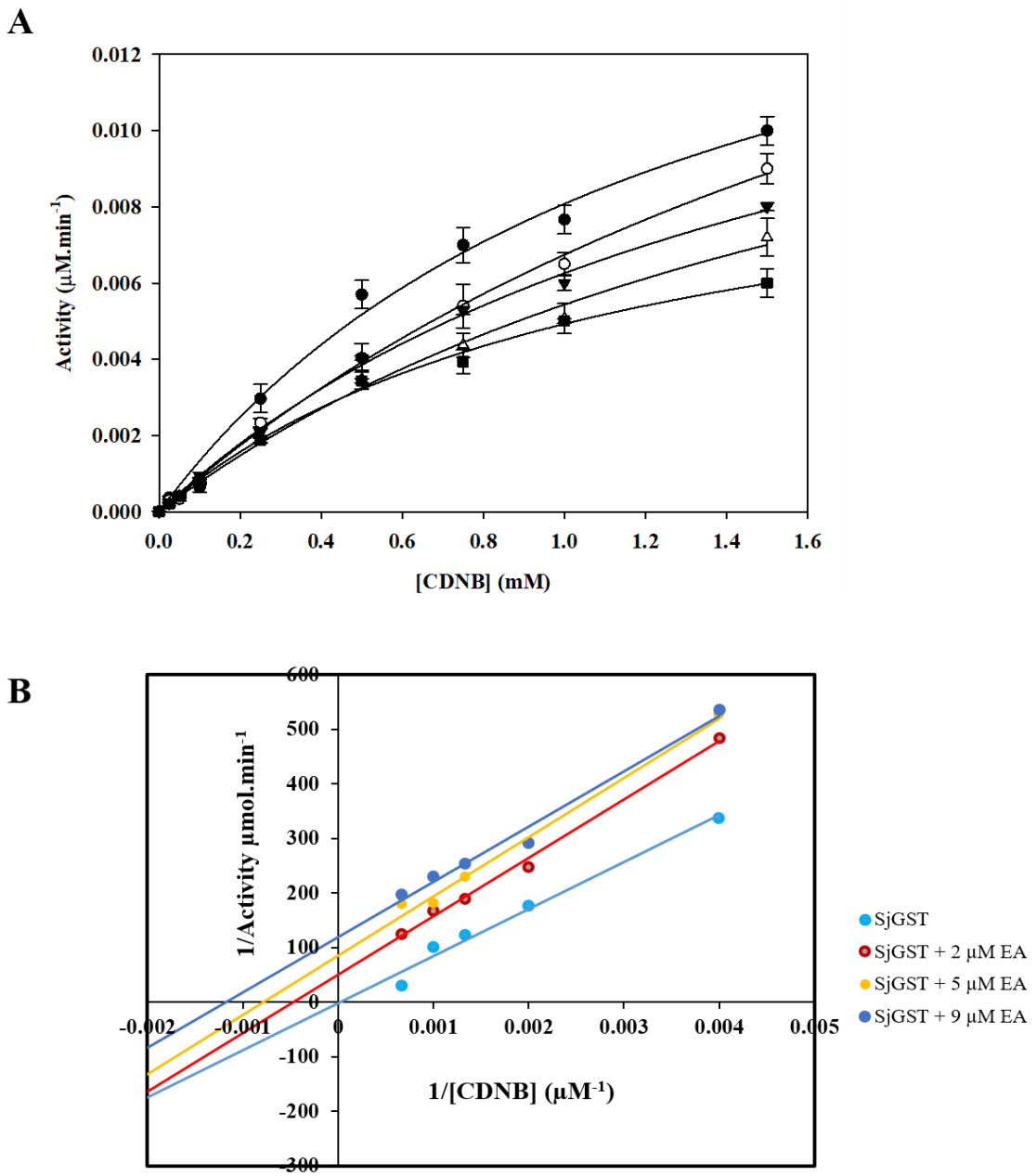


Figure 4.11 Kinetic analysis of SjGST in the presence and absence of EA. (*A*) Michaelis Menten kinetics of SjGST-CDNB conjugation in the presence of 1 mM GSH monitored at 340 nm for 60 seconds. Hyperbolic curve (●) represents the reaction of SjGST in the absence of EA, (○) is the curve obtained when 0.9 µM of EA was added, (▼) shows the curve for 2 µM EA, (Δ) 5 µM EA and (■) 9 µM EA. The reaction velocity was plotted against a varying concentration of CDNB (0 - 1.5 mM). (*B*) Lineweaver burke double reciprocal plot of the rate of inactivation of SjGST activity as a function of the concentration of EA using CDNB as the substrate. The reaction was monitored for 60 seconds. The error bars represent ± SD of each replicate experiment.

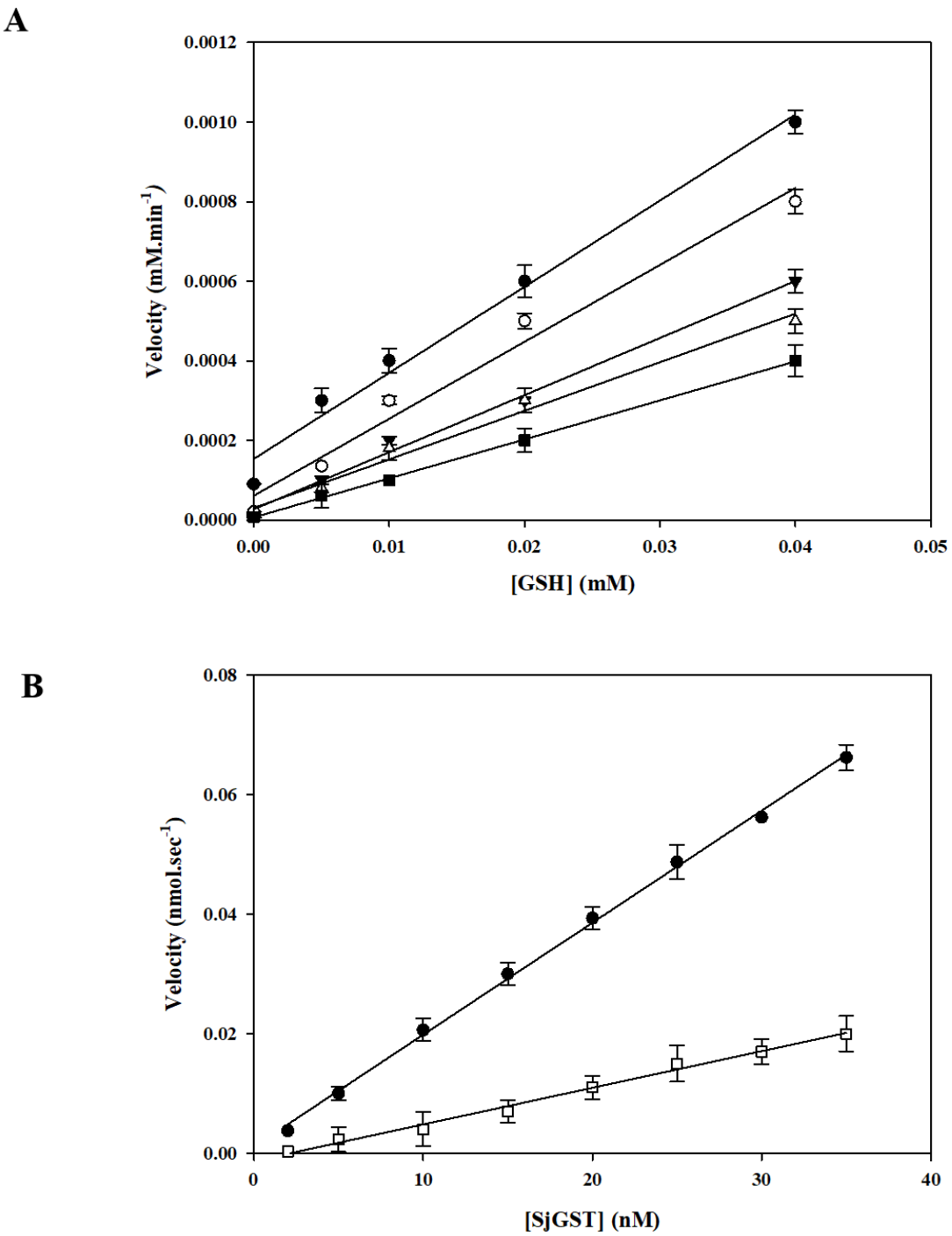


Figure 4.12 Inhibition kinetics of EA on SjGST. (*A*) k_{cat}/K_M linear plot of SjGST (30 nM) in the presence of varied EA concentration. The data plots of the reaction in the absence of EA (●), in the presence of 0.9 µM EA (○), 2 µM EA (▼), 5 µM EA (Δ) and 9 µM EA (■) were obtained in triplicate and was monitored at 340 nm for 60 seconds. The reaction velocity was plotted against varied substrate (GSH) concentration. (*B*) The linear plot of SjGST in the absence and presence of EA (9 µM) derives the k_{cat}. Velocity was plotted against varied enzyme concentration to obtain the k_{cat}. The error bars represent ± SD of each replicate experiment.

Table 4.2

Kinetic parameters of SjGST in the presence of EA

[EA](μM)	*V*max (μmol.min^{-1})		K_M (mM)		k_{cat} (sec^{-1})	k_{cat}/K_M (M^{-1}s^{-1})
	GSH	CDNB	GSH	CDNB		
0.00	0.007 ± 0.0002	0.018 ± 0.002	0.48 ± 0.03	2.05 ± 0.03	0.0019	0.021 ± 0.003
0.90	0.006 ± 0.0002	0.024 ± 0.003	0.51 ± 0.02	1.89 ± 0.02		0.019 ± 0.001
2.00	0.005 ± 0.0001	0.016 ± 0.001	0.53 ± 0.03	1.68 ± 0.04		0.014 ± 0.001
5.00	0.004 ± 0.0001	0.016 ± 0.002	0.55 ± 0.04	1.11 ± 0.03		0.012 ± 0.002
9.00	0.003 ± 0.0001	0.011 ± 0.001	0.62 ± 0.03	1.14 ± 0.01	0.0006	0.009 ± 0.0001

4.4 Thermodynamics of Ellagic acid-SjGST interaction

The energetics of EA binding to SjGST was investigated by isothermal titration calorimetry at 20℃, this analysis will also give more insight on the structural basis of EA-SjGST binding interaction and energy profile of the associated ligand binding sites. EA was titrated into the SjGST sample until saturation of the binding sites was achieved. The interaction between EA and SjGST is exothermic as shown in Figure 4.14. Heat of dilution was corrected by averaging the post saturation peaks and subtracting the value from the raw data, and the data was analysed using *Nano*Analyze™ software. The binding isotherm and fitted data displays profile of an exothermic reaction (ΔH = -9.48 ± 0.42 kJ/mol). The result shows that the reaction was enthalpically driven with a favourable entropy ($-T\Delta S$ = 20.40 ± 0.08 kJ/mol). The reaction proceeded spontaneously (ΔG = -29.88 ± 0.07 kJ/mol). The dissociation constant (K_d = 4.79 ± 0.04 μM) is in the micro molar range, with a stoichiometry of 4 molecules of EA per mole of the dimeric SjGST.

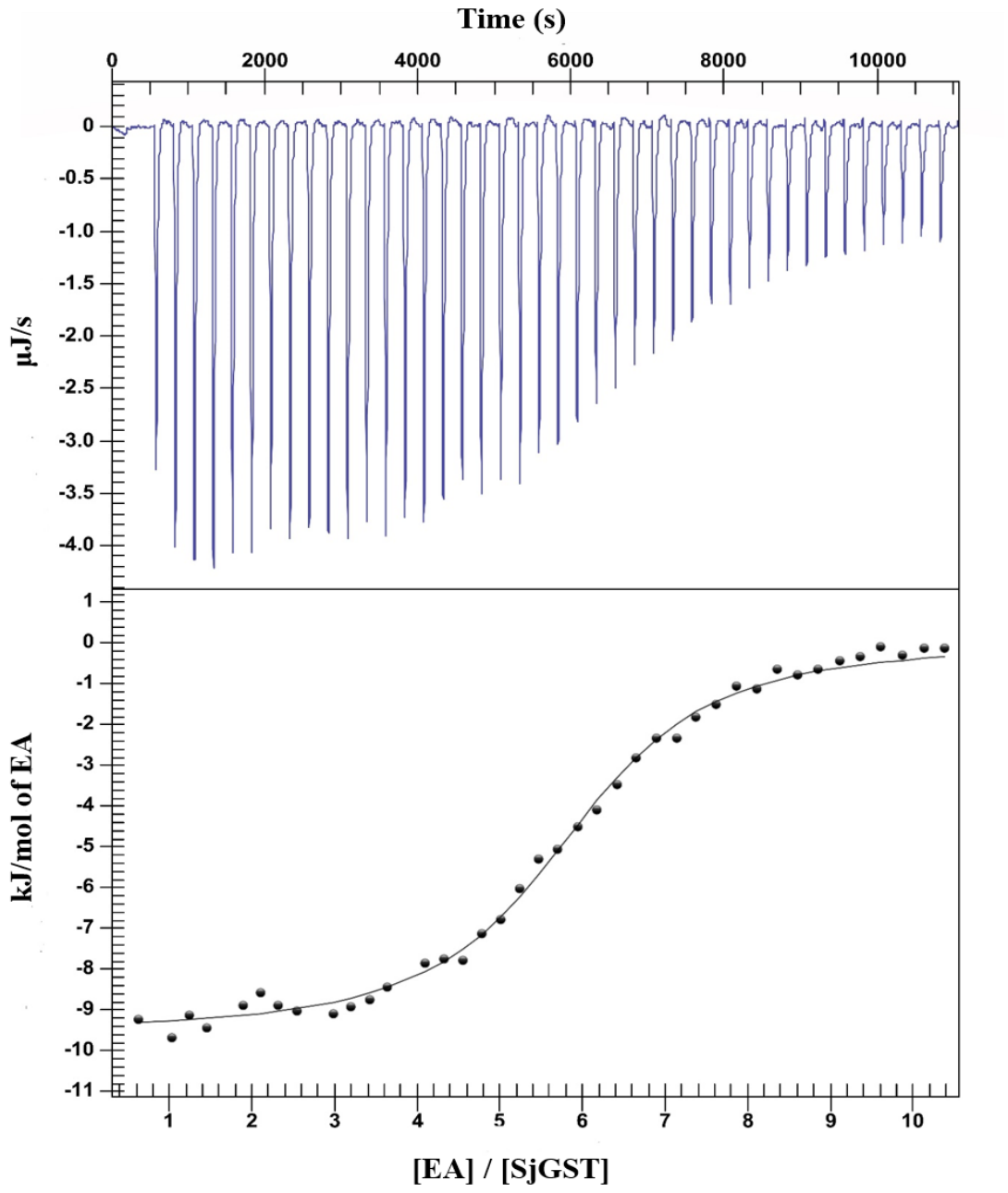


Figure 4.13 Calorimetric profile of the titration of SjGST with EA in 20 mM sodium phosphate buffer containing 2 mM TCEP-HCL and 0.02% (w/v) NaN_3 at 20°C. Top panel represents the raw exothermic heats generated upon each injection of 25 µL of 2 mM EA into 1.8 mL of 50 µM of SjGST. The panel below shows the corrected binding isotherm for each peak in top panel plotted against the molar ratio of EA to SjGST. The solid line represents the non-linear best fit of the experimental data for n = 4 ± 0.08, K_d = 4.73 ± 0.04 µM, ΔH = -9.48 ± 0.42 kJ/mol, $-T\Delta S$ = 20.40 ± 0.08 kJ/mol and ΔG = -29.88 ± 0.07 kJ/mol.

4.5 Molecular modelling studies

In the absence of the crystal structure of SjGST-EA complex, molecular docking analysis was performed to gain more information (theoretical) on the binding and interaction between SjGST and EA. EA was also docked into human GSTP1-1 (Figure 4.16) to compare the interaction with that of SjGST. The docking was performed using Induced Fit™ ligand docking and Glide docking algorithms implemented in Schrödinger Suite 2017-3. The 3D coordinates of SjGST used was extracted from the Protein Data Bank (PDB: 1DUG). The structure of EA was flexible while that of SjGST was kept rigid. The obtained results by Glide™ indicates that EA binds to the dimer interface as well as in the H-site active site sub-structure of SjGST (Figure 4.14 and 4.15). A higher Emodel energy of induced fit docking (-80.328 kcal/mol) was obtained for the binding on the dimer interphase while (-74.200 kcal/mol) was obtained for the binding on the active site. The result obtained for the best docking pose for human GST P1-1 (hGSTP1-1) produced Emodel energy of -78.4 kcal/mol. Hydrogen bond interaction was observed (Figure 4.16). The two-dimensional representation of EA bound to the dimer interface (Figure 4.14B) shows hydrogen bonding interaction between EA and SjGST with Asp100 and Glu95 residues. Binding of EA to the active site (Figure 4.15B) shows hydrogen bonding interaction with Asp100, Arg107, Ser106, Tyr110 and Tyr6. EA also shows contact with Tyr104 which is absent in mammalian GSTs of known structures. It is also in contact with Tyr6, a residue critical for GST catalysis, it is also responsible for stabilising GSH thiolate anion and enhances nucleophilicity of protonated thiol (Andújar-Sánchez *et al.*, 2003). There is also hydrogen bond between EA and Tyr110 residue which is important for water molecule coordination in SjGST active site. EA docked into GSTP1-1 shows hydrogen bond interaction with Gly205, a water molecule and GSH on the G-site. A pi-pi stacking interaction also occurred with Tyr108. The accuracy of the docking process performed, produced RMSD of 0.024 Å. A bar graph (Figure 4.17) was plotted using the mean and standard deviation of Emodel energy (kJ/mol). The average Emodel energy obtained for EA was -285.75 kJ/mol, for L-site poses -311.3 kJ/mol, and -257.03 kJ/mol for H-site poses. Emodel energy of -305.8 kJ/mol was obtained for EA docked into hGSTP1-1. EA has a higher affinity to SjGST when bound the L-site in comparison to the H-site.

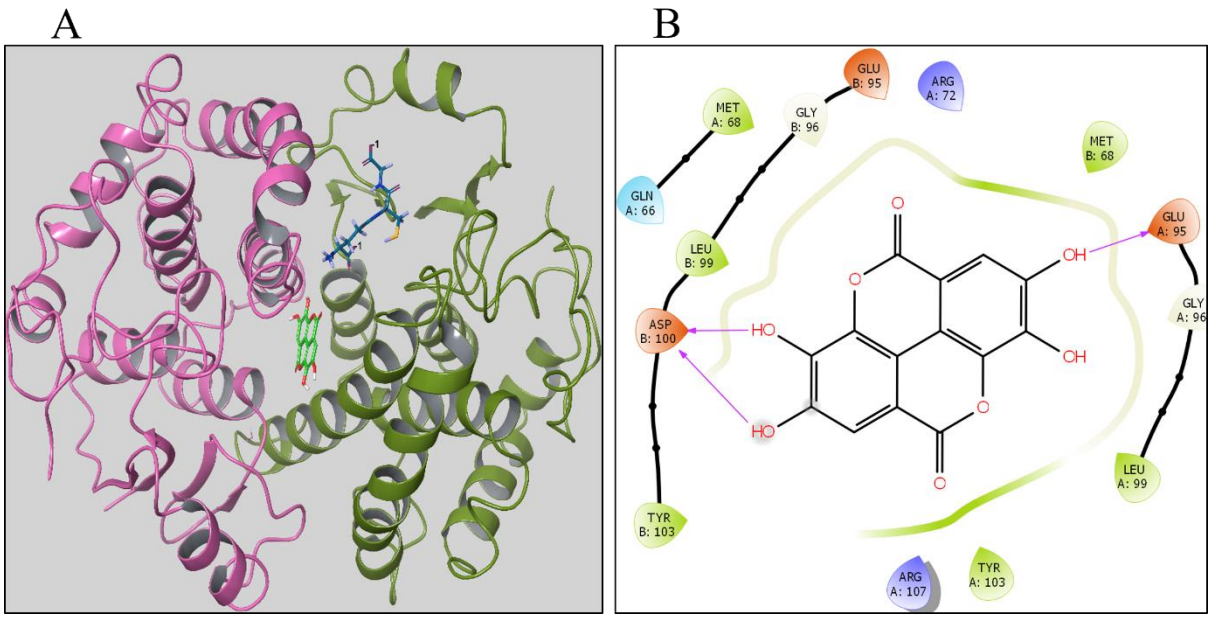


Figure 4.14 Molecular docking of SjGST bound EA. (*A*) Ribbon representation of the top scoring pose of SjGST in complex with EA (green ball and stick structure) bound at the dimer interface. GSH is shown on the G-site (blue ball and stick structure). (*B*) 2D representation showing Hydrogen bonding between EA and the amino acid residues (Asp100 and Glu95) within 4Å.

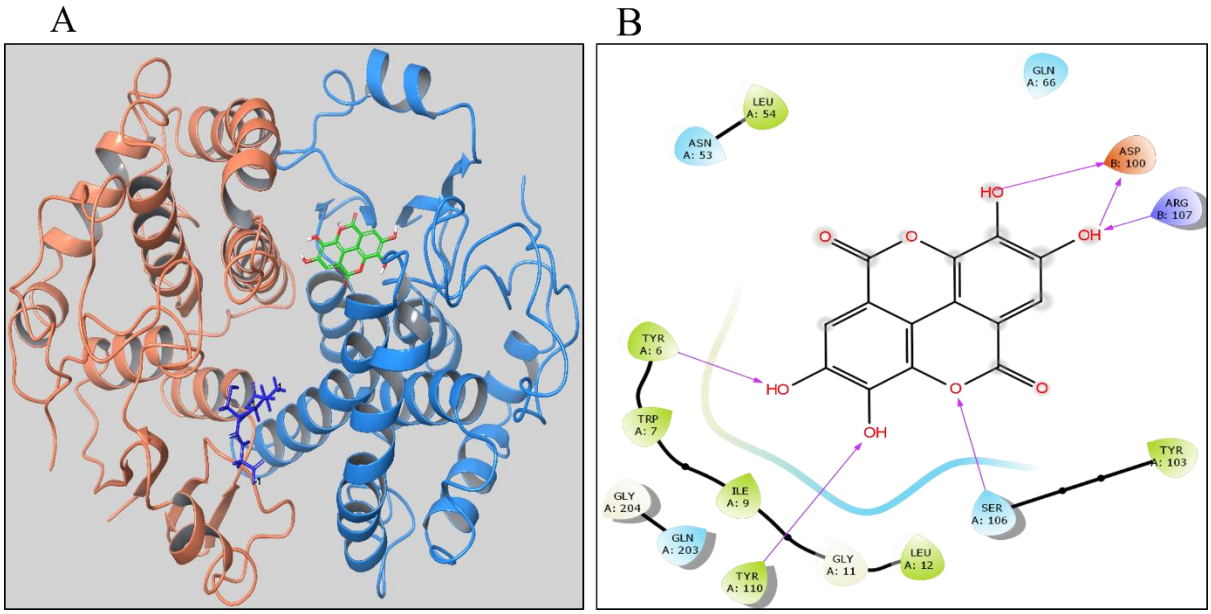


Figure 4.15 Molecular docking of EA bound to the H-site of SjGST. (*A*) Ribbon model of SjGST in complex with GSH (ball and stick model on blue ribbon) showing EA (ball and stick model on green ribbon) bound to the H-site, the amino acid residues are also shown. (*B*) 2D structure representation showing the hydrogen bonding between EA and the amino acid residues (Tyr6, Tyr110, Ser106, Asp100, Arg107) of SjGST.

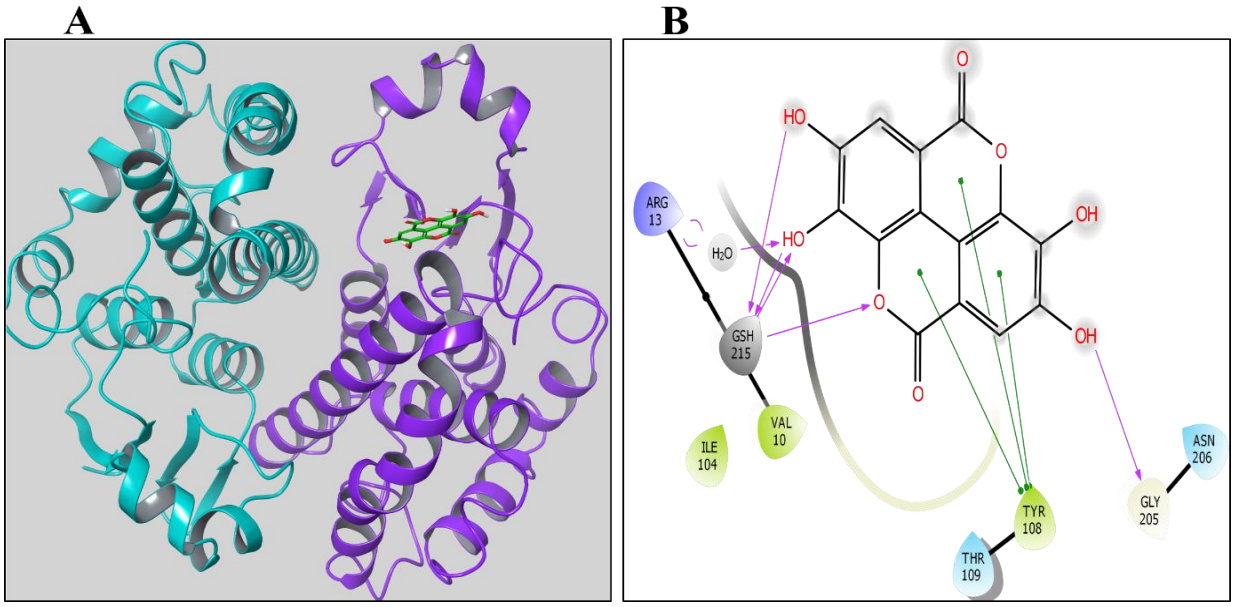


Figure 4.16 Molecular docking of EA bound to GSTPi. (*A*) Ribbon model of GSTPi showing EA (ball and stick model on green ribbon) bound to the H-site, the amino acid residues are also shown. (*B*) 2D structure representation showing the hydrogen bonding between EA, GSH and the amino acid residues (Tyr108, Tyr205) of SjGST.

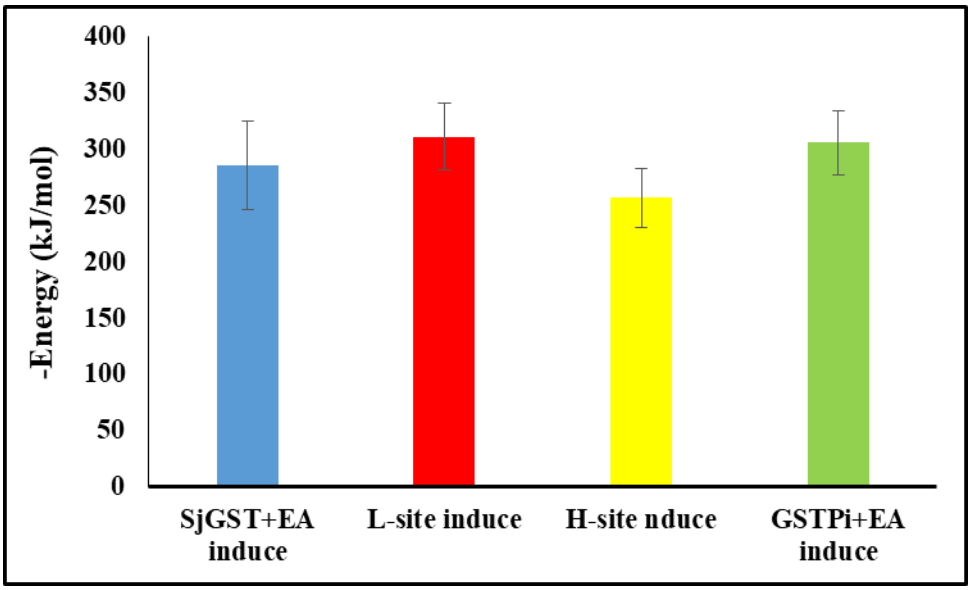


Figure 4.17 Glide Emodel energy bar chart showing the average energy (285.75 kJ/mol) obtained for EA docked in SjGST (blue), average energy obtained for L-site poses (red, 311.3 kJ/mol), and average energy for the H-site (yellow, 257.03 kJ/mol). Energy obtained (305.8 kJ/mol) for EA docked into hGSTP1-1 is represented in green bar. Error bars represents the standard deviation, to determine the differential binding of EA to the L-site, H-site, and in comparison, to hGSTP1-1.

Chapter 5

Discussion

Schistosomiasis is an acute and chronic disease caused by parasitic helminths (blood flukes) of the genus *Schistosoma*. This neglected disease is prevalent in tropical and subtropical rural communities, affecting millions of people worldwide. *S. japonicum* is recognised as the most virulent specie of the three-major species affecting humans. Praziquantel is the only drug available for the treatment of schistosomiasis. The drug is not effective on schistosomula compared with the adult worms. Some high endemic areas have recorded drug resistance of praziquantel by these parasites, and there are no alternative drugs that can be used as substitute. Hence, this raises a major concern to the public health sector because there is need for an alternative drug to be developed. GSTs are phase II detoxification enzymes, identified as putative therapeutic drug targets in parasitic helminth (Wu *et al.*, 2005). GSTs play a vital role in the catalytic conjugation of GSH, passive ligandin binding, and they could be selectively targeted by different inhibitors. SjGST can bind non-substrate ligands; hence, it has the capacity to reduce oxidative damage and formation of toxic haematin crystals by expropriating host-derived heme in the parasite (McTigue *et al.*, 1995; Smith *et al.*, 1986). There has been an emergence of different GST inhibitors which are potential therapeutic agents against parasitic worms. EA is a known GST inhibitor (Mukhtar *et al.*, 1985; Sturm *et al.*, 2009). This study is aimed at investigating the effect of EA on SjGST and its potential as a prodrug for the treatment of schistosomiasis by performing structural, functional, kinetic analysis and ligand docking (molecular modelling) studies.

Recombinant expression of SjGST was performed with pGEX-4T-1 expression vector, which employs SjGST as a fusion tag. The electrophoretogram (Figure 4.2) obtained from SDS-PAGE analysis of the expression samples shows that there was no protein expression on the uninduced sample. This indicates that the P_{tac} promoter was tightly controlled. Hence, no leaky or background expression was observed. There was a minimal amount of insoluble protein observed in the lysate, suggesting that SjGST is highly soluble, as previously reported by Smith & Johnson, 1988. The high levels of soluble expressed protein observed could be attributed to the cold induction condition used (Bader and Leisinger, 1994; Hartman *et al.*, 1992). Obtaining a pure protein is crucial for the characterisation and molecular recognition studies of proteins. A one step purification using GSH-Agarose affinity chromatography was performed, to obtain

pure protein samples. A single predominant protein band was observed on the SDS-PAGE electrophoretogram and a single peak on the SE-HPLC chromatogram, indicating the absence of contaminants (Figure 4.3B and 4.8). Molecular weight of 26.3 kDa was obtained (SDS-PAGE), which is similar to previously published results (Walker *et al.*, 1993). A buffer containing free GSH is normally used to elute proteins purified using this technique. However, in this study, glycine was used for the elution. Eluting SjGST in the presence of GSH will interfere with the actual concentration of GSH required to measure the specific activity and other GSH-CDNB conjugation assays. In addition, it may be difficult to completely eliminate GSH entirely through dialysis; therefore, it may compromise the result of kinetic studies if GSH was in the elution buffer.

Assessing the quality of purified protein is a crucial step required for further downstream applications in this study. The typical protein spectra obtained (Figure 4.4A) shows a peak at 280 nm and no peak was observed at 340 nm, indicating the absence of protein aggregation. The shoulder observed on the peak at 280 nm indicates exposed tryptophan residues. Furthermore, the quality of SjGST was also assessed by SDS-PAGE (Figure 4.3B) and SE-HPLC (Figure 4.8), the later also assessed the native quaternary state of SjGST; hence, establishing that the purified SjGST is almost completely devoid of other protein contaminants. Quantifying the obtained pure protein sample enabled the determination of the working sample concentrations. The concentration of the purified sample was reasonable, at 100 mg/g wet cells (1.5 L culture). SjGST was over-expressed in such a manner that a 1.5 L culture was enough for an entire kinetic and enzymatic studies.

Structural characterisation of recombinant proteins enables a better understanding of structure-function dynamics of protein ligand interactions (Otaki *et al.*, 2010). In this study, SjGST bound to EA was probed for possible structural changes. Because there is no information with regards to SjGST-EA complex, I postulated that EA may have the propensity to induce structural changes in SjGST, especially within the active site of the enzyme. However, Secondary structure of SjGST characterised both in the absence and presence of EA suggest that the interaction of EA did not induce any noticeable structural changes. SjGST exhibits similar structural characteristics with other known GSTs, because it is a homodimer and predominantly α-helical with few β-strands. Secondary structural analysis elucidated the polypeptide backbone of SjGST and the effect of EA on the structure. There was no observable difference

in the spectra of SjGST incubated with EA, this implies that the protein conformation was not distorted by the interaction between SjGST and EA.

The tertiary structure of SjGST was analysed using intrinsic fluorescence spectroscopy of tryptophan. SjGST contains eight tryptophan residues (Trp7, Trp40, Trp200 and Trp205), four per monomer, hence it is difficult to differentiate their individual spectral contributions (Albrecht *et al.*, 2008). The obtained spectra indicate that some of the tryptophans are partially exposed to solvent with maximum emission wavelength at 341 nm and a shoulder (vibrational fine structure) at 330 nm wavelength. Binding of EA to SjGST reduced the intensity of the fluorescence emission spectrum (Figure 4.6). This indicates that the local environment of the tryptophans has become more polar or solvent-exposed and not necessarily a change in the global structure of the protein because the circular dichroism data shows almost no changes in the secondary structure of SjGST. Furthermore, fluorescence characteristics of hydrophobic probes such as ANS is very useful in analysing conformational changes in protein structures. ANS was used to probe hydrophobic binding cavities in SjGST. The increased quantum yield and a blue shift (from 520 nm – 492 nm) of ANS when bound to SjGST is consistent with hydrophobic binding sites observed in GSTs class Mu (Kinsley *et al.*, 2008a). The spectra obtained for ANS bound to SjGST-EA complex shows reduced emission maxima. This could suggest that the ANS binding pockets became more hydrophobic (increased blue shift) as a result of the binding of EA to SjGST. More so, it is also possible that both ANS and EA binds at the same active site (H-site). It has been shown that ANS binds mostly at the H-site of most GSTs (Dirr *et al.*, 2005; Mannervik B1 and UH., 1988; Mannervik *et al.*, 1988; Oakley *et al.*, 1997). However, it has been reported that ANS also binds to a site distinct from the H-site of SjGST (Yassin *et al.*, 2004), which could be at the dimer interface groove (Ligandin site) (McTigue *et al.*, 1995). The displacement of ANS by EA in a concentration dependent manner (Figure 4.7B) further confirms that EA and ANS binds at the H-site or a similar site other than the H-site. SjGST has lower affinity for ANS, which agrees with the observation reported by Yassin, *et al* (2004) when they compared ANS and BS (Bromosulfophthalein) affinity to SjGST; hence, EA (stronger binder) was able to displace ANS (weaker binder). The affinity of SjGST for ANS (K_d = 30.3 μM) was further decreased in SjGST-EA complex (K_d = 40.6 μM) suggesting that both ANS and EA may be binding at the same site, and affinity of ANS for SjGST reducing in the presence of EA. From ANS binding study, one could conclude that ANS and EA may be competing for the same binding site in SjGST. Because studies have shown that ANS binds

within the H-site of cGSTs (Litwack *et al.*, 1971), this suggests that EA may be binding to SjGST at the H-site.

Characterisation of the quaternary structure of SjGST was performed using SE-HPLC to analyse the hydrodynamic volume and molecular mass of SjGST both in the absence and presence of EA. SjGST is a cytoplasmic protein, existing in a reduced environment. Hence the analysis was performed in the presence of a reducing agent (DTT). In the absence of DTT the protein forms a high order oligomer. SjGST (in the presence of DTT) eluted at a size indicating a dimeric quaternary structure (54 kDa) (Figure 4.8), although this differs from the theoretical size of 52 kDa. However, this difference is within a reasonable limit. The observed size is comparable with the crystal structure reported by Lim *et al*. (Lim *et al.*, 1994). The presence of EA (10 μM) did not change the quaternary structure of SjGST. Studies have shown that ligandin function of GSTs does not induce any noticeable structural changes within the global structure of the enzymes (Liebau *et al.*, 1997). The ability of SjGST to retain its native structure is fundamental for functional characterisation, because a dimeric structure is required to maintain functional active sites (Dirr *et al.*, 2005; Liebau *et al.*, 2005).

SjGST is the main detoxification system in *S. japonicum* due to the absence of cytochromes P450 activity in the parasite (Tracy and Vande Waa, 1995). The active site of cytosolic GSTs is proximal to the dimer interface. The active site is positioned between two subunits of the protein (Figure 2.5); the G-site which binds GSH is located at the N-terminal domain and H-site which binds electrophilic compounds, at the C-terminal domain. The catalytic activity of SjGST was analysed using GSH-CDNB conjugation assay. SjGST catalyses GSH-CDNB conjugation at the rate of 24 μmol min^{-1} mg^{-1}, this specific activity is high when compared with the result (10.8 μmol min^{-1} mg^{-1}) obtained by Kaplan *et al*. (1997). In the presence of EA, SjGST shows residual activity, indicating that an inhibition of the enzyme by the ligand occurred. EA has not been reported to inhibit SjGST previously. However, it has been shown to inhibit *Plasmodium falciparum* GST (Sturm *et al.*, 2009) and human cytosolic GSTs with very low affinities (Hayeshi *et al.*, 2007). In view of the fact that this study has established that EA inhibits SjGST activity, it was important to measure the inhibition potency of EA for further downstream applications. This was achieved using GSH-CDNB assay in the presence of different concentrations of EA and the IC_{50} (2.4 μM) was obtained by constructing a dose response curve. When compared with the value obtained by Sturm et al. (2009), EA binds

tighter to SjGST than to *plasmodium falciparum* GST ($IC_{50} \approx 74.40$ μM) and human cGSTs ($IC_{50} \approx 74.40$ μM).

Bisubstrate inhibition kinetics were used to evaluate the kinetic mechanism of SjGST in the presence and absence of different EA concentrations, using GSH and CDNB as the probe for G-site and H-site, respectively. The obtained IC_{50} value formed the bases of the choice of various EA concentrations used in the steady state kinetic analysis for this study. Ordered binding of substrates has been observed in most GSTs, however, random, ping-pong and sequential mechanism has also been reported (Valenzuela-Chavira *et al.*, 2017). A correlation between kinetic mechanism and the structure of an enzyme has been reported by Valenzuela-Chavira (2017). Hence, in ordered mechanisms, the binding of the second substrate is dependent on the conformational changes induced on the active site by the binding of the first substrate. In this study it was observed that SjGST catalytic mechanism proceeded with the formation of a ternary complex which exhibits random substrate binding order, this is consistent with the observation made by (Stefanidis *et al.*, 2018). Although Michaelis-Menten behaviour was followed by both substrates (GSH and CDNB) in this study, however the curve obtained for CDNB (Figure 4.16) did not show proper saturation at 1.5 mM (CDNB) concentration. Double reciprocal plots of the Michaelis-Menten data was used to determine modes of inhibition, which suggests non-competitive inhibition for the G-site and un-competitive for the H-site. The un-competitive mode of inhibition observed in the H-site suggests the possibility of EA binding somewhere else other than the H-site. The K_M and V_{max} values (Table 4.2) obtained in the absence of EA are consistent with the values obtained by Walker et al 1993. The K_M values indicates that SjGST has more affinity for GSH than CDNB, which is expected because GSH is their natural substrate. GSH is majorly synthesised in the cytosol, with a concentration of 1-10 mM, and SjGST is a cytosolic enzyme, hence the preference or higher affinity for the G-site. The obtained rate constant (k_{cat}) at which the SjGST-substrate complex is converted to a product in the absence of EA indicates that the enzyme exhibits moderate affinity towards the non-substrate ligand (CDNB). The conjugation of GSH to CDNB was not very rapid. This is in line with the observation made by Fabrini *et al* (2010). Accelerated detoxification of toxic compounds requires enzyme-substrate complex. However low affinity of some cytosolic GSTs towards some non-substrates (ligand) is hugely compensated by high enzyme concentration in the cell (Fabrini *et al.*, 2010). Additionally, Huang *et al*. (Huang *et al.*, 2012) also reported that $kJmol^{-1}$ have limited antioxidant capacity when compared to their human host, this could also explain the low k_{cat} observed in this study. The

k_{cat}/K_M values (Table 4.2) indicate that the catalytic efficiency of SjGST was reduced as the concentration of EA increases. This supports the previous observation that the binding of EA to SjGST reduces the activity of the enzyme. Kinetic parameters for cytosolic GSTs have not been previously well characterised and most of the available data were obtained under different conditions.

Thermodynamic insights from ITC studies are of significant interest for drug development (Draczkowski *et al.*, 2014). The energetics of EA binding to SjGST was explored using ITC. This was performed to probe further the structural basis of EA-SjGST binding interaction and energy profile of the associated ligand binding sites. The observed binding affinity (K_d = 4.73 ± 0.04 μM) of EA to SjGST is in the lower micromole range, which is consistent with the IC_{50} (2.4 μM). Yassin et al. (2004) obtained the K_d of ANS to SjGST to be 357 μM, this is more than fifty-fold higher than the K_d of EA to SjGST obtained in this study. This indicates that EA binds tighter to SjGST than ANS, as earlier observed in our ANS binding studies. Binding of EA to SjGST is enthalpy driven, accompanied by a negative entropy change ($T\Delta S$). This denotes favourable non-covalent interactions such as H-bonding, electrostatic and van der Waals between the enzyme and the ligand. Net formation of these bonds as observed in the docking studies (Figure 4.15B and 4.16B) produces negative enthalpy change (ΔH) (Pattanayak *et al.*, 2017). Phenolic hydroxyl group of EA can interact with the O, C and NH of the SjGST polypeptide chain with strong hydrogen bonding, leading to the rearrangement of the carbonyl hydrogen bonding network of the polypeptide backbone. The negative value obtained for ΔG indicates that the formation of SjGST-EA complex occurred spontaneously. The binding profile obtained in this study indicates that EA binding to SjGST is strong with respect to the affinity constant in the range of 10^5 M^{-1}. Binding stoichiometry (4) obtained could not have been precisely determined, it is known that SjGST has one H-site per monomer and a ligandin site (L-site) at the dimer interface. However, in the absence of a crystal structure of SjGST-EA complex, it is assumed that EA (being a planer molecule) could possibly bind at other places apart from these two identified sites. Thus, the obtained stoichiometry value.

The un-competitive mode of inhibition observed in the H-site and the ambiguity of the obtained stoichiometry in ITC prompted further probe using molecular docking studies. Molecular modelling provides better understanding and information about the binding sites and the binding mode at the atomic level in the absence of a crystal structure (Pattanayak *et al.*, 2017). Molecular docking was performed using Induced fit™ ligand and Glide docking algorithms

implemented in Schrödinger Suite (2017-3). To ensure that the protein is within its lowest energy conformation before docking, energy minimisation was performed in a solvated environment. Ligand minimisation was also performed on EA, to prevent occurrence of any significant internal strain. Residues within 4 Å of the EA bound to the L-site for chain-A include: Arg72, Glu95, Gly96, Leu99, Tyr103, Arg107 and for chain-B Tyr103, Asp100, Leu99, Gly96, Met68 and Glu95. EA bound to H-site is in close proximity with Tyr6, Trp7, Ile9, Try110, Gly11, Leu12, Ser106, Tyr103, Gln66, Asn53 and Leu54 on Chain-A, and on chain-B Asp100 and Arg107. Hydrogen bond interaction was observed between EA and some residues for both L-site (Asp100 on chain-B and a double interaction with Glu95 on chain-B) and H-site (Tyr6, Tyr110, Ser106 on Chain A, on Chain-B Asp100 and Arg107). EA bound to H-site exhibits more hydrogen bond interaction with the residues. The crystal structure of SjGST-Praziquantel complex has been solved by McTigue et al 1995, it was observed that Praziquantel binds at the L-site of SjGST. However, it could not inhibit activity of SjGST as observed in this study with EA. The L-site of SjGST is distinct from that of mammalian GST due to the presence of Tyr104 (McTigue *et al.*, 1995) and the site is not totally hydrophobic, therefore binding of ligands depends on the structure, size and nature of the ligand (Yassin *et al.*, 2004). Binding of EA at two distinct sites as observed in molecular docking studies could explain the inconsistent stoichiometry value obtained with the ITC experiment. In addition, this compliments the mode of inhibition observed with CDNB. It is possible that EA binds to the H-site together with CDNB and also binds to the L-site. In addition, it was reported that proteins usually possess various binding sites where polyphenols could bind and that polyphenols have a number of ends which can bind to proteins (Siebert *et al.*, 1996). The obtained RMSD (0.02Å) is less than 2Å hence, validating the accuracy of the overall docking process.

It is very necessary to perform MD simulation on the SjGST-EA complex in subsequent studies, to ascertain how firm EA binds to the protein. X-ray crystallography of the protein-ligand complex (SjGST-EA) would be great tool which, can elucidate the exact conformational changes in the SjGST-EA complex and the binding properties.

In summary, EA is a potent inhibitor of SjGST catalytic ability, which binds at the H-site and more tighter at the L-site of the dimer interface. Binding of EA to SjGST did not change the overall structural conformation of the enzyme, but the functional characteristics were altered. The observed structural differences at the H-site of SjGST when compared with mammalian GSTs (McTigue *et al.*, 1995) provides the structural basis for selective drug design for selective inhibition of SjGST. Barch et al reported that the various portions (lactone and hydroxyl group)

of EA molecule are required for different inhibitory activities. Slight modifications of EA structure could produce derivatives with high chemotherapeutic capabilities against schistosomiasis (Barch *et al.*, 1996a). Thus, this study under pins the potential to re-model EA for stronger and more effective inhibition of SjGST. This therefore answers the research question that EA can be a template for a rational approach to drug design against schistosomiasis.

References

Adedapo, A., Alex, Adeoye Bisi, O., Sofidiya Margaret, O., Oyagbemi Ademola, A., (2015). Antioxidant, antinociceptive and anti-inflammatory properties of the aqueous and ethanolic leaf extracts of Andrographis paniculata in some laboratory animals, Journal of Basic and Clinical Physiology and Pharmacology, p. 327.

Adenowo, A.F., Oyinloye, B.E., Ogunyinka, B.I., Kappo, A.P., (2015). Impact of human schistosomiasis in sub-Saharan Africa. *Brazilian Journal of Infectious Diseases* 19, 196-205.

Ahmed, S.H., (2016a). Schistosomiasis: Background, Pathophsiology, Etiology. *Medscape* 228392, 3-12.

Ahmed, S.H., (2016b). Schistosomiasis: Background, Pathophsiology, Etiology. *Medscape* 3-12.

Al-Waheeb, S., Al-Murshed, M., Dashti, F., Hira, P.R., Al-Sarraf, L., (2009). Disseminated peritoneal Schistosoma japonicum: a case report and review of the pathological manifestations of the helminth. *Ann Saudi Med* 29, 149-152.

Albrecht, C., Russinova, E., Kemmerling, B., Kwaaitaal, M., de Vries, S.C., (2008). Arabidopsis SOMATIC EMBRYOGENESIS RECEPTOR KINASE Proteins Serve Brassinosteroid-Dependent and -Independent Signaling Pathways. *Plant Physiology* 148, 611-619.

Alias, Z., (2016). The Role of Glutathione Transferases in the Development of Insecticide Resistance, in: Trdan, S. (Ed.), Insecticides Resistance. InTech, Rijeka, p. Ch. 16.

Andújar-Sánchez, M., Clemente-Jiménez, J.M., x, Las Heras-Vázquez, F.J., Rodrı, x, guez-Vico, F., Cámara-Artigas, A., Jara-Pérez, V., (2003). Thermodynamics of glutathione binding to the tyrosine 7 to phenylalanine mutant of glutathione S-transferase from Schistosoma japonicum. *International Journal of Biological Macromolecules* 32, 77-82.

Babatunji, O., Fatimah, A., Nomagugu, G., Abidemi, K., (2014). The Promise of Antimicrobial Peptides for Treatment of Human Schistosomiasis. *Current Drug Targets* 15, 852-859.

Bader, R., Leisinger, T., (1994). Isolation and characterization of the Methylophilus sp. strain DM11 gene encoding dichloromethane dehalogenase/glutathione S-transferase. *Journal of Bacteriology* 176, 3466-3473.

Baiocco, P., Gourlay, L.J., Angelucci, F., Fontaine, J., Hervé, M., Miele, A.E., Trottein, F., Brunori, M., Bellelli, A., (2006). Probing the Mechanism of GSH Activation in Schistosoma haematobium Glutathione-S-transferase by Site-directed Mutagenesis and X-ray Crystallography. *Journal of Molecular Biology* 360, 678-689.

Bala, I., Bhardwaj, V., Hariharan, S., Kumar, M.N.V.R., (2006). Analytical methods for assay of ellagic acid and its solubility studies. *Journal of Pharmaceutical and Biomedical Analysis* 40, 206-210.

Barch, D.H., Rundhaugen, L.M., Stoner, G.D., Pillay, N.S., Rosche, W.A., (1996a). Structure-function relationships of the dietary anticarcinogen ellagic acid. *Carcinogenesis* 17, 265-269.

Barch, D.H., Rundhaugen, L.M., Stoner, G.D., S., P.N., Rosche, W., (1996b). Structure-function relationships of the dietary anticarcinogen ellagic acid. *Carcinogenesis* 17, 265-269.

Bottegoni, G., Kufareva, I., Totrov, M., Abagyan, R., (2008). A New Method for Ligand Docking to Flexible Receptors by Dual Alanine Scanning and Refinement (SCARE). *Journal of computer-aided molecular design* 22, 311-325.

Bottieau, E., Clerinx, J., de Vega, M.R., Van den Enden, E., Colebunders, R., Van Esbroeck, M., Vervoort, T., Van Gompel, A., Van den Ende, J., (2006). Imported Katayama fever: Clinical and biological features at presentation and during treatment. *Journal of Infection* 52, 339-345.

Bowden, A.C., (1995). Analysis of enzyme kinetic data. Oxford University Press, London.

Caffrey, C.R., (2007). Chemotherapy of schistosomiasis: present and future. *Current Opinion in Chemical Biology* 11, 433-439.

Caffrey, C.R., Rohwer, A., Oellien, F., Marhöfer, R.J., Braschi, S., Oliveira, G., McKerrow, J.H., Selzer, P.M., (2009). A Comparative Chemogenomics Strategy to Predict Potential Drug Targets in the Metazoan Pathogen, Schistosoma mansoni. *PLoS ONE* 4, e4413.

Cardoso, R.M.F., Daniels, D.S., Bruns, C.M., Tainer, J.A., (2003). Characterization of the electrophile binding site and substrate binding mode of the 26- kDa glutathione S- transferase from Schistosoma japonicum. *Proteins: Structure, Function, and Bioinformatics* 51, 137-146.

Chung, C.T., Niemela, S.L., Miller, R.H., (1989). One-step preparation of competent Escherichia coli: transformation and storage of bacterial cells in the same solution. *Proceedings of the National Academy of Sciences of the United States of America* 86, 2172-2175.

Colley, D.G., Bustinduy, A.L., Secor, W.E., King, C.H., (2014). Human schistosomiasis. *The Lancet* 383, 2253-2264.

Cornell, W.D., Cieplak, P., Bayly, C.I., Gould, I.R., Merz, K.M., Ferguson, D.M., Spellmeyer, D.C., Fox, T., Caldwell, J.W., Kollman, P.A., (1995). A Second Generation Force Field for the Simulation of Proteins, Nucleic Acids, and Organic Molecules. *Journal of the American Chemical Society* 117, 5179-5197.

Dirr, H.W., Little, T., Kuhnert, D.C., Sayed, Y., (2005). A Conserved N-capping Motif Contributes Significantly to the Stabilization and Dynamics of the C-terminal Region of Class Alpha Glutathione S-Transferases. *Journal of Biological Chemistry* 280, 19480-19487.

Doenhoff, M.J., Cioli, D., Utzinger, J., (2008). Praziquantel: mechanisms of action, resistance and new derivatives for schistosomiasis. *Current opinion in infectious diseases* 21, 659-667.

Doerig, C., Grevelding, C.G., (2015). Targeting kinases in Plasmodium and Schistosoma: Same goals, different challenges. *Biochimica et Biophysica Acta (BBA) - Proteins and Proteomics* 1854, 1637-1643.

Draczkowski, P., Matosiuk, D., Jozwiak, K., (2014). Isothermal titration calorimetry in membrane protein research. *Journal of Pharmaceutical and Biomedical Analysis* 87, 313-325.

Fabrini, R., Bocedi, A., Pallottini, V., Canuti, L., De Canio, M., Urbani, A., Marzano, V., Cornetta, T., Stano, P., Giovanetti, A., Stella, L., Canini, A., Federici, G., Ricci, G., (2010). Nuclear Shield: A Multi-Enzyme Task-Force for Nucleus Protection. *PLoS ONE* 5, e14125.

Farid, R., Day, T., Friesner, R.A., Pearlstein, R.A., (2006). New insights about HERG blockade obtained from protein modeling, potential energy mapping, and docking studies. *Bioorganic & Medicinal Chemistry* 14, 3160-3173.

Fenwick, A., Savioli, L., Engels, D., Robert Bergquist, N., Todd, M.H., (2003). Drugs for the control of parasitic diseases: current status and development in schistosomiasis. *Trends in Parasitology* 19, 509-515.

Ferreira, L.G., Oliva, G., Andricopulo, A.D., (2015). Target-based molecular modeling strategies for schistosomiasis drug discovery. *Future Medicinal Chemistry* 7, 753-764.

Frova, C., (2006). Glutathione transferases in the genomics era: new insights and perspectives. *Biomol Eng.* 23, 149-169.

Galano, A., Francisco Marquez, M., Pérez-González, A., (2014). Ellagic Acid: An Unusually Versatile Protector against Oxidative Stress. *Chemical Research in Toxicology* 27, 904-918.

Gasteiger E., Hoogland C., Gattiker A., Duvaud S., Wilkins M.R., Appel R.D., A.;, B., (2005). Protein Identification and Analysis Tools on the ExPASy Server;. Humana Press.

GHO, (2016). Schistosomiasis: Situations and trends, in: data, G.H.O.G. (Ed.). Global Health Observatory (GHO).

Greenfield, N.J., (2006). Using circular dichroism spectra to estimate protein secondary structure. *Nature protocols* 1, 2876-2890.

Gregorio Weber, Young, L.B., (1964). Fragmentation of Bovine Serum Albumin by Pepsin *The Journal of Biological Chemistry* 239, 1415-1423.

Gryseels, B., Polman, K., Clerinx, J., Kestens, L., (2009). Human schistosomiasis. *The Lancet* 368, 1106-1118.

Habig, W.H., Pabst, M.J., Jakoby, W.B., (1974). Glutathione S-transferases the first enzymatic step in mercapturic acid formation. *Journal of biological Chemistry* 249, 7130-7139.

Halperin, I., Ma, B., Wolfson, H., Nussinov, R., (2002). Principles of docking: An overview of search algorithms and a guide to scoring functions. *Proteins: Structure, Function, and Bioinformatics* 47, 409-443.

Hartman, J., Daram, P., Frizzell, R.A., Rado, T., Benos, D.J., Sorscher, E.J., (1992). Affinity purification of insoluble recombinant fusion proteins containing glutathione- S-transferase. *Biotechnology and Bioengineering* 39, 828-832.

Hawe, A., Sutter, M., Jiskoot, W., (2008). Extrinsic Fluorescent Dyes as Tools for Protein Characterization. *Pharmaceutical Research* 25, 1487-1499.

Hayeshi, R., Mutingwende, I., Mavengere, W., Masiyanise, V., Mukanganyama, S., (2007). The inhibition of human glutathione S-transferases activity by plant polyphenolic compounds ellagic acid and curcumin. *Food and Chemical Toxicology* 45, 286-295.

Head-Gordon, M., Head-Gordon, T., (1994). Analytic MP2 frequencies without fifth-order storage. Theory and application to bifurcated hydrogen bonds in the water hexamer. *Chemical Physics Letters* 220, 122-128.

Heur, Y.H., Toledo, O., Zeng, W.G., Stoner, G.D., Nemeth, G.A., (1992). Synthesis of ellagic acid 0-alkyl derivatives and isolation of ellagic acid as a tetrahexanoyl derivative from Fragaria ananassa, Ohio USA.

Hotez, P.J., Fenwick, A., (2009). Schistosomiasis in Africa: An Emerging Tragedy in Our New Global Health Decade. *PLOS Neglected Tropical Diseases* 3, e485.

Hu, H., Elstner, M., Hermans, J., (2003). Comparison of a QM/MM force field and molecular mechanics force fields in simulations of alanine and glycine "dipeptides" (Ace- Ala- Nme and Ace- Gly- Nme) in water in relation to the problem of modeling the unfolded peptide backbone in solution. *Proteins: Structure, Function, and Bioinformatics* 50, 451-463.

Huang, H.-H., Rigouin, C., Williams, D.L., (2012). The Redox Biology of Schistosome Parasites and Applications for Drug Development. *Current pharmaceutical design* 18, 3595-3611.

Jakobsson, P.J., Morgenstern, R., Mancini, J., Ford-Hutchinson, A., Persson, B., (1999). Common structural features of MAPEG -- a widespread superfamily of membrane associated proteins with highly divergent functions in eicosanoid and glutathione metabolism. *Protein Science : A Publication of the Protein Society* 8, 689-692.

Jia, T.-W., Zhou, X.-N., Wang, X.-H., Utzinger, J., Steinmann, P., Wu, X.-H., (2007). Assessment of the age-specific disability weight of chronic schistosomiasis japonica. *Bulletin of the World Health Organization* 85, 458-465.

Jiang, Y.-G., Zhang, M.-M., Xiang, J., (2008). Spinal cord schistosomiasis japonica: a report of 4 cases. *Surg Neurol* 69, 392-397.

Joannes Clerinx, Soentjens., P., (2017). Epidemiology, pathogenesis, and clinical manifestations of schistosomiasi, in: Weller, P.F. (Ed.).

John, R., Ezekiel, M., Philbert, C., Andrew, A., (2008). Schistosomiasis transmission at high altitude crater lakes in Western Uganda. *BMC Infectious Diseases* 8, 110-110.

Jorgensen, W.L., (2004). The Many Roles of Computation in Drug Discovery. *Science* 303, 1813-1818.

Khanduja, K.L., Gandhi, R.K., Pathania, V., Syal, N., (1999). Prevention of N-nitrosodiethylamine-induced lung tumorigenesis by ellagic acid and quercetin in mice. *Food and Chemical Toxicology* 37, 313-318.

King, C.H., Dangerfield-Cha, M., (2008). The unacknowledged impact of chronic schistosomiasis. *Chronic Illness* 4, 65-79.

Kinsley, N., Sayed, Y., Armstrong, R.N., Dirr, H.W., (2008a). Characterization of the binding of 8-anilinonaphthalene sulphonate to rat class Mu GST M1-1. *Biophysical Chemistry* 137, 100-104.

Kinsley, N., Sayed, Y., Mosebi, S., Armstrong, R.N., Dirr, H.W., (2008b). Characterization of the binding of 8-anilinonaphthalene sulfonate to rat class Mu GST M1-1. *Biophysical Chemistry* 137, 100-104.

Kramer CV, Zhang F, Sinclair D, PL., O., (2014). Drugs for treating urinary schistosomiasis. Cochrane Database of Systematic Reviews. *Cochrane Library*.

Labieniec, M., Gabryelak, T., (2006). Interactions of tannic acid and its derivatives (ellagic and gallic acid) with calf thymus DNA and bovine serum albumin using spectroscopic method. *Journal of Photochemistry and Photobiology B: Biology* 82, 72-78.

Laemmli, U.K., (1970). Cleavage of Structural Proteins during the Assembly of the Head of Bacteriophage T4. *Nature* 227, 680-685.

Landete, J.M., (2011). Ellagitannins, ellagic acid and their derived metabolites: A review about source, metabolism, functions and health. *Food Research International* 44, 1150-1160.

Liebau, E., De Maria, F., Burmeister, C., Perbandt, M., Turella, P., Antonini, G., Federici, G., Giansanti, F., Stella, L., Lo Bello, M., Caccuri, A.M., Ricci, G., (2005). Cooperativity and Pseudo-cooperativity in the Glutathione S-Transferase from Plasmodium falciparum. *Journal of Biological Chemistry* 280, 26121-26128.

Liebau, E., Eckelt, V.H., Wildenburg, G., Teesdale-Spittle, P., Brophy, P.M., Walter, R.D., Henkle-Dührsen, K., (1997). Structural and functional analysis of a glutathione S-transferase from Ascaris suum. *Biochemical Journal* 324, 659-666.

Lim, K., Ho, J.X., Keeling, K., Gilliland, G.L., Ji, X., Rüker, F., Carter, D.C., (1994). Three-dimensional structure of Schistosoma japonicum glutathione S-transferase fused with a six-amino acid conserved neutralizing epitope of gp41 from HIV. *Protein Science : A Publication of the Protein Society* 3, 2233-2244.

Listowsky, I., (1993). Glutathione 5-transferases: intracellular binding detoxification and adaptive responses. . *Hepatic Anion Transport and Bile Secretion: Physiology and Pathophysiol- ogv. New York: Raven Press.*, 397-405.

Litwack, G., Ketterer, B., Arias, I.M., (1971). Ligandin: a Hepatic Protein which Binds Steroids, Bilirubin, Carcinogens and a Number of Exogenous Organic Anions. *Nature* 234, 466.

Liu, J., Dyer, D., Wang, J., Wang, S., Du, X., Xu, B., Zhang, H., Wang, X., Hu, W., (2013). 3-Oxoacyl-ACP Reductase from Schistosoma japonicum: Integrated In Silico-In Vitro Strategy for Discovering Antischistosomal Lead Compounds. *PLoS ONE* 8, e64984.

Loarca-Piña, G., Kuzmicky, P.A., González de Mejía, E., Kado, N.Y., (1998). Inhibitory effects of ellagic acid on the direct-acting mutagenicity of aflatoxin B1 in the Salmonella microsuspension assay. *Mutation Research/Fundamental and Molecular Mechanisms of Mutagenesis* 398, 183-187.

Madhavi Sastry, G., Adzhigirey, M., Day, T., Annabhimoju, R., Sherman, W., (2013). Protein and ligand preparation: parameters, protocols, and influence on virtual screening enrichments. *Journal of Computer-Aided Molecular Design* 27, 221-234.

Mannervik B1, UH., D., (1988). Glutathione transferases--structure and catalytic activity. *CRC Crit Rev Biochem.* 23, 283-337.

Mannervik, B., Helena Danielson, U., Ketterer, B., (1988). Glutathione transferases—structure and catalytic activit. *Critical Reviews in Biochemistry* 23, 283-337.

Martín-Santamaría, S., (2017). Computational Tools for Chemical Biology. Royal Society of Chemistry.

Masamba, P., Adenowo, A.F., Oyinloye, B.E., Kappo, A.P., (2016). Universal Stress Proteins as New Targets for Environmental and Therapeutic Interventions of Schistosomiasis. *International Journal of Environmental Research and Public Health* 13, 972.

Maurer, H.R., (1971). Disc Electrophoresis, and Related Techniques of Polyacrylamide Gel Electrophoresis 2nd ed. De

Gruyter, New York.

McTigue, M.A., Williams, D.R., Tainer, J.A., (1995). Crystal Structures of a Schistosomal Drug and Vaccine Target: Glutathione S-Transferase fromSchistosoma japonicaand its Complex with the Leading Antischistomal Drug Praziquantel. *Journal of Molecular Biology* 246, 21-27.

Meltzer, E., Artom, G., Marva, E., Assous, M.V., Rahav, G., Schwartz, E., (2006). Schistosomiasis among Travelers: New Aspects of an Old Disease. *Emerging Infectious Diseases* 12, 1696-1700.

Milhon, J.L., Thiboldeaux, R.L., Glowac, K., Tracy, J.W., (1997). Schistosoma japonicumGSHS-TransferaseSj26 Is Not the Molecular Target of Praziquantel Action. *Experimental Parasitology* 87, 268-274.

Mukhtar, H., Benjamin J. Del Tito, J., Marcelo, C.L., Das, M., Bickers, D.R., (1985). Ellagic acid: a potent naturally occurring inhibitor of benzo[a]pyrene metabolism and its subsequent glucuronidation, sulfation and covalent binding to DNA in cultured BALB/C mouse keratinocytes. *Carcinogenesis* 5, 565–1571.

Murugan, V., Mukherjee, K., Maiti, K., Mukherjee, P.K., (2009). Enhanced Oral Bioavailability and Antioxidant Profile of Ellagic Acid by Phospholipids. *Journal of Agricultural and Food Chemistry* 57, 4559-4565.

Nakashima, T., Kage, M., Hirata, M., (2003). A historical view of schistosomiasis japonica in the Chikugo river basin. What can we learn from autopsy? *Parasitol Int* 52, 327-334.

Nare, B., Smith, J.M., Prichard, R.K., (1992). Mechanisms of inactivation of Schistosoma mansoni and mammalian glutathione S-transferase activity by the antischistosomal drug oltipraz. *Biochemical Pharmacology* 43, 1345-1351.

Neubign, R.R., Spedding, M., Kenakin, T., Christopoulos, A., (2003). International Union of Pharmacology Committee on Receptor Nomenclature and Drug Classification. XXXVIII. Update on Terms and Symbols in Quantitative Pharmacology. *Pharmacological Reviews* 55, 597-606.

Nmorsi O., U.N., Ogoinja S, Blackie T., Odike C., (2007). rinary tract pathology in some Schistosoma haematobium infected Nigerians *African Journal of Biotechnology* 6(2), 123-127.

Nour, N.M., (2010). Schistosomiasis: Health Effects on Women. *Reviews in Obstetrics and Gynecology* 3, 28-32.

Oakley, A.J., Bello, M.L., Battistoni, A., Ricci, G., Rossjohn, J., Villar, H.O., Parker, M.W., (1997). The structures of human glutathione transferase P1-1 in complex with glutathione and various inhibitors at high resolution11Edited by R. Huber. *Journal of Molecular Biology* 274, 84-100.

Otaki, J.M., Tsutsumi, M., Gotoh, T., Yamamoto, H., (2010). Secondary Structure Characterization Based on Amino Acid Composition and Availability in Proteins. *Journal of Chemical Information and Modeling* 50, 690-700.

Palermo, G., Vivo, M.D., (2015). Encyclopedia of Nanotechnology, Encyclopedia of Nanotechnology, 1 ed. ed. s.l.:Springer, Netherlands.

Pattanayak, R., Basak, P., Sen, S., Bhattacharyya, M., (2017). An insight to the binding of ellagic acid with human serum albumin using spectroscopic and isothermal calorimetry studies. *Biochemistry and Biophysics Reports* 10, 88-93.

Pierce, J., Raymond, Dubois-Abdesselem, F., Lancelot, J., Andrade, L., Oliveira, G., (2012). Targeting Schistosome Histone Modifying Enzymes for Drug Development. *Current Pharmaceutical Design* 18, 3567-3578.

Ramsay, E.E., Dilda, P.J., (2014). Glutathione S-conjugates as prodrugs to target drug-resistant tumors. *Frontiers in Pharmacology* 5, 181.

Renganathan, E., Cioli, E., (1998). An International Initiative on Praziquantel Use. *Parasitology Today* 14, 390-391.

Ross, A.G., McManus, D.P., Farrar, J., Hunstman, R.J., Gray, D.J., Li, Y.-S., (2012). Neuroschistosomiasis. *Journal of Neurology* 259, 22-32.

Ross, A.G., Vickers, D., Olds, G.R., Shah, S.M., McManus, D.P., (2007). Katayama syndrome. *The Lancet Infectious Diseases* 7, 218-224.

Ross , A.G.P., Bartley , P.B., Sleigh , A.C., Olds , G.R., Li , Y., Williams , G.M., McManus , D.P., (2002). Schistosomiasis. *New England Journal of Medicine* 346, 1212-1220.

Rufer, A.C., Thiebach, L., Baer, K., Klein, H.W., Hennig, M., (2005). X-ray structure of glutathione S-transferase from Schistosoma japonicum in a new crystal form reveals flexibility of the substrate-binding site. *Acta Crystallographica Section F* 61, 263-265.

Sabhiya Majid, Krishan Lal KHANDUJA, Sanjay KAPUR, SHARMA, R.R., (1991). Effect of Feeding Ellagic Acid on Glutathione-S-Transferase Activity and Reduced Glutathione Levels inLiver and Lungs of Mice. *J. Clin. Biochem.* 10, 119-126.

Sarkar, S., Siddiqui, A.A., Mazumder, S., De, R., Saha, S.J., Banerjee, C., Iqbal, M.S., Adhikari, S., Alam, A., Roy, S., Bandyopadhyay, U., (2015). Ellagic Acid, a Dietary Polyphenol, Inhibits Tautomerase Activity of Human Macrophage Migration Inhibitory Factor and Its Pro-inflammatory Responses in Human Peripheral Blood Mononuclear Cells. *Journal of Agricultural and Food Chemistry* 63, 4988-4998.

Schrödinger, S., (2017a). Induced Fit Docking protocol; Glide, Schrödinger. Schrödinger LLC New York, New York.

Schrödinger, S., (2017b). Protein Preparation Wizard; , New York, NY.

Secor, W.E., Sundstrom, J.B., (2007). Below the belt: new insights into potential complications of HIV-1/schistosome coinfections. *Current Opinion in Infectious Diseases* 20, 519-523.

Sheehan, D., Meade, G., Foley, V.M., Dowd, C.A., (2001). Structure, function and evolution of glutathione transferases: implications for classification of non-mammalian members of an ancient enzyme superfamily. *Biochemical Journal* 360, 1.

Shivakumar, D., Williams, J., Wu, Y., Damm, W., Shelley, J., Sherman, W., (2010). Prediction of Absolute Solvation Free Energies using Molecular Dynamics Free Energy Perturbation and the OPLS Force Field. *Journal of Chemical Theory and Computation* 6, 1509-1519.

Siebert, K.J., Troukhanova, N.V., Lynn, P.Y., (1996). Nature of Polyphenol−Protein Interactions. *Journal of Agricultural and Food Chemistry* 44, 80-85.

Sivasankar, C., Maruthupandiyan, S., Balamurugan, K., James, P.B., Krishnan, V., Pandian, S.K., (2016). A combination of ellagic acid and tetracycline inhibits biofilm formation and the associated virulence of Propionibacterium acnes in vitro and in vivo. *Biofouling* 32, 397-410.

Smith, D.B., Davern, K.M., Board, P.G., Tiu, W.U., Garcia, E.G., Mitchell, G.F., (1986). Mr 26,000 antigen of Schistosoma japonicum recognized by resistant WEHI 129/J mice is a parasite glutathione S-transferase. *Proceedings of the National Academy of Sciences of the United States of America* 83, 8703-8707.

Sreerama, N., Woody, R.W., (2000). Estimation of Protein Secondary Structure from Circular Dichroism Spectra: Comparison of CONTIN, SELCON, and CDSSTR Methods with an Expanded Reference Set. *Analytical Biochemistry* 287, 252-260.

Stefanidis, L., Scinto, K.V., Strada, M.I., Alper, B.J., (2018). Bisubstrate Kinetics of Glutathione S-Transferase: A Colorimetric Experiment for the Introductory Biochemistry Laboratory. *Journal of Chemical Education* 95, 146-151.

Steinmann, P., Keiser, J., Bos, R., Tanner, M., Utzinger, J., (2006). Schistosomiasis and water resources development: systematic review, meta-analysis, and estimates of people at risk. *The Lancet infectious diseases* 6, 411-425.

Sturm, N., Hu, Y., Zimmermann, H., Fritz-Wolf, K., Wittlin, S., Rahlfs, S., Becker, K., (2009). Compounds Structurally Related to Ellagic Acid Show Improved Antiplasmodial Activity. *Antimicrobial Agents and Chemotherapy* 53, 622-630.

Taylor, R.D., Jewsbury, P.J., Essex, J.W., (2002). A review of protein-small molecule docking methods. *Journal of Computer-Aided Molecular Design* 16, 151-166.

Tayyab, S., Qamar, S., Islam, M., (1991). Size exclusion chromatography and size exclusion HPLC of proteins. *Biochemical Education* 19, 149-152.

Torres-Rivera, A., Landa, A., (2008). Glutathione transferases from parasites: A biochemical view. *Acta Tropica* 105, 99-112.

Tracy, J.W., Vande Waa, E.A., (1995). 10 - Xenobiotic Metabolism A2 - Marr, J. Joseph, in: Müller, M. (Ed.), Biochemistry and Molecular Biology of Parasites. Academic Press, San Diego, pp. 161-175.

Trottein, F., Godin, C., Pierce, R.J., Sellin, B., Taylor, M.G., Gorillot, I., Silva, M.S., Lecocq, J.-P., Capron, A., (1992). Inter-species variation of schistosome 28-kDa glutathione S-transferases. *Molecular and Biochemical Parasitology* 54, 63-72.

Utzinger, J., N'Goran, E.K., N'Dri, A., Lengeler, C., Shuhua, X., Tanner, M., (2000). Oral artemether for prevention of Schistosoma mansoni nfection: randomised controlled trial. *The Lancet* 355, 1320-1325.

Utzinger, J., Raso, G., Brooker, S., de Savigny, D., Tanner, M., Ornbjerg, N., Singer, B., N'Goran, E., (2009). Schistosomiasis and neglected tropical diseases: towards integrated and sustainable control and a word of caution. *Parasitology* 136, 1859-1874.

Utzinger, J., Tozan, Y., Singer, B.H., (2001). Efficacy and cost- effectiveness of environmental management for malaria control. *Tropical Medicine & International Health* 6, 677-687.

Valenzuela-Chavira, I., Contreras-Vergara, C.A., Arvizu-Flores, A.A., Serrano-Posada, H., Lopez-Zavala, A.A., García-Orozco, K.D., Hernandez-Paredes, J., Rudiño-Piñera, E., Stojanoff, V., Sotelo-Mundo, R.R., Islas-Osuna, M.A., (2017). Insights into ligand binding to a glutathione S-transferase from mango: Structure, thermodynamics and kinetics. *Biochimie* 135, 35-45.

Walker, A.J., (2011). Insights into the functional biology of schistosomes. *Parasites & Vectors* 4, 203.

Walker, J., Crowley, P., Moreman, A.D., Barrett, J., (1993). Biochemical properties of cloned glutathione S-transferases from Schistosoma mansoni and Schistosoma japonicum. *Molecular and Biochemical Parasitology* 61, 255-264.

Walle, T., Vincent, T.S., Walle, U.K., (2003). Evidence of covalent binding of the dietary flavonoid quercetin to DNA and protein in human intestinal and hepatic cells. *Biochemical Pharmacology* 65, 1603-1610.

Whitley, A.C., Stoner, G.D., Darby, M.V., Walle, T., (2003). Intestinal epithelial cell accumulation of the cancer preventive polyphenol ellagic acid—extensive binding to protein and DNA. *Biochemical Pharmacology* 66, 907-915.

Whitmore, L., Wallace, B.A., (2008). Protein secondary structure analyses from circular dichroism spectroscopy: Methods and reference databases. *Biopolymers* 89, 392-400.

Whittle, P.J., Blundell, T.L., (1994). Protein Structure-Based Drug Design. *Annual Review of Biophysics and Biomolecular Structure* 23, 349-375.

WHO, (2016). Schistosomiasis, Schistosomiasis fact sheet.

WHO, (2017). Crossing the billion: lymphatic filariasis, onchocerciasis, schistosomiasis, soil-transmitted helminthiases and trachoma: preventive chemotherapy for neglected tropical diseases.

Woodrow, C.J., Haynes, R.K., Krishna, S., (2005). Artemisinins. *Postgraduate Medical Journal* 81, 71.

Wright, M.D., Harrison, R.A., Melder, A.M., Newport, G.R., Mitchell, G.F., (1991). Another 26-kilodalton glutathioneS-transferase ofSchistosoma mansoni. *Molecular and Biochemical Parasitology* 49, 177-179.

Wu, Z.-D., Lü, Z.-Y., Yu, X.-B., (2005). Development of a vaccine against Schistosoma japonicum in China: a review. *Acta Tropica* 96, 106-116.

Yassin, Z., Ortiz-Salmerón, E., García-Maroto, F., Barón, C., García-Fuentes, L., (2004). Implications of the ligandin binding site on the binding of non-substrate ligands to Schistosoma japonicum-glutathione transferase. *Biochimica et Biophysica Acta (BBA) - Proteins and Proteomics* 1698, 227-237.

Young, D.C., (2001). Computational Chemistry: A Practical Guide for Applying Techniques to Real-World Problems. A John Wiley & Sons, INC, Newyork.

Yourgenome, (2016). What is Schistosomiasis, FACTS: Targeting disease. Wellcome Genome Campus, UK.

Appendix A

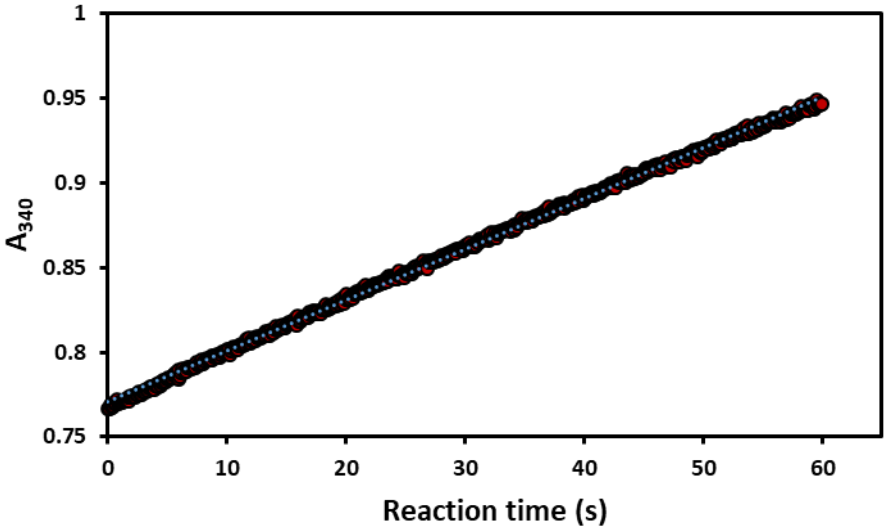


Figure Append. 1: A representative of the progress curves of GSH-CDNB conjugation reaction catalysed by SjGST. The monitored production of 1-(S-glutathionyl)-2,4-dinitrobenzene, as measured by an increasing A340 reading, immediately following initiation of the assay reaction by the addition of 1 mM CDNB to the buffered protein solution for a period of 60 s. The change in absorbance at 340 nm over the period of 60 seconds was determined by linear regression and used to calculate the initial velocity (υ_0) (R^2 = 0.998)

Table 5

Summary of the results obtained from each conjugation assay progress curve for different enzyme concentration and their activity. The figures represent the average of triplicate experimental data.

[SjGST] (nM)	Slope	R^2	Average activity
2	0.0002	0.9332	0.004
5	0.005	0.9911	0.010
10	0.0032	0.9950	0.021
15	0.0016	0.9977	0.030
20	0.0021	0.9989	0.039
25	0.0026	0.9989	0.048
30	0.003	0.9992	0.056
35	0.0035	0.9989	0.066

$$Activity = \frac{\Delta A_{340 \times time \times volume\ of\ sample}}{\varepsilon} \times 1\ 000\ 000 \qquad Eqn.\ 1.$$

$$Mass\ of\ enzyme\ (mg) = C \times Mr \times V \times 1000 \qquad Eqn.2.$$

Equation four and five were used to calculate the enzyme activity and the mass of enzyme.

Appendix B

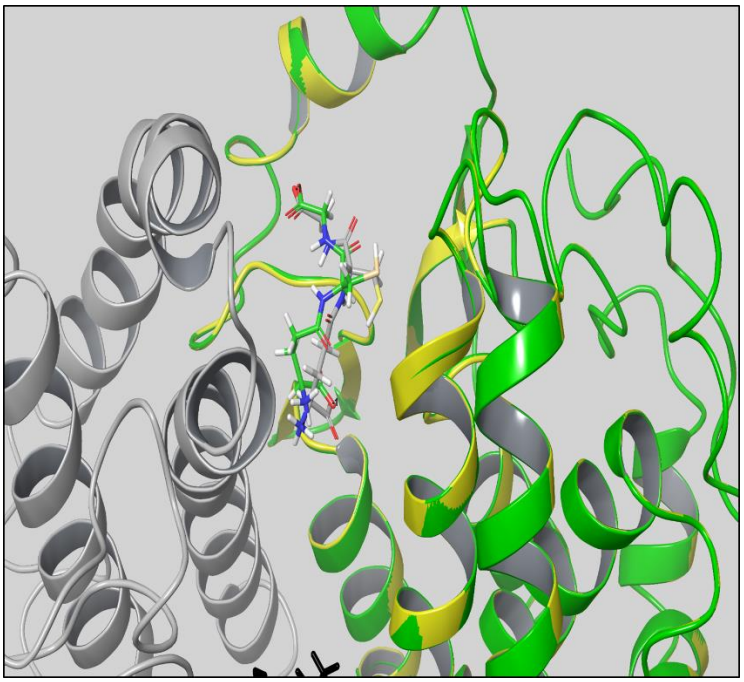


Figure Append 2. Validation of the molecular modelling dockings. The docking results was validated by obtaining the RMSD using the solved crystal structure (PDB ID: 1DUG) and the redocked structure. RMSD value of 0.024 Å was obtained.